NUMERICAL SOLUTION, ANALYSIS AND APPLICATIONS OF GEOMETRICAL NONLINEAR DIFFUSION EQUATIONS

Karol Mikula *

Abstract

We present recent results and applications of nonlinear diffusion equations. We focus on the so-called geometrical nonlinearities which are often expressed in a dependence of diffusion coefficient on the solution and/or its gradient. As working examples we consider generalized mean curvature flow equations in direct and level-set formulations, nonlinear diffusions of Perona-Malik type and nonlinear degenerate porous-medium equations. They model, for example, the motion of interface in free boundary problems and they are also used in image processing applications like image selective smoothing or image segmentation. We present related mathematical models, computational schemes for their solution, numerical examples and applications, and stability and convergence analysis of the numerical methods.

1 Introduction and motivations

In this work we are going to discuss several recent applications of geometrical nonlinear diffusion equations. We will mainly deal with generalized mean curvature flow equations in direct and level set formulations, nonlinear diffusions of Perona-Malik type and nonlinear degenerate porous-medium type problems. They are related, e.g., to motion of free boundaries in phase transition and to image processing applications like selective smoothing or segmentation. In this first Chapter we present mathematical models related to image processing and phase transition applications and illustrate some of their properties on the number of examples. In the second Chapter we describe how curve evolution equations can be solved by the so-called direct (Lagrangian) approach. In the third Chapter we concentrate on a solution of level-set-like equations and Perona-Malik type diffusion by means of variational techniques, namely finite element and finite/complementary volume methods.

Acknowledgements The particular results presented or cited in this publication were obtained together with Angela Handlovičová, Zuzana Krivá, Fiorella Sgallari, Eberhard Bänsch, Michal Beneš, Jozef Kačur, Claudio Lamberti, Tobias Preusser, Martin Rumpf, Narisoa Ramarosy, Alessandro Sarti and Daniel Ševčovič. The author is greatly indebted to all these colleagues for cooperation in numerical solution of geometrical nonlinear diffusion equations

*Department of Mathematics, Slovak University of Technology, Radlinského 11, 813 68 Bratislava, Slovak Republic, mikula@vox.svf.stuba.sk

and applications. He also thanks to organizers of the programme Computational Challenges in Partial Differential Equations, especially to Professor Charlie Elliott, for invitation to Isaac Newton Institute for Mathematical Sciences, University of Cambridge, where this work was finished.

1.1 Why nonlinear diffusion equations are used in image processing

In many applications computers analyse images or image sequences which are often contaminated by noise, and their quality can be poor (e.g. in medical imaging). Nonlinear partial differential equations (PDEs) can be used to automatically produce an image of higher quality, enhance its sharpness, filter out the noise, extract shapes, etc. From the mathematical point of view, the input processed image can be modelled by a real function $u^0(x)$, $u^0 : \Omega \to \mathbb{R}$, where $\Omega \subset \mathbb{R}^d$ represents a spatial domain. Typically Ω is rectangular and $d = 2$ or 3. In the case of an input image sequence $u^0(x, \theta)$, $u^0 : \Omega \times [0, T_A] \to \mathbb{R}$, it depends on the additional parameter θ representing a point in a real time interval of acquisition $[0, T_A]$.

Image processing operations involving PDEs are nonlinear image filtration, edge detection, deblurring and image enhancement, restoration, image inpainting, shape extraction and analysis, image segmentation, motion analysis, motion based filtering etc. [3, 5, 117, 133, 136, 30, 105, 120, 109]. Typical 2D examples are given by a large variety of medical images, satellite or camera system images, old archive documents, texts pre-processed for automatic reading, old corrupted photographs or any other digital images of poor quality. 3D examples arise in bioengineering, medicine or in material quality control, where 3D volumetric aquisition methods are widely used nowadays. The processing of image sequences can be found in the restoration of movies, video sequence analysis, visual recording of growth (of human organs, leaves of plants, etc.) or in improvement of the quality of medical image sequences. For example, the ultrasound acquisition of a beating heart in 3D echocardiography gives one interesting application.

The first step to use PDEs for image processing was done in the beginning of eighties [80, 140]. By the simple observation that the Gauss function

$$G_\sigma(x) = \frac{1}{(4\pi\sigma)^{d/2}} e^{-|x|^2/4\sigma} \tag{1.1}$$

is a fundamental solution of the linear heat (diffusion) equation, it has been possible to replace the classical image processing operation – convolution of an image with G_σ with a given variance $v = \sqrt{2\sigma}$ (Gaussian smoothing) – by solving the linear heat equation for a corresponding time $t = \sigma$ with initial condition given by the processed image. It is well known that Gaussian smoothing (linear diffusion) blurs edges in the images and moves their positions. Although such a phenomenon can cause no problems in some examples of data analysis, in image processing, where the visual impression is important and a precise localization of edges is also necessary (e.g. to compute volumes of segmented objects), the linear image smoothing is generally not the best choice. A way has been found to overcome these shortcomings, namely to switch to nonlinear diffusion models.

Due to the evolutionary character of the process which controls the processing using diffusion equations, application of any PDE to an initially given image is understood as its embedding in the so-called *scale space*. The Gaussian smoothing represents *linear scale space*. In the case of nonlinear PDEs one speaks about *nonlinear scale space*. The axioms and

fundamental properties of such embeddings have been summarized and studied by Alvarez, Guichard, P.L. Lions and Morel in [3, 5, 65], where the notion of *image multiscale analysis* has been introduced. The image multiscale analysis associates with a given image $u^0(x)$ a family $u(t,x)$ of smoothed-simplified images depending on an abstract parameter $t \in [0,T]$, the *scale*. As has been proved in [3], if such a family fulfills certain basic assumptions – pyramidal structure, regularity and local comparison principle – then $u(t,x)$, $u : [0,T] \times \Omega \to \mathbb{R}$, can be represented as the unique viscosity solution (in the sense of [34]) of a general second order (degenerate) parabolic partial differential equation. This theoretical result has also an important practical counterpart. The equations of (degenerate) parabolic type have a smoothing property, so they are a natural tool for filtering (image simplification) by removing spurious structures, e.g. noise. Moreover, the simplification should be "image oriented", e.g. it should respect edges and not blur them. Or, it should recognize motion of a structure in an image sequence, and consequently the smoothing (diffusion) should respect the motion coherence in consecutive frames. Such requirements, or even more sophisticated ones related to the geometrical characteristics of the image, bring strong nonlinearity into the parabolic PDEs, and make this field interesting not only because of the applications but also from a mathematical and numerical point of view.

1.2 Anisotropic diffusion of Perona-Malik type

Since the end of the 80s, the nonlinear diffusion equations have been used for processing of 2D and 3D images. After the pioneering work of Perona and Malik [114] who modified the linear heat equation to nonlinear diffusion preserving edge positions, there has been a great deal of interest in the application and analysis of such equations. At present, the following nonlinear PDE suggested by Catté, P.L.Lions, Morel and Coll [31] is widely used

$$u_t - \nabla.(g(|\nabla G_\sigma * u|)\nabla u) = 0, \tag{1.2}$$

where $u(t,x)$ is an unknown function defined in $Q_T \equiv [0,T]\times\Omega$. The equation is accompanied by zero Neumann boundary conditions and the initial condition

$$\frac{\partial u}{\partial n} = 0 \quad \text{on} \quad I \times \partial\Omega, \tag{1.3}$$

$$u(0,x) = u^0(x) \quad \text{in} \quad \Omega, \tag{1.4}$$

where n is the unit normal vector to the boundary of Ω. We assume that $\Omega \subset \mathbb{R}^d$ is a bounded rectangular domain, $I = [0,T]$ is a scaling interval,

$$g : \mathbb{R}_0^+ \to \mathbb{R}^+ \text{ is a nonincreasing function,} \quad g(\sqrt{s}) \text{ is smooth,} \tag{1.5}$$
$$g(0) = 1, \quad \text{and we admit } g(s) \to 0 \text{ for } s \to \infty,$$

$$G_\sigma \in C^\infty(\mathbb{R}^d) \text{ is a smoothing kernel (e.g. the Gauss function),} \tag{1.6}$$
$$\int_{\mathbb{R}^d} G_\sigma(x)\,dx = 1, \qquad \int_{\mathbb{R}^d} |\nabla G_\sigma|\,dx \le C_\sigma,$$
$$G_\sigma(x) \to \delta_x \text{ for } \sigma \to 0, \quad \delta_x \text{ is the Dirac measure at the point } x,$$

$$u^0 \in L_\infty(\Omega), \tag{1.7}$$

and

$$\nabla G_\sigma * u = \int_{\mathbb{R}^d} \nabla G_\sigma(x-\xi)\tilde{u}(\xi)\,d\xi, \tag{1.8}$$

where $\tilde{u}$ is an extension of u to $\mathbb{R}^d$. One can consider the extension of u by 0 outside Ω or the reflective periodic extension of the image [31].

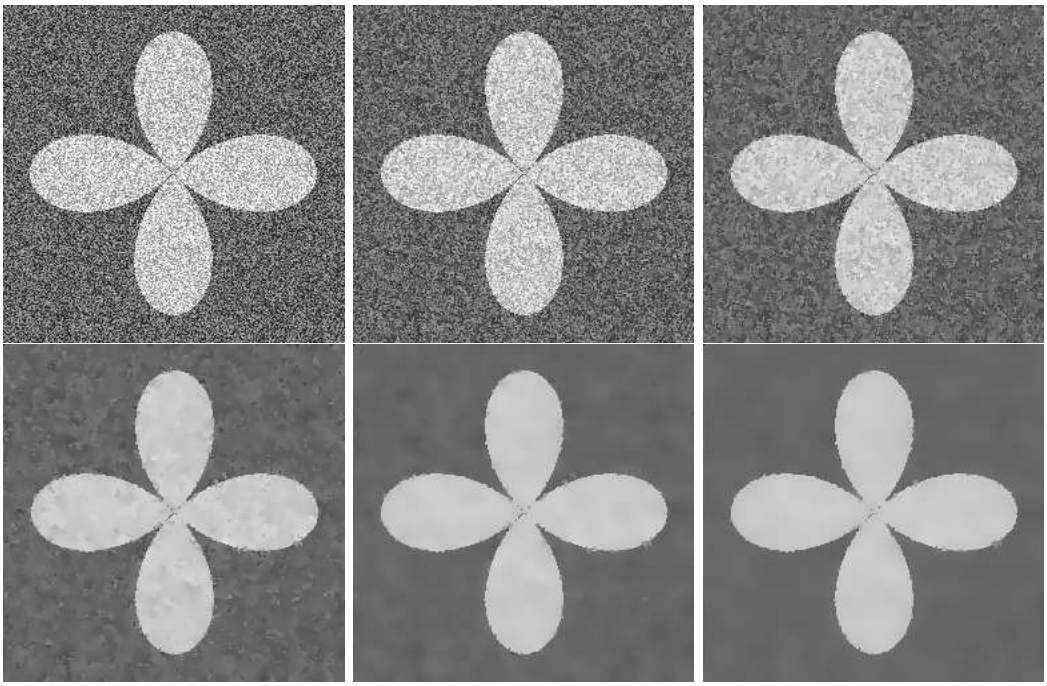

Figure 1: Smoothing of the noisy image keeping the edges using anisotropic diffusion. Shown are the 0th, 10th, 20th, 30th, 40th and 50th discrete steps of a semi-implicit finite volume algorithm [96].

The equation (1.2) represents a modification of the original Perona-Malik model [114, 106, 74]

$$u_t - \nabla.(g(|\nabla u|)\nabla u) = 0, \tag{1.9}$$

called also *anisotropic diffusion* in the computer vision community. Perona and Malik introduced (1.9) in the context of edge enhancement. The equation selectively diffuses the image in the regions where the signal has small variance in intensity in contrast with those regions where the signal changes its tendency. Such a diffusion process is governed by the shape of the diffusion coefficient given by the function g in (1.5) and by its dependence on ∇u, which is understood as an edge indicator [114]. Since $g \to 0$ for large gradients, the diffusion is strongly slowed down on edges, while outside them it provides averaging of pixel intensities as in the linear case. From a mathematical point of view, for practical choices of g (e.g. $g(s) = 1/(1+s^2)$, $g(s) = e^{-s^2}$), the original Perona-Malik equation can behave locally like the backward heat equation. It is, in general, an ill-posed problem which suffers from

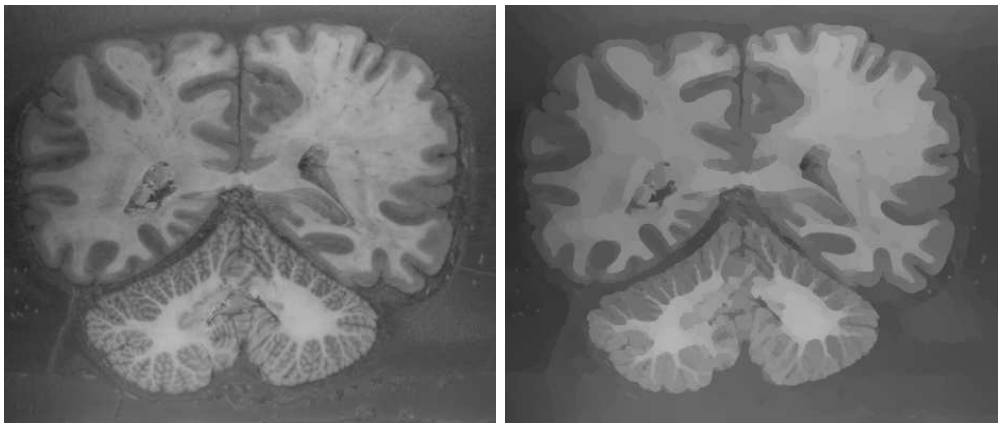

Figure 2: Initial image (left); result after 20 steps of regularized Perona-Malik filtering (right) using semi-implicit complementary volume discretization [60].

non-uniqueness and whose solvability is a difficult problem [74]. One way to overcome this disadvantage has been proposed by Catté, P.L.Lions, Morel and Coll in [31]. They introduced the convolution with the Gaussian kernel G_σ into the decision process for the value of the diffusion coefficient. Since convolution with the Gaussian is equivalent to linear diffusion, their model combines ideas of linear and nonlinear scale space equations. Such a slight modification made it possible to prove the existence and uniqueness of solutions for the modified equation, and to keep the practical advantages of the original formulation. Moreover, usage of the *Gaussian gradient* $\nabla G_\sigma * u$ combines the theoretical and implementation aspects of the model. The convolution (with prescribed σ) gives a unique way to compute gradients of a piecewise constant image. It also bounds (depending on σ) the gradient of the solution as input of the function g in the continuous model – which corresponds to the situation in numerical implementations where gradients evaluated on a discrete grid are finite. Also, the local edge enhancement is more understandable in the presence of noise.

We illustrate behaviour of the regularized Perona-Malik equation (1.2) in three examples. First, the artificial image (Fig. 1, 256×256 pixels) with additive noise is processed by our finite volume scheme [96]; then nonlinear multiscale analysis of the medical image (Fig. 2, 463×397 pixels) computed by the co-volume discretization [60] is given; and finally, there is an application of the 3D adaptive finite element method [70, 16, 17] to 3D echocardiographic image of one moment of the cardiac cycle with the left ventricle in open phase. In Fig. 3, one can see a visualization of the isosurface representing the boundary between blood and muscle forming an edge in 3D image intensity.

1.3 Slow and fast degenerate diffusion added to Perona-Malik equation

The following generalization of the Perona-Malik equation has been introduced by Kačur and Mikula [71, 72]:

$$\partial_t b(x,u) - \nabla.(g(|\nabla G_\sigma * \beta(x,u)|)\nabla\beta(x,u)) = f(u^0 - u). \tag{1.10}$$

The functions b and β represent new nonlinearities which make the image multiscale analysis locally dependent on values of the intensity function u and on the position in the image x.

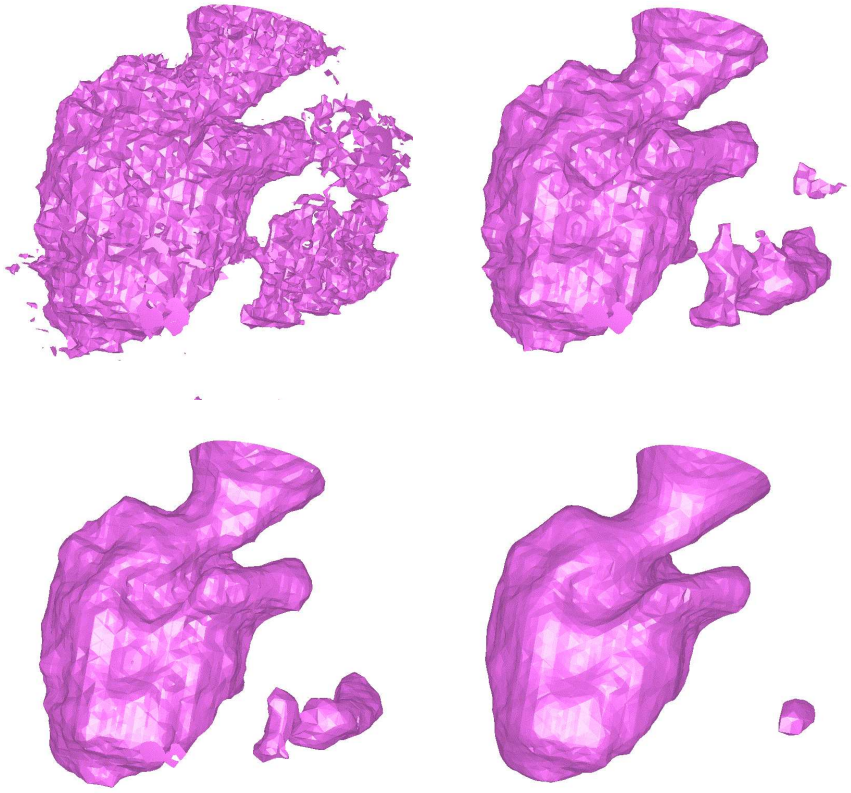

Figure 3: Smoothing of the human left ventricle by anisotropic diffusion. We visualize corresponding level surfaces in the 0th, 2nd, 4th and 8th discrete steps of the semi-implicit adaptive finite element algorithm [17].

Such a generalization is useful in any situation where properties of the image or requirements to the image processing operation can be expressed in dependence on x and u. For example, if a different speed of the diffusion process is desirable in different parts of the image or for different ranges of the intensity function, then equation (1.10) can be used. In the points, where the derivative β'_u is small (b'_u is large), the diffusion process is slowed down, while where β'_u is large (b'_u is small) the diffusion process is speeded up. Degenerate cases from the point of view of the theory of parabolic PDEs, when either β'_u or b'_u is equal 0 or ∞, can also be included. The degenerate cases can be interpreted as total stopping of diffusion, or as diffusion with the infinite speed in some image regions. Applying the regularized anisotropic diffusion (1.2) improves some set of edges. On the other hand, it destroys details which are under the edge threshold (given by g) or undistinguished from the noise at some scale. If such details are contained in certain ranges of greylevels, then they can be conserved by a special choice of the function β or b. As a demonstration we present Fig. 4. In that image, the colors of Flora's face are demaged only. We present the reconstruction of the original (left image) by anisotropic diffusion accompanied with the *slow diffusion effect* (image on the right). Using the proper choice of β (b is linear), which is constant for darker (lower) greylevels and linear for

the upper range of u, the face is selectively smoothed and the details around it are conserved. For the existence of the solution to (1.10) and numerical algorithm which converges to this solution we refer to [72]. The right-hand side of (1.10) with nondecreasing function f can be used to force the solution to be close to original u^0 [108]. The Lipschitz continuous f causes no important difference in numerical analysis compared to the zero right-hand side [70, 72, 96].

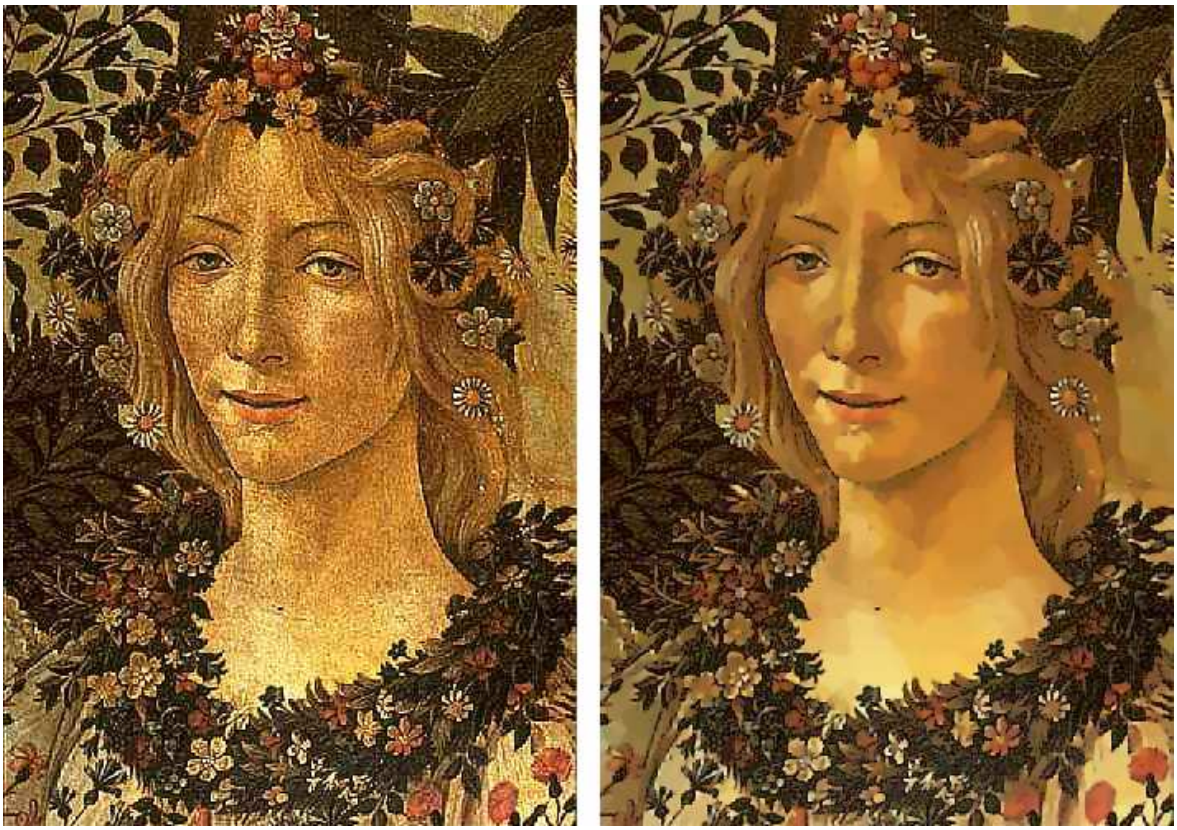

Figure 4: Processing of a color image using slowed anisotropic diffusion [72].

1.4 Structural tensor based anisotropic diffusion

Weickert (see e.g. [136, 137, 138]) introduced a generalization of the Perona-Malik equation of the form

$$u_t - \nabla.(D\nabla u) = 0 \tag{1.11}$$

where D is a matrix depending on the eigenvalues and eigenvectors of a regularization of the so-called *structure tensor* $\nabla u(\nabla u)^T$. The dependence is such that diffusion strongly prefers direction of line structures in the image. That idea has also been used by Preusser and Rumpf in multiscale flow field visualization in computational fluid dynamics [115, 40].

Figure 5: In the top: red, green, and blue channels before smoothing (from left to the right). In the bottom: red, green, and blue channels (from left to the right) after 8 steps of the synchronized smoothing model (1.12). In the middle: composition of smoothed channels.

1.5 Diffusion systems and color image processing

There exist generalizations of the basic equations from the previous Sections to the processing of color images. An RGB image can be viewed as a composition of three greyscale images (channels) representing the levels of intensity for red, green and blue colors. Then it is natural to consider a Perona-Malik-type system of equations adapted to the RGB image. The image in Fig. 4 was processed using independent diffusion processes (1.10) for each channel. It gives good result, but certainly a better idea is not to apply the Perona-Malik-like anisotropic diffusion to each channel independently, but to synchronize the diffusion by computing a common diffusion coefficient depending on the information coming from all three colors. In [139, 138, 81], dealing with color images and vector valued diffusion, the following

system of nonlinear partial differential equations has been considered:

$$\partial_t u_i - \nabla.(g(\sum_{j=1}^{3} |\nabla G_\sigma * u_j|^2)\nabla u_i) = 0, \quad i = 1, 2, 3. \tag{1.12}$$

The equations are accompanied by initial and zero Neumann boundary conditions for each color. In the case (1.12) the edges of a highly destroyed channel can be recovered by information coming from the remaining channels [81]. The experiment documented in Fig. 5 was performed on the RGB image of the size 512×402 pixels. The picture is a result of scanning and has a significantly damaged blue channel (top of Fig. 5). The Fig. 5 shows, that with help of red and green channels, which are of much better quality, the synchronized smoothing (1.12) recovered the blue channel to the form shown in the bottom of the Fig. 5, on the right.

1.6 Space-time filtering of image sequences

A given 3D space-time image sequence (e.g. in 3D echocardiography) $u^0(x, \theta)$ is a special 4D image where a motion coherence of subsequent frames is present. Usually, the aim is to extract relevant motion information from the sequence, filter out the noise, and enhance moving structures. To that end, it seems reasonable to use additional information (in comparison with still image processing) given by the motion correspondence in the image sequence.

We can assume that certain objects acquired at different times, and thus being in different frames of the sequence, are formed by points that preserve their intensity along the motion trajectory. Such objects are called *Lambertian structures*. Moreover, we assume that *motion is smooth* in time, and thus the motion trajectories are close to straight lines locally. Designing the model we consider the following quantity [3, 5] proposed by Guichard [53]:

$$\begin{aligned} clt_u(t, x, \theta) = \min_{w_1, w_2} \frac{1}{(\Delta\theta)^2} (&\Delta\theta \; |\langle \nabla u(t, x, \theta), w_1 - w_2 \rangle| \\ &+ |u(t, x - w_1, \theta - \Delta\theta) - u(t, x, \theta)| \\ &+ |u(t, x + w_2, \theta + \Delta\theta) - u(t, x, \theta)|) \end{aligned} \tag{1.13}$$

where w_1, w_2 are arbitrary vectors in $\mathbb{R}^N$ and $\Delta\theta$ is a time increment. The scalar function clt_u will introduce a measure of coherence in time for the moving structures. It consists of the sum of three positive parts and we want to find the minimum in all possible directions w_1, w_2. The last two terms in the sum on the right-hand side of (1.13) are related to the differences in the intensities of end-points of the candidate Lambertian velocity vectors w_1, w_2. To find the directions of such vectors, we look at the points whose intensity value is closest to the intensity $u(t, x, \theta)$ in the previous frame (term $|u(t, x - w_1, \theta - \Delta\theta) - u(t, x, \theta)|$) and in the next frame (term $|u(t, x + w_2, \theta + \Delta\theta) - u(t, x, \theta)|$). Those differences are scaled by the factor $1/(\Delta\theta)^2$. Note that if we find corresponding Lambertian points, then both terms vanish. The first term in the sum, namely $|\langle \nabla u(t, x, \theta), w_1 - w_2 \rangle|/(\Delta\theta)$, corresponds to the so-called *apparent acceleration*, i.e. to the difference between the candidate Lambertian velocity vectors w_1 and w_2 in the direction of ∇u. For details and some more background from the *optic flow* point of view we refer to [3, 5, 53]. The quantity clt_u is thus related to the curvature of the space-time level curve passing through the space-time point (x, θ) in the scale t (curvature of the Lambertian trajectory). The value of clt_u vanishes for the Lambertian points that are

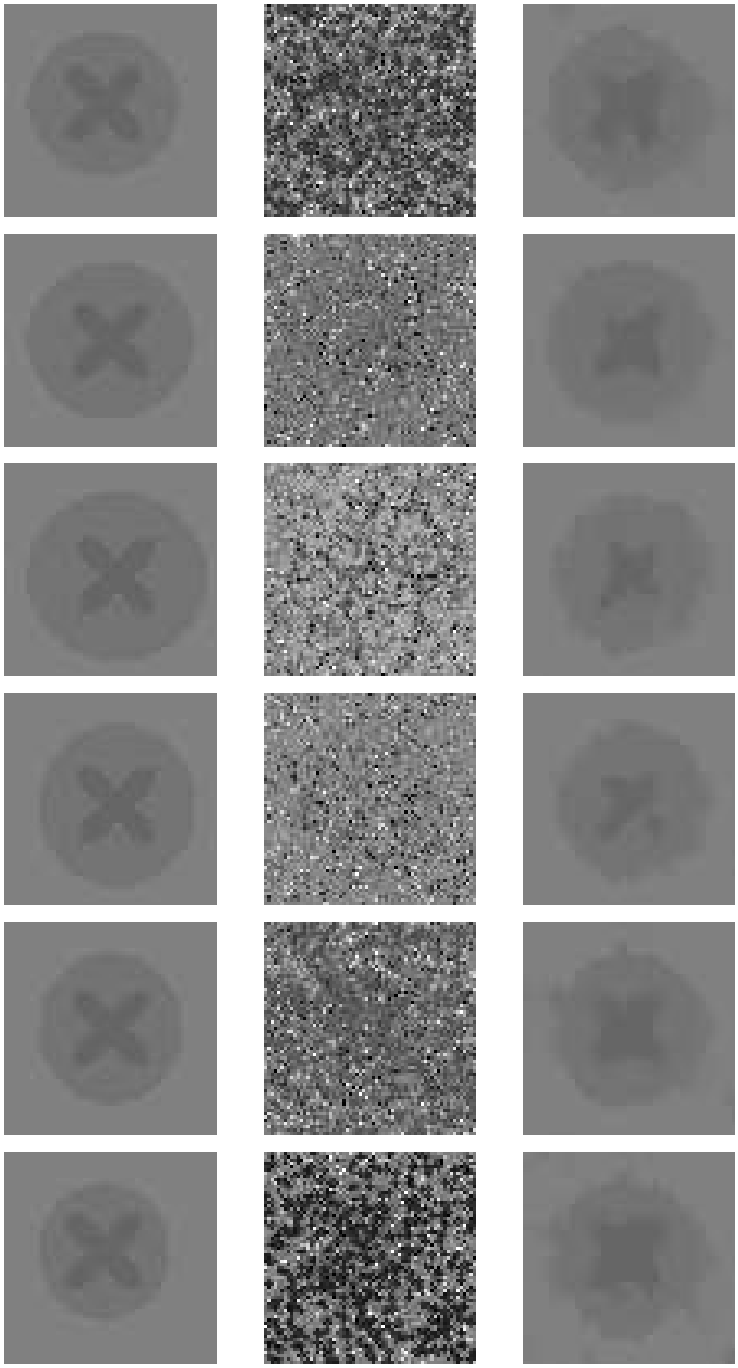

Figure 6: 2D phantom image sequence - original (left), noisy (middle) and processed (right) images by the equation (1.14) [126].

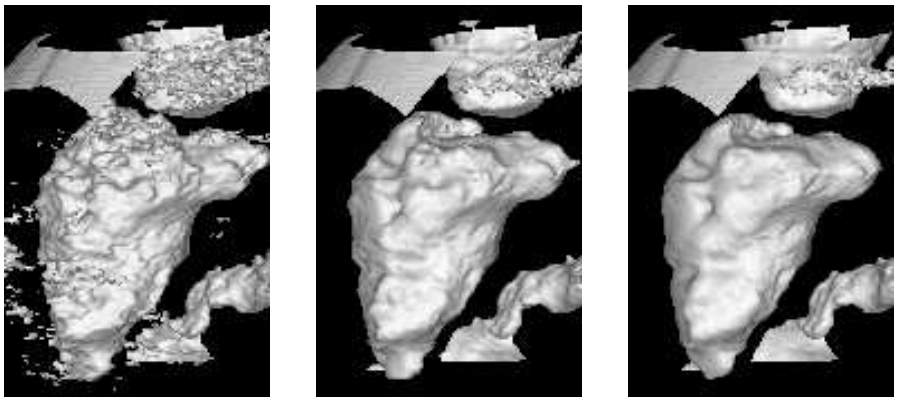

Figure 7: The multiscale analysis of the 1st frame of a 3D-echocardiographic image sequence by the equation (1.14) [125].

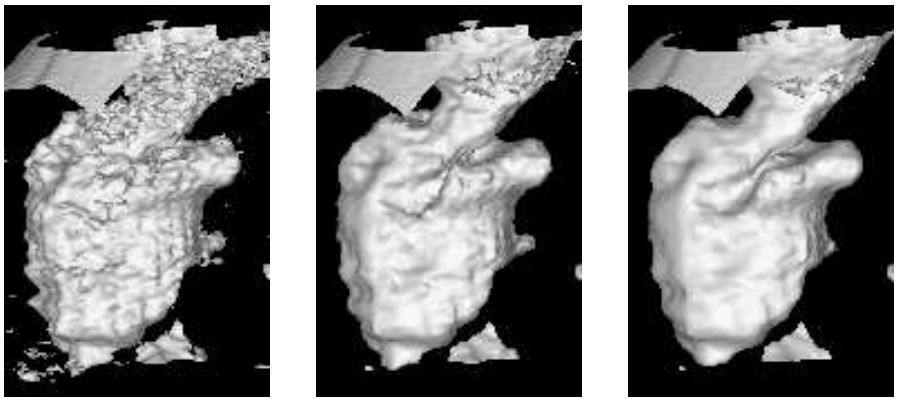

Figure 8: The multiscale analysis of the 7th frame of a 3D-echocardiographic image sequence by the equation (1.14) [125].

in uniform motion. This is consistent with the purpose not to alter such trajectories. On the other hand, for the noisy points there is no motion coherence and thus clt_u will be large there.

Concerning the space coherence, we assume that distinguished structures are located in the regions with a certain mean value of the image intensity, and that the object boundary forms an edge in the image. In order to construct a spatial diffusion process we thus require specific behavior on the edges as in the Perona-Malik anisotropic diffusion equation.

To combine time coherence of moving objects with their spatial localization we consider the following equation for the processing of image sequences [125]:

$$u_t = clt_u \nabla.(g(|\nabla G_\sigma * u|)\nabla u). \tag{1.14}$$

As an application, we are dealing with a phantom-like image sequence consisting of expanding, slightly deforming and moving ellipses with the inner structure in the form of quatrefoils. We add impulsive (salt & pepper), Gaussian noise and blurring to the frames of the image sequence. The original six-frame sequence and its destroyed version are shown in the first two columns of Fig. 6. The reconstruction of any noisy frame of this sequence by a

standard (still image) filtering algorithm is very difficult task (by our experience impossible). The right-hand column of Fig. 6 represents the results of (1.14) applied to the noisy sequence after 10 discrete scale steps of the numerical implementation from [125].

Next we have applied the method to 3D echocardiographic sequence. In Figs. 7–8 the iso-surfaces corresponding to the blood-muscle interface have been visualized. Figs. 7–8 consist of three sub-figures. For each row, on the left we show the echo-volume visualized using the original noisy data, in the middle the result after three discrete scale steps, and on the right after nine discrete scale steps of the model (1.14). Some further experiments (also in parallel implementation) and more detailed discussion can be found in [125, 92, 126, 127].

1.7 The curvature-driven nonlinear diffusion equations

In rather general situations, edges corresponds to specific level lines (level surfaces in 3D) of the image intensity function [23]. For example, as one can see in Fig. 9, the edge representing the blood-cardiac muscle interface corresponds also to an isosurface of the greylevel image intensity function. In the three subfigures, the corresponding isolines are visible in 2D cutting slices. The isoline gives a curve in 2D plane representing the boundary of the left ventricle in the slice. If one would like to smooth it in order to remove the large acquisition errors, one way how to proceed is to move the curve (surface in 3D) in the direction of its inner normal with the velocity proportional to its (mean) curvature. The motion of convex and concave pieces is opposite due to the sign of the curvature, and the large fingers shrink much faster than the smoother parts, due to the curvature dependence of the flow. This motion by (mean) curvature is governed by heat equation (Gaussian smoothing), but applied in the intrinsic curve (surface) geometry. In Fig. 10 we present the smoothing effect of such *geometrical diffusion* [91, 97]. On the left, the cuttings of unfiltered iso-surfaces are plotted, on the right the filtered ones (all after binarization with the same treshold). We can see an immediate extinction of small structures (noise) due to their high curvature, and a smoothing of the larger structures in the image. Recently, Perona-Malik-like effects have been included into geometrical diffusion models by Preusser and Rumpf [116] which allow smoothing of the image level lines (surfaces) together with enhancing of their edges and corners. Geometrical diffusion models based on representation of a color image as a hypersurface in 3D space which is then moved by mean curvature motion are used for processing of color images, too (e.g. [77]). An image sequence analysis based on anisotropic geometrical diffusion in space and time which, in spite of the previous Section, is capable to take into account highly accelerated motions in motion based filtering, has been suggested by Mikula, Preusser and Rumpf ([94], see also [95]).

The level lines (level surfaces) of the image intensity function correspond to plane curves (hypersurfaces in 3D) and, in geometrical diffusion models, the smoothing corresponds to their properly designed motion. Since usually objects which are of particular interest are contained inside the image, without lost of generality (in 3D case it is similar), we may restrict attention to evolutions of closed plane curves $\Gamma_t = \mathrm{Image}(x(p,t))$, where $x : \mathbb{R} \times [0, T_{max}) \to \mathbb{R}^2$ is a C^2 vector function, periodic in the first argument with a period given by the range of a curve parametrization p. The motion is driven by the normal velocity v which is assumed to be a function of the curvature k, tangential angle ν and position vector $x \in \Gamma_t$:

$$v = \beta(x, k, \nu)\,. \tag{1.15}$$

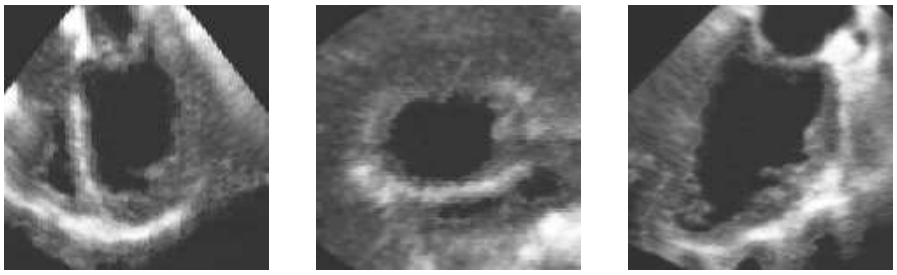

Figure 9: 2D orthogonal slices crossing in the centre of the 3D echocardiographic cube with the image of the human left ventricle.

The experiment presented in Fig. 10 corrresponds to the simple linear curve shortening flow (linear intrinsic diffusion) equation $\beta(x,k,\nu) = k$ (see e.g. [49, 52, 1, 45, 6, 8, 9, 10]) Let us note that geometric equations of the form (1.15) can be found not only in image processing but in a large variety of applied problems like e.g. multiphase fluid dynamics, material science, dynamics of phase boundaries in thermomechanics, modelling of flame front propagation in combustion, computational geometry, robotics, semiconductors industry, etc. For an overview of important applications of (1.15) we refer to a recent books by Sethian [133], Sapiro [120] and Osher and Fedkiw [109]. They have not only the practical application in image filtering but also special conceptual importance in computer vision. Namely, *affine invariant scale space* which is a generalization of the linear intrinsic diffusion (curve shortening flow) is given by equation (1.15) provided $\beta(x,k,\nu) = k^{1/3}$ [3, 121, 122, 123, 124, 14].

There exists a mathematical theory for evolving curve and surface problems [46, 33]; also, numerical methods are available and in further development. From the computational point of view there are two main approaches for solving curve or surface evolution. In the so-called *Lagrangian (or direct) approach*, the curve, respectively surface, itself is discretized and moved. In spite of that, the so-called *Eulerian (or level-set) approach* implicitly handles the motion by passing the problem to a higher dimensional space and solving there the evolution equation for a graph whose evolving level sets correspond to the evolving curve or surface. So one looks for the function $u : \mathbb{R}^2 \times \mathbb{R}_0^+ \to \mathbb{R}$, for which the moving curve x is the same level line at each time moment t, i.e.

$$u(x(t),t) = c \tag{1.16}$$

for every $t \in I = [0, T_{max})$ and certain $c \in \mathbb{R}$. As initial datum for u one can consider e.g. the so-called signed distance function [133, 109] given by

$$u(x,0) = \pm d(x), \tag{1.17}$$

where $d(x)$ is distance from the point x to the initial curve Γ_0 and the plus (minus) sign is chosen if the point x is outside (inside) the initial curve Γ_0. Differentiating (1.16) in time one gets

$$\nabla u . \frac{\partial x}{\partial t} + \frac{\partial u}{\partial t} = 0. \tag{1.18}$$

Since only normal component of velocity influences image of the evolution (see e.g. [14]) by

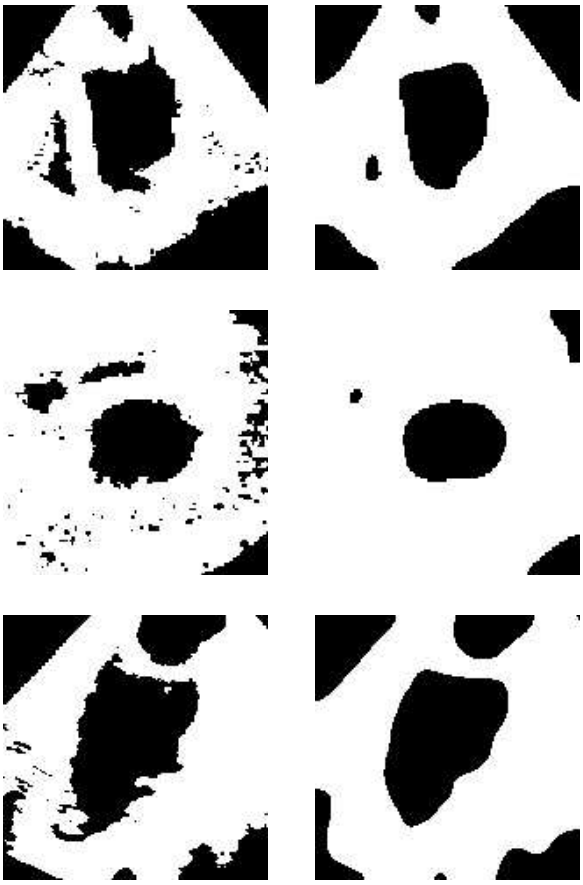

Figure 10: 2D cuts of the result of 3D processing by geometrical diffusion of mean curvature flow type.

(1.15) we get

$$\frac{\partial x}{\partial t} = \beta \vec{N} \tag{1.19}$$

where

$$\vec{N} = \frac{\nabla u}{|\nabla u|} \tag{1.20}$$

is the outer normal vector to the level line of u. Using (1.19) and (1.20) in (1.18) we obtain the Hamilton-Jacobi partial differential equation

$$\frac{\partial u}{\partial t} + \beta |\nabla u| = 0 \tag{1.21}$$

for the unknown function u. This equation is a basis for construction of the Osher-Sethian numerical *level set method* ([110], [131]). Due to the relation

$$k = -\nabla . \left(\frac{\nabla u}{|\nabla u|} \right)$$

which holds for the curvature k of the level line of u passing through point x, we get, provided $\beta(x, k, \nu) = k$, the well-known *level set equation*

$$u_t = |\nabla u| \nabla . \left(\frac{\nabla u}{|\nabla u|} \right) \tag{1.22}$$

for curvature-driven motion. As noticed in the beginning of the Section, it is well suited for image processing applications, since it smoothes intrinsically any level set and moreover the smoothing is done at once for all level sets. It also fulfills the so-called *morphological principle*: if u is a solution then, for any nondecreasing function φ, $\varphi(u)$ is a solution as well. This *contrast invariant* property has large significance in the axiomatic theory of the image processing and computer vision [3]. It also means that level sets move independently of each other; they diffuse only intrinsically, there is no diffusion across them in the normal direction. The level set equation (1.22) provides a directional smoothing of the image along its level lines and contains implicitly the idea of Weickert's directional diffusion (see Section 1.4) if we think about level lines instead of edges. Such an idea was used by Alvarez, P.L.Lions and Morel in [4], where the equation

$$u_t = g(|\nabla G_\sigma * u|) |\nabla u| \nabla . \left(\frac{\nabla u}{|\nabla u|} \right) \tag{1.23}$$

has been suggested for computational image and shape analysis. It is accompanied by the same boundary and initial conditions (1.3)–(1.4) as in the case (1.2). Equation (1.23) can be used for image silhouettes smoothing ($g \equiv 1$, see e.g. [3, 5, 91, 97]), or it can be used for edge-preserving smoothing in a similar way as equation (1.2). The Perona-Malik function $g(s)$ depending on $|\nabla G_\sigma * u|$ is used to strongly slow down the motion of silhouettes which are at the same time edges. The regions between them are smoothed by the mean curvature flow.

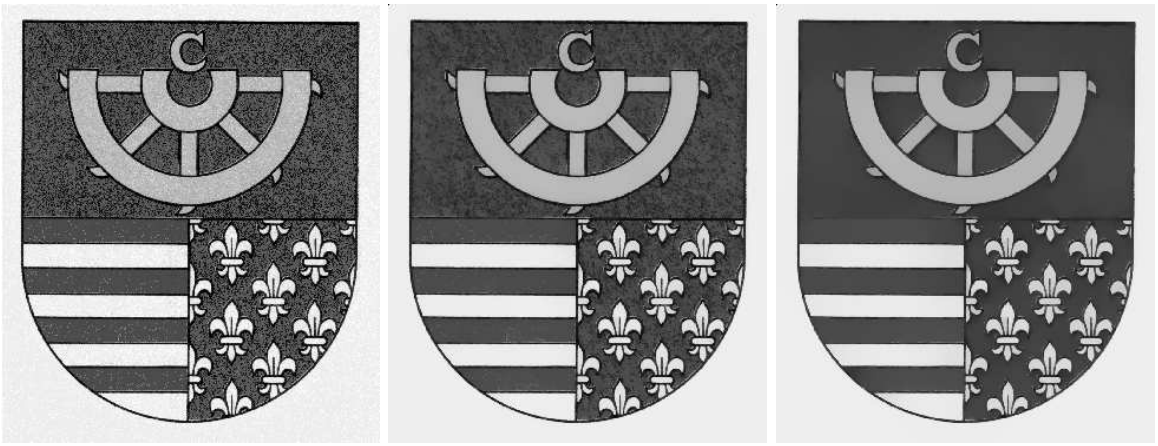

Figure 11: Initial image (left); result of smoothing after 5 (middle) and 10 (right) scale steps using equation (1.23) and co-volume discretization [59].

In Fig. 11 we smooth an initial 321×373 pixel image (ancient coat-of-arms of the Slovak town Kremnica shown on the left), scanned from a book with neither paper nor colors of good quality. Also shown are the results after 5 and 10 discrete scale steps of the co-volume

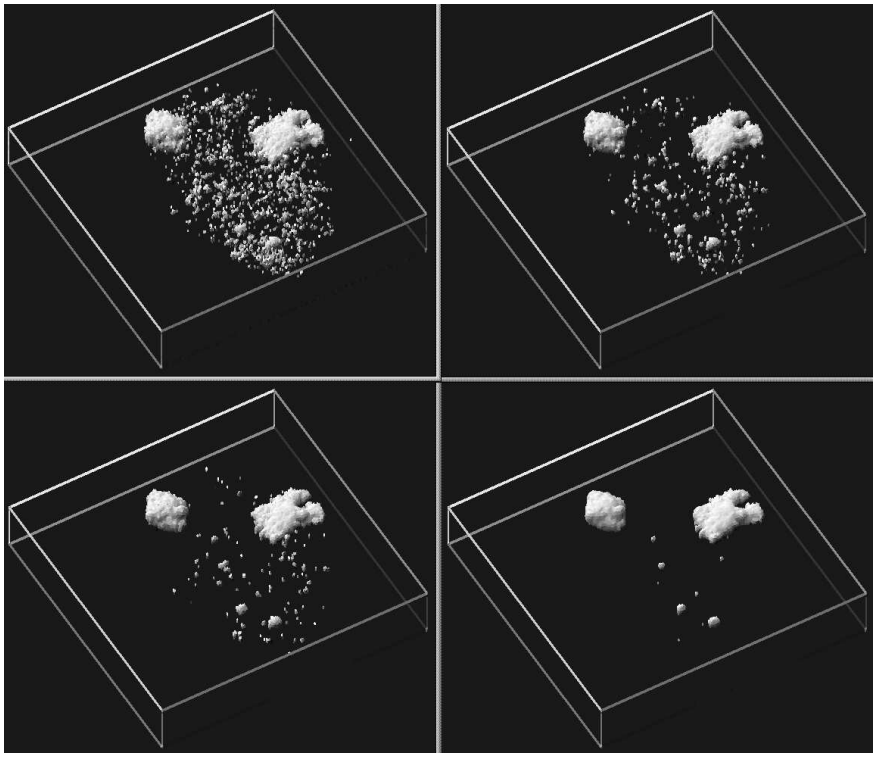

Figure 12: Extraction of two chromosomes in a human cell using geometrical diffusion (1.23) [58].

scheme [59] for equation (1.23) with $g(s) = 1/(1+s^2)$. We also present Fig. 12, where two chromosomes are extracted from an initial noisy 3D image of a human cell by image selective smoothing (1.23) with the same g.

To end of this Section, let us mention a general useful use of viewing gradient-dependent nonlinear diffusion equations. The nonlinear diffusion term $\nabla.(g(|\nabla u|)\nabla u)$ can be rewritten in 2D as

$$\nabla.(g(|\nabla u|)\nabla u) = g(|\nabla u|)u_{\xi\xi} + H'(|\nabla u|)u_{\eta\eta},$$

where $H(s) = sg(s)$ and ξ, η are tangential and orthogonal vectors to the level line, respectively. From this form one can clearly see how diffusion works along and across the image silhouettes with different choices of g. There is always positive, but possibly strongly slowed-down (depending on the shape of g) diffusion *along* level lines. *Across* level lines there can be forward diffusion (when $H'(s)$ is positive), zero diffusion (e.g. in the Rudin-Osher-Fatemi model [118, 111] dealing with total variation denoising, and also in the mean curvature flow equation in the level set formulation, where $g(s) = 1/s$), or backward diffusion (in the original Perona-Malik model [114] where $g(s) = 1/(1+s^2)$).

1.8 Interface dynamics in phase transition

If a solid phase occupies a subset $\Omega_s(t) \subset \Omega$ and a liquid phase - a subset $\Omega_l(t) \subset \Omega$, $\Omega \subset \mathbb{R}^2$, at a time t, then the phase interface is the set $\Gamma_t = \partial\Omega_s(t) \cap \partial\Omega_l(t)$ which is assumed to be a

closed smooth embedded curve. The sharp-interface description of the solidification process is then described by the Stefan problem with a surface tension

$$\begin{aligned} \rho c \partial_t U &= \lambda \Delta U \qquad \text{in } \Omega_s(t) \text{ and } \Omega_l(t), && (1.24)\\ [\lambda \partial_{\nu^\perp} U]_s^l &= -Lv \qquad \text{on } \Gamma_t, && (1.25)\\ \frac{\delta e}{\sigma}(U - U^*) &= -\gamma_2(\nu)k + \gamma_1(\nu)v \text{ on } \Gamma_t, && (1.26) \end{aligned}$$

subject to initial and boundary conditions for the temperature field U and initial position of the interface Γ (see e.g. [19, 21, 128, 129]). The constants ρ, c, λ represent material characteristics (density, specific heat and thermal conductivity), L is the latent heat per unit volume, U^* is a melting point and v is normal velocity of the interface. Discontinuity in the heat flux on the interface Γ_t is described by the Stefan condition (1.25). The relationship (1.26) is referred to as the Gibbs – Thomson law on the interface Γ_t, where δe is difference in entropy per unit volume between liquid and solid phases, σ is a constant surface tension, γ_1 is a coefficient of attachment kinetics and dimensionless function γ_2 describes anisotropy of the interface. One can see that the Gibbs – Thomson condition can be viewed as a geometric equation having the form (1.15). Let us note that solution of (1.26) is an important part of the solution and in general it is connected to (1.24)–(1.25) by the term on the left side of (1.26). Such coupling allows computer simulations of complex physical phenomena, e.g. the dendrite growth in solidification process presented by Bänsch and Schmidt [128, 129, 18].

In the series of papers [11, 12, 13], see also [54], Angenent and Gurtin studied perfect conductors where the problem can be reduced to a single equation on the interface. Following their approach and assuming a constant kinetic coefficient one obtains the equation

$$v = \beta(x, k, \nu) \equiv \gamma(\nu)k + F$$

describing the interface dynamics. It is often referred to as the *anisotropic curve shortening equation* with a constant driving force F (energy difference between bulk phases) and a given anisotropy function γ.

1.9 Geodesic curvature driven flow and image segmentation

Let us now consider a flow of curves on a two dimensional surface $\mathcal{M}$ in $\mathbb{R}^3$. The surface $\mathcal{M} = \{(x, \phi(x)) \in \mathbb{R}^3,\ x \in \Omega\}$ is assumed to be represented by a graph of a smooth function $\phi : \Omega \subset \mathbb{R}^2 \to \mathbb{R}$ defined in a domain $\Omega \subset \mathbb{R}^2$. We assume the simplest possible case in which the normal velocity $\mathcal{V}$ of a curve $\mathcal{G}$ on $\mathcal{M}$ is a linear function of its geodesic curvature $\mathcal{K}_g$ and external force [101, 103]

$$\mathcal{V} = \mathcal{K}_g + \mathcal{F} \tag{1.27}$$

where $\mathcal{F}$ is the normal component of a given external force $\vec{G}$, i.e. $\mathcal{F} = \vec{G}.\vec{\mathcal{N}}$ and $\vec{\mathcal{N}}$ is the unit normal vector to $\mathcal{G}$ belonging to the tangent space $T_x(\mathcal{M})$.

Hereafter, we will frequently use the abbreviation (x, z) standing for a vector $(x_1, x_2, z) \in \mathbb{R}^3$ where $x = (x_1, x_2) \in \mathbb{R}^2$. Any smooth closed curve $\mathcal{G}$ on the surface $\mathcal{M}$ can be then represented by its vertical projection to Ω, i.e.

$$\mathcal{G} = \{(x, \phi(x)) \in \mathbb{R}^3,\ x \in \Gamma\}$$

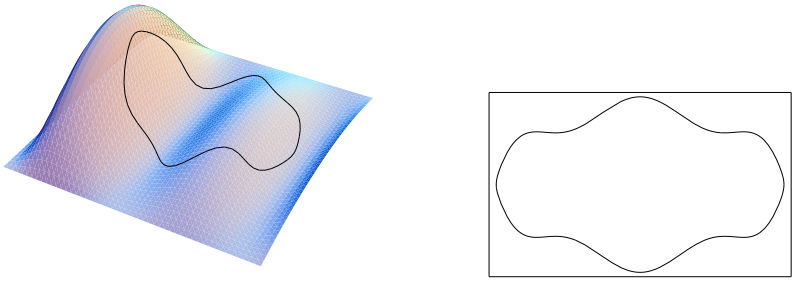

Figure 13: A surface curve $\mathcal{G}$ (left) and its projection Γ to the plane $\mathbb{R}^2$ (right).

where Γ is a planar curve in $\Omega \subset \mathbb{R}^2$ (see Fig. 13).

It is possible to derive a geometric equation for evolution of the family of planar curves $\Gamma_t, t \geq 0$, provided that the flow $\mathcal{G}_t, t \geq 0$, of surface curves satisfies (1.27) [101, 103]. For that goal, we have to find how the normal velocity v of Γ_t depends on geometric quantities corresponding to Γ_t. Straightforward calculations enables us to conclude that the unit inward normal and tangent vectors $\vec{\mathcal{N}}, \vec{\mathcal{T}} \in T_x(\mathcal{M})$ to a surface curve $\mathcal{G} \subset \mathcal{M}$ relative to $\mathcal{M}$ are given by

$$\vec{\mathcal{T}} = \frac{\left(\vec{T},\ \nabla\phi.\vec{T}\right)}{\left(1+(\nabla\phi.\vec{T})^2\right)^{\frac{1}{2}}},$$

$$\vec{\mathcal{N}} = \frac{\left((1+(\nabla\phi.\vec{T})^2)\vec{N} - (\nabla\phi.\vec{T})(\nabla\phi.\vec{N})\vec{T},\ \nabla\phi.\vec{N}\right)}{\left((1+|\nabla\phi|^2)(1+(\nabla\phi.\vec{T})^2)\right)^{\frac{1}{2}}}.$$

For a curve $\mathcal{G} = \{(x, \phi(x)) \in \mathbb{R}^3,\ x \in \Gamma\}$ on a surface $\mathcal{M} = \{(x_1, x_2, \phi(x_1, x_2)) \in \mathbb{R}^3,\ (x_1, x_2) \in \Omega\}$ the geodesic curvature $\mathcal{K}_g$ is given by

$$\begin{aligned}\mathcal{K}_g \ = \ & -\sqrt{EG-F^2}\Big(x_1''x_2' - x_1'x_2'' - \Gamma_{11}^2 x_1'^3 + \Gamma_{22}^1 x_2'^3 \\ & -(2\Gamma_{12}^2 - \Gamma_{11}^1)x_1'^2 x_2' + (2\Gamma_{12}^1 - \Gamma_{22}^2)x_1' x_2'^2\Big)\end{aligned}$$

where E, G, F are coefficients of the first fundamental form and Γ_{ij}^k are Christoffel symbols of the second kind. Here $(.)'$ denotes the derivative with respect to the unit speed parametrization of a curve on a surface. Taking into account that the surface $\mathcal{M}$ is a graph of a smooth function ϕ we obtain, after some calculations, that

$$\mathcal{K}_g = \frac{\left(1+|\nabla\phi|^2\right)^{\frac{1}{2}}\ k + \frac{\vec{T}^T\nabla^2\phi\vec{T}}{(1+|\nabla\phi|^2)^{\frac{1}{2}}}\nabla\phi.\vec{N}}{\left(1+(\nabla\phi.\vec{T})^2\right)^{\frac{3}{2}}} \tag{1.28}$$

where $k, \vec{T}, \vec{N}$ are the curvature, unit tangent and inward normal vector of a plane curve $\Gamma \subset \Omega$. The external vector field $\vec{G}$ is assumed to be perpendicular to the plane $\mathbb{R}^2$ and it depends on the vertical coordinate $z = \phi(x)$ only. As a typical example one can consider gravitational like external force

$$\vec{G}(x) = -(0, 0, \bar{\gamma}) .$$

where $\bar{\gamma} = \bar{\gamma}(z) = \bar{\gamma}(\phi(x))$ is a given scalar "gravity" functional. Taking the normal component of such an external force we obtain expression for the driving term $\mathcal{F} = \vec{G}.\vec{\mathcal{N}}$ in the form

$$\mathcal{F} = -\frac{\bar{\gamma}(\phi(x))}{\left((1 + |\nabla\phi|^2)(1 + (\nabla\phi.\vec{T})^2)\right)^{\frac{1}{2}}} \nabla\phi.\vec{N} . \tag{1.29}$$

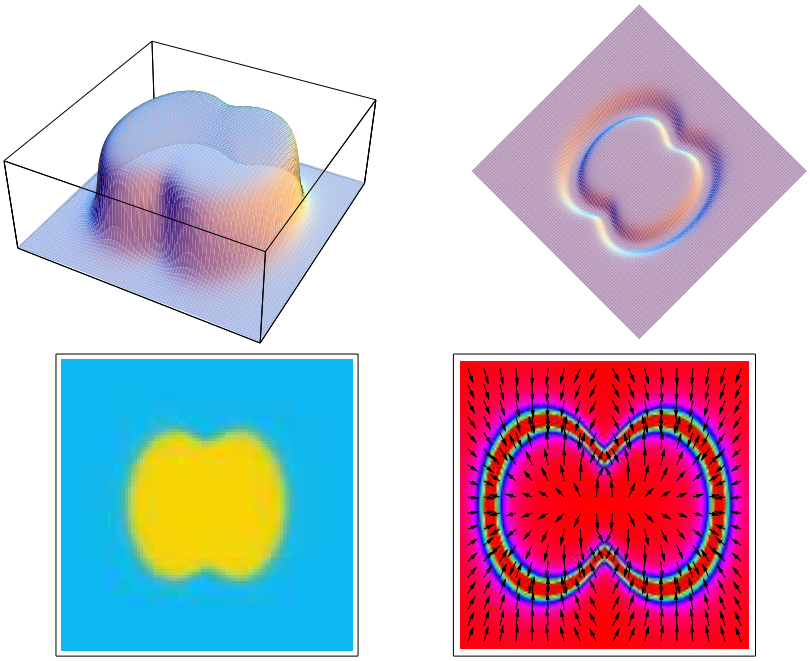

Figure 14: An image intensity function $I(x)$ (left-top) corresponding to a "dumb-bell" image (left-bottom). The plot of function $\phi(x) = g(|\nabla I(x)|)$ (right-top) and its density plot together with the corresponding vector field $-\nabla\phi(x)$ (right-bottom).

Now we are in a position to derive a geometric equation $v = \beta(x, k, \nu)$ having the form of (1.15) for the normal velocity v of Γ_t in such way that corresponding family of surface curves $\mathcal{G}_t$ satisfies (1.27). For description of the evolution of the position vector $x = x(., t) \in \mathbb{R}^2$ of a planar curve Γ_t we consider the position vector equation

$$\partial_t x = \beta\vec{N} + \alpha\vec{T} \tag{1.30}$$

where β and α are normal and tangential velocities of Γ_t, resp. Since $\mathcal{G}_t = \{(x, \phi(x)),\ x \in \Gamma_t\}$ the normal velocity $\mathcal{V}$ of $\mathcal{G}_t$ satisfies

$$\begin{aligned} \mathcal{V} &= \partial_t(x,\phi(x)).\vec{\mathcal{N}} = (\vec{N}, \nabla\phi.\vec{N}).\beta\vec{\mathcal{N}} \\ &= \left(\frac{1+|\nabla\phi|^2}{1+(\nabla\phi.\vec{T})^2}\right)^{\frac{1}{2}} \beta. \end{aligned}$$

It follows from (1.28) and (1.29) that the flow of surface curves $\mathcal{G}_t \subset \mathcal{M}, t \geq 0$, fulfills (1.27) if and only if the normal velocity v of the flow of planar curves $\Gamma_t, t \geq 0$, satisfies the geometric equation

$$v = \beta(x,k,\nu) \equiv a(x,\nu)\, k - b(x,\nu)\, \nabla\phi(x).\vec{N} \tag{1.31}$$

where $a = a(x,\nu) > 0$ and $b = b(x,\nu)$ are smooth functions given by

$$\begin{aligned} a(x,\nu) &= \frac{1}{1+(\nabla\phi.\vec{T})^2}, \\ b(x,\nu) &= \frac{1}{1+|\nabla\phi|^2}\left(\bar{\gamma}(\phi(x)) - \frac{\vec{T}^T\nabla^2\phi\,\vec{T}}{1+(\nabla\phi.\vec{T})^2}\right). \end{aligned} \tag{1.32}$$

Here $\phi = \phi(x)$ and $\vec{T} = (\cos\nu, \sin\nu), \vec{N} = (-\sin\nu, \cos\nu)$. Notice that the function b is positive provided that $\bar{\gamma} \gg 1$ is large enough. Furthermore, β is a 2π periodic function in ν variable and β is C^{k-2} smooth provided that $\phi \in C^k$.

A similar equation to (1.31) arises from the theory of image segmentation. A given greylevel image can be represented by its intensity function I. The aim of segmentation is to find boundaries of distinguished object of the image, i.e. closed planar curves on which the gradient ∇I is large [114]. The idea behind the so-called *active contour models* is to construct an evolving family of plane curves converging to an edge [73]. One can construct such a family respecting the geometric equation $v = \gamma k + c$ where $c = c(x,\nu)$ is a driving force and $\gamma = \gamma(x,\nu) > 0$ is a smoothing coefficient [25, 88]. These functions may depend on the position vector x as well as orientation angle ν of a curve. If $c > 0$ then the driving force shrinks the curve whereas the impact of c is reversed in the case $c < 0$. Let us consider an auxiliary function $\phi(x) = g(|\nabla I(x)|)$ where g is a smooth edge detector function like e.g. the Perona-Malik one $g(s) = 1/(1+s^2)$. The gradient $-\nabla\phi(x)$ has the important geometric property: it points towards regions where the norm of the gradient ∇I is large (see Fig. 14). Let us therefore take $c(x,\nu) = -b_2(\phi(x))\nabla\phi(x).\vec{N}$ and $\gamma(x,\nu) = b_1(\phi(x))$ where $b_1, b_2 > 0$ are given smooth functions. Now, if an initial curve belongs to a neighborhood of an edge of the image and it is evolved according to the geometric equation (cf. (1.31))

$$v = \beta(x,k,\nu) \equiv b_1(\phi(x))k - b_2(\phi(x))\nabla\phi(x).\vec{N}$$

then it is smoothly driven towards this edge. In the context of level set methods, segmentation techniques based on this idea were first discussed by Caselles et al. [25] and Malladi, Sethian and Vemuri [88]. Later on, the models have been revisited and significantly improved by finding the proper driving force in the form $-\nabla\phi(x)$ by Caselles, Kimmel and Sapiro ([26, 27], also [28, 29]) and Kichenassamy et al. [75, 76].

2 Computational methods for the curve evolution equations

From the computational point of view, two main approaches are used for solving the equation (1.15):

1. Direct (or Lagrangian) approach, in which the geometrical parameters of the evolving curve itself are unknowns in related initial boundary value problems. For example, there are methods of this type based on computing the
- position vector in intrinsic heat equations, e.g. [41, 42, 43, 35, 99, 100, 78, 79, 128, 129]
- curvature or crystalline curvature in porous-medium like equations [93, 90, 50, 51, 134]
- nonlinear intrinsic systems for geometrical quantities describing curve [61, 62, 101, 102, 103]
- morphological methods based on erosion of polygons [104, 24], etc..

2. Level set (or Eulerian) approach based on introducing of an auxiliary function $v(x,t)$, $v : \mathbb{R}^d \times \mathbb{R}_0^+ \to \mathbb{R}$ specific level set of which corresponds to the evolving curve (surface) and which is solution to the
- level set formulation (1.21) (see e.g. [110, 131, 132, 133, 109]) or
- various phase-field formulations in the form of reaction-diffusion equations (see e.g. [22, 107, 44, 112, 19, 20, 21]).

The level set equation is used in sharp interface motion modelling while the phase-field equations are used to describe motion of diffussive interface and the curve evolution by (1.15) is then given as a limit when thickness of diffusive interface tends to zero.

In this Chapter we will be mainly concerned with direct methods for curve evolution and postpone discussion on the level set approach to Chapter 3. The computational techniques and applications of the phase-field equations have been extensively studied in the last decades, we refer e.g. to [107] or [19] for numerical methods of this type; we will not present more detailed discussion on these methods in this publication.

We will consider a regular plane curve Γ which can be parametrized by a C^2 smooth function $x : S^1 \to \mathbb{R}^2$ such that $\Gamma = \mathrm{Image}(x) = \{x(u), u \in [0,1]\}$ and $|\partial_u x| > 0$. One can define the unit tangent vector $\vec{T} = \partial_u x/|\partial_u x|$ and the unit normal vector $\vec{N}$ in such a way that $\vec{T} \wedge \vec{N} = 1$ where $\vec{a} \wedge \vec{b}$ is the determinant of the 2×2 matrix with column vectors $\vec{a}, \vec{b}$. Henceforth, we will denote $\vec{a} \,.\, \vec{b}$ the Euclidean inner product of two vectors. By $|\vec{a}| = (\vec{a} \,.\, \vec{a})^{1/2}$ we denote the Euclidean norm of a vector $\vec{a}$. The derivative of a function $f = f(\xi)$ with respect to ξ we will be denoted by $\partial_\xi f$ or $\frac{\partial f}{\partial \xi}$. The arc-length parametrization will be denoted by s. We denote by $g = |\partial_u x|$ the local length. Then clearly, $ds = g du$. Note, that in the first and third Chapter we use u and g as greylevel image intensity resp. Perona-Malik function while in this Chapter as unit interval parametrization resp. local length, but since the contexts are quite different we hope no confusion can appear. By k we denote the signed curvature of the curve $\Gamma = \mathrm{Image}(x)$ defined as

$$k = \partial_s x \wedge \partial_s^2 x = \frac{\partial_u x \wedge \partial_u^2 x}{|\partial_u x|^3} \tag{2.1}$$

then Frenet's formulae read as follows $\vec{T}_s = k\vec{N}, \vec{N}_s = -k\vec{T}$. The angle ν of the tangential vector is given by $\nu = \arg(\vec{T})$, i.e. $(\cos\nu, \sin\nu) = \partial_s x = \vec{T}$. To describe the time evolution $\{\Gamma_t\}, t \in [0,T)$ of an initial curve $\Gamma = \Gamma_0 = \mathrm{Image}(x^0)$ we adopt the notation $\Gamma_t = \{x(u,t), u \in [0,1]\}, \quad t \in [0,T)$, where $x \in C^2(Q_T, \mathbb{R}^2)$ and $Q_T = S^1 \times [0,T)$. We will frequently identify

Q_T with $[0,1]\times[0,T)$ and the space $C^l(Q_T,\mathbb{R}^2)$ with the space of C^l differentiable functions defined on $[0,1]$ and satisfying periodic boundary conditions. We will study a motion driven by the normal velocity v which is assumed to be a function of the curvature k, tangential angle ν and position vector $x\in\Gamma_t$:

$$v=\beta(x,k,\nu)\,. \tag{2.2}$$

Assumptions on a specific form of the governing function β will be given in subsequent Sections. First, we will describe convex curves evolution, driven by anisotropy and nonlinear function of curvature, solving doubly-nonlinear asymptotically degenerate porous-medium type equation. Then we use intrinsic heat equation formulation to solve general nonconvex curvature driven evolution. Next, we will stabilize the intrinsic diffusion based method by suitable tangential redistribution. Finally we develop formulation and solution method for system of ordinary-partial differential equations of convection-diffusion-reaction type governing evolution of all geometric quantities (curvature, tangent angle, local length and position vector), which is well suited for numerical solution and can be used in very general situations of anisotropic and geodesic curvature motions with strong external driving forces depending on current position of the curve.

2.1 Solution using porous-medium like equations

In this Section, let us consider closed and convex initial curve $x(u,0)$ and evolution of the form

$$v=\beta(k,\nu), \tag{2.3}$$

with β smooth, increasing in k. Then, due to [12, 14], the evolution by equation (2.3) preserves convexity. The evolving curve admits various parametrizations. In convex case, ν - the angle of the tangent to the curve with the horizontal axes - gives a convenient parametrization varying in fixed interval $[0,2\pi\omega]$, where $\omega\in\mathbb{N}$ corresponds to the index of the curve.

Let the initial closed convex curve $x^0=x(\nu,0)$ be parametrized by ν and let $k_0(\nu)$ be its curvature. Then we have that the flow $x(\nu,t)$ of the curves, which solves the problem (2.3) with the initial curve x^0, is given uniquely up to a translation by the formula [49, 11]

$$x(\nu^*,t)=x(0,t)-\int_0^{\nu^*}\frac{e^{i\nu}}{k(\nu,t)}d\nu,\quad \nu^*\in[0,2\pi\omega], \tag{2.4}$$

in which the curvature $k(\nu,t)$ is the solution of the following doubly nonlinear porous-medium type initial boundary value problem:

$$\begin{aligned} \partial_t b(k) &= \partial_{\nu\nu}\beta(k,\nu)+\beta(k,\nu), \\ k(\nu,t) &= k(\nu+2\pi\omega,t), \\ k(\nu,0) &= k_0(\nu), \end{aligned} \tag{2.5}$$

with $b(k)=-1/k$. Doubly nonlinear porous-medium type equations can be solved efficiently by the so-called Jäger-Kačur algorithm ([63, 68, 64, 67], see also [55, 56, 57, 89]). The approach based on Jäger-Kačur method for solving the curve evolution problem (2.4)-(2.5) was

suggested by Mikula and Kačur in [69, 93, 90] and has been applied first to classical (i.e. linear in k) anisotropic curve shortening [69, 93] and then to general nonlinear curve shortening problem [90]. The discrete curvature function is computed in each discrete time step of the numerical scheme designed to solve equation (2.5) and the curve flow is reconstructed by the formula (2.4). Using the so-called Rothe's technique [66], the ideas of Alt and Luckhaus [2], Magenes, Nochetto and Verdi [87] and the Jäger-Kačur method we were able to prove convergence of the scheme to the true solution. By our knowledge, the methods from [69, 93, 90] were first computational techniques which have guaranteed the convergence to anisotropic as well as nonlinear curve shortening problem, although only in convex curve evolution case. Due to that theoretical property we have used these methods to test and compare behaviour of more general schemes given e.g. in [99, 100, 101, 19, 59] for which such complete theory is not yet available.

Let us briefly recall the main ideas of approximation of the equation (2.5). In [93, 90], we consider the case of separated anisotropy and nonlinearity in the form

$$\beta(k,\nu) = \gamma_1(\nu)\beta_1(k) + \gamma_2(\nu),$$

where $\gamma_1 \geq q > 0, \gamma_1', \gamma_1'', \gamma_2$ are bounded measurable functions, periodic in interval $[0, 2\pi\omega]$ and β_1 is C^2-function in $\mathbb{R} - \{0\}$ with $\beta_1'(s) > 0, s \neq 0$, $\beta_1'(0) \geq 0$, $\beta_1(0) = 0$. The mathematical and numerical difficulties are caused by degeneracies in the equation (2.5). Namely, asymptotical degeneracy of *slow diffusion type* ($b' = \infty$, $\beta_1' = 0$) is related to the parts of the curve, where curvature is close to 0 and plays the role in the presence of anisotropy and porous-medium-like nonlinearity, $\beta_1(s) = s^m, m > 1$. Asymptotical degeneracy of *fast diffusion type* ($b' = 0$, $\beta_1' = \infty$) is related to both, large and small curvatures, and plays the role near the shrinking, singularities formation and influences a more shape preserving (e.g. affine invariant, $\beta(k) = k^{1/3}$) evolution. The special form of the problem causes a blow up of the curvature in a finite time which corresponds to the shrinking of the curve to a point or to other singular behaviour [48, 10].

If we denote $I = [0, T_{max}]$, $J = [0, 2\pi\omega]$, $V = \{w \in W_2^1(0, 2\pi\omega) : w(0) = w(2\pi\omega)\}$, V^* its dual space, and assuming that $\beta_1(k_0) \in V$, we can define weak solution of (2.5) as a function $k \in L_2(I, L_2(J))$ with $\partial_t b(k) \in L_2(I, V^*)$ for which $\beta(k,\nu) \in L_2(I, V)$, $k(\nu, 0) = k_0(\nu)$ and

$$\int_I \int_J \partial_t b(k)\varphi d\nu dt + \int_I \int_J \partial_\nu \beta(k,\nu)\varphi_\nu d\nu dt = \int_I \int_J \beta(k,\nu)\varphi d\nu dt, \ \forall \varphi \in L_2(I, V).$$

In order to find the weak solution we use the following **approximation scheme for the porous-medium curve evolution equation (2.5)**[93, 90]:
Let $m \in \mathbb{N}, \tau = \frac{T_{max}}{m}, t_j = j\tau$ for $j = 0, \ldots, m$, $k^0 = k_0(\nu), K^0 = \beta_1(k_0)$. For $j = 1, \ldots, m$ we look for the functions $K^j \in V$ ($K^j \approx \beta_1(k^j)$), $\mu^j \in L_\infty(\Omega)$ such that

$$\int_J \mu^j (K^j - \beta_1(k^{j-1}))\varphi d\nu + \tau \int_J \partial_\nu \tilde{\beta}(K^j, \nu)\varphi_\nu d\nu = \tau \int_J \tilde{\beta}(K^j, \nu)\varphi d\nu, \ \forall \varphi \in V \tag{2.6}$$

where $\tilde{\beta}(s,\nu) = \beta(\beta_1^{-1}(s), \nu) = \gamma_1(\nu)s + \gamma_2(\nu)$, provided the *convergence condition*

$$\alpha\frac{\lambda}{2} \leq \mu^j \leq \frac{b(\beta_1^{-1}(\alpha K^j + (1-\alpha)\beta_1(k^{j-1}))) - b(k^{j-1})}{K^j - \beta_1(k^{j-1})}, \tag{2.7}$$

holds with $0 < \alpha < 1$ (α close to 1) and λ is a lower bound of derivative of a regularized $b \circ \beta_1^{-1}$ function (details and a role of the regularization are given in [93, 90]). The curvature function k^j is obtained by the *algebraic correction*

$$b(k^j) := b(k^{j-1}) + \mu^j (K^j - \beta_1(k^{j-1})). \tag{2.8}$$

In the scheme (2.6)-(2.8), the nonlinearity of equation is treated by the optimal choice of relaxation function μ^j corresponding to $\partial_s(b \circ \beta_1^{-1})$ constructed in an iterative way (for details we refer to [93, 90]). The linear elliptic convection-diffusion equation (2.6) can be solved by finite element discretization (see e.g. [32]) or by finite volume method including up-wind principle (see e.g. [113, 47]).

Using k^j, K^j obtained in each time step of (2.6)-(2.8), the Rothe functions

$$\overline{k}^{(n)}(t) = k^j, \text{for } t_{j-1} < t \le t_j, j = 1, \dots, m, \quad \overline{k}^{(n)}(0) = k_0, \tag{2.9}$$

$$\overline{K}^n(t) = K^j, \text{for } t_{j-1} < t \le t_j, j = 1, \dots, m, \quad \overline{K}^n(0) = K_0 \tag{2.10}$$

are constructed. Then due to [93] and [90] we have

2.1 Theorem *Let $\overline{k}^{(n)}, \overline{K}^n$ be given by* (2.9)-(2.10). *Then*

$$\overline{k}^{(n)} \to k \ \text{ in } L_2(I, L_2(J)), \quad \overline{K}^n \to \beta_1(k) \ \text{ in } L_2(I, V),$$

where k is unique bounded weak solution of the initial-boundary value problem (2.5).

2.2 Solution by intrinsic heat equation

In the concept presented above, the existence and uniqueness of the solution as well as convergence and error estimates of approximations has been proved in [93, 90]. However, such approach holds only for convex curve motions and, from practical point of view, we would like to handle general nonconvex curve evolution governed by equation (2.3). In the nonconvex case, ν-parametrization seems to be not convenient due to a changing of its range during the evolution for each convex/concave piece of a curve. Another idea, originating in the Dziuk algorithm for evolutionary surfaces [41] can be used. Let us first consider isotropic but possibly in nonlinear way dependent on curvature normal velocity v,

$$v = \beta(k) \tag{2.11}$$

and assume that β is a smooth increasing function of k. Mikula and Ševčovič in [99] use the representation of equation (2.11) by the *(generalized) intrinsic heat equation*

$$\frac{\partial x}{\partial t} = \frac{\partial^2 x}{\partial s_*^2} \tag{2.12}$$

where s_* is a special curve parametrization related to standard arc-length parametrization s by

$$ds_* = \vartheta(s) ds, \vartheta = k^{1/2} \beta(k)^{-1/2}. \tag{2.13}$$

Then clearly

$$\frac{\partial x}{\partial t} = \frac{1}{\vartheta(s)}\frac{\partial}{\partial s}\left(\frac{1}{\vartheta(s)}\frac{\partial x}{\partial s}\right) = \beta(k)\vec{N} - \frac{\vartheta'(s)}{\vartheta^3(s)}\vec{T}. \tag{2.14}$$

Hence the normal velocity $v = (\frac{\partial x}{\partial t}, \vec{N})$ fulfills the equation (2.11). If s_* is equal to s, i.e. $\beta(k) = k$, we get standard intrinsic heat equation (see e.g. [42]).

Let us define scalar valued function $G : \mathbb{R}^2 \times \mathbb{R}^2 \to \mathbb{R}_0^+$,

$$G(p,q) = |p|k(p,q)^{1/2}\beta(k(p,q))^{-1/2}$$

where

$$k(p,q) = |p|^{-3}\left(|p|^2|q|^2 - (p,q)^2\right)^{1/2} \quad p,q \in \mathbb{R}^2.$$

With this notation, (2.12) can be rewritten as follows

$$\frac{\partial x}{\partial t} = \frac{1}{G(x_u, x_{uu})}\frac{\partial}{\partial u}\left(\frac{1}{G(x_u, x_{uu})}\frac{\partial x}{\partial u}\right), \quad (u,t) \in [0,1] \times [0, T_{max}). \tag{2.15}$$

The system of two nonlinear PDEs (2.15) is subject to the initial condition $x(u,0) = x^0(u), u \in [0,1]$ and periodic boundary conditions at $u = 0, 1$.

Approximation scheme for the curve evolution based on intrinsic heat equation: Let $\tau = \frac{T_{max}}{m}, m \in \mathbb{N}$ denote time discretization step. By $x^j, j = 0, 1, ..., m$, we denote the approximation of a solution of (2.15) at time $t = j\tau$, i.e. $x^j(.) = x(., j\tau)$. The idea of the construction of a time discretization scheme is based on approximation of the intrinsic heat equation (2.12) by the backward Euler method

$$\frac{x^j - x^{j-1}}{\tau} = \frac{\partial^2 x^j}{\partial s_*^2}, \quad j = 1, 2, ..., m,$$

where the parametrization s_* is computed from the previous time step x^{j-1}. The semidiscrete scheme thus reads as follows

$$x^j - \frac{\tau}{G^{j-1}}\frac{\partial}{\partial u}\left(\frac{1}{G^{j-1}}\frac{\partial x^j}{\partial u}\right) = x^{j-1}, \quad j = 1, 2, ..., m, \tag{2.16}$$

where $G^{j-1} = G(x_u^{j-1}, x_{uu}^{j-1})$ and x^0 is the initial condition. One can prove (see [99]) that the length of the curve $\Gamma_j = \text{Image}(x^j)$ decreases along the semidiscrete evolution generated by (2.16) which represents a kind of stability property for the scheme.

To derive a fully discrete analogue of (2.16) we use the uniform spatial grid $u_i = ih$ $(i = 0, ..., n)$ with $h = 1/n$. The smooth solution x is then approximated by the discrete values x_i^j corresponding to $x(ih, j\tau)$ which are solutions to the following semi-implicit fully discrete scheme

$$\frac{1}{2}(G_i^{j-1} + G_{i+1}^{j-1})\frac{x_i^j - x_i^{j-1}}{\tau} = \frac{x_{i+1}^j - x_i^j}{G_{i+1}^{j-1}} - \frac{x_i^j - x_{i-1}^j}{G_i^{j-1}} \tag{2.17}$$

$i = 1, ..., n, j = 1, ..., m$, where (we slightly regularize G_i^{j-1} in order to avoid zeroes in denominator)

$$G_i^{j-1} = h_i^{j-1} \sqrt{\frac{k_i^{j-1}+\varepsilon}{\beta(k_i^{j-1}+\varepsilon)}}, \quad h_i^{j-1} = |x_i^{j-1} - x_{i-1}^{j-1}|,$$

$$k_i^{j-1} = \frac{|\arccos\big((x_{i+1}^{j-1}-x_{i-1}^{j-1}, x_i^{j-1}-x_{i-2}^{j-1})/(|x_{i+1}^{j-1}-x_{i-1}^{j-1}||x_i^{j-1}-x_{i-2}^{j-1}|)\big)|}{h_i^{j-1}}.$$

The scheme is subject to periodic boundary conditions $x_{i+n}^j = x_i^j$ $(i = 0, 1)$. In each discrete computational time step $j\tau$ the scheme (2.17) leads to solving of two tridiagonal systems for the new curve position which is fast procedure. Let us mention that (2.17) does not involve the spatial grid parameter h (i.e. the scheme respects the intrinsic character of the equation) and in the linear case $\beta(k) = k$ it coincides with Dziuk's scheme [42].

Recently, the previous approach based on solution to the intrinsic heat equation has been adopted to anisotropic case with β linear in k by Dziuk [43], and also to the general anisotropic and nonlinear case (2.3) by Mikula and Ševčovič [100]. Such approach we will explain in the next Section.

We present several computational results related to the schemes (2.6)-(2.8) and (2.17). They show good correspondence of both methods in convex case (until formation of singularities) and also successful computation of nonconvex curves evolution.

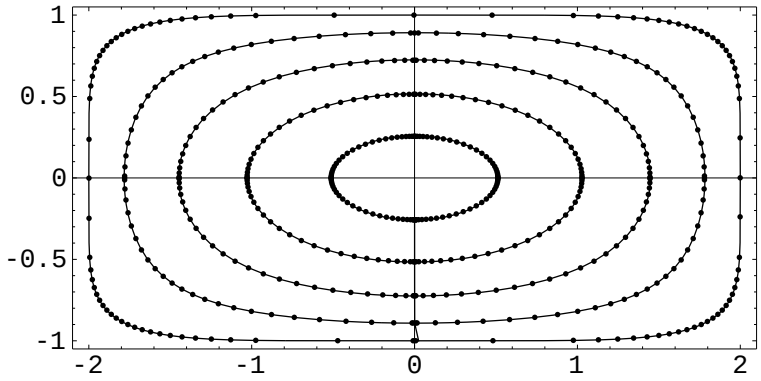

Figure 15: Comparison of two different methods for evolution of convex curve; tick marks - method (2.17), solid lines - method (2.6)-(2.8), affine invariant case $\beta(k) = k^{1/3}$. We also remark, a proper redistribution of flowing points representing the discrete curve in the method (2.17) due to the presence of convenient (for this experiment) tangential velocity, see (2.14).

2.3 Solution by intrinsic heat equation with tangential velocity preserving relative local length

In this Section, let us consider anisotropic and nonlinear in curvature normal velocity

$$v = \beta(k, \nu) = \gamma(\nu)|k|^{m-1}k \tag{2.18}$$

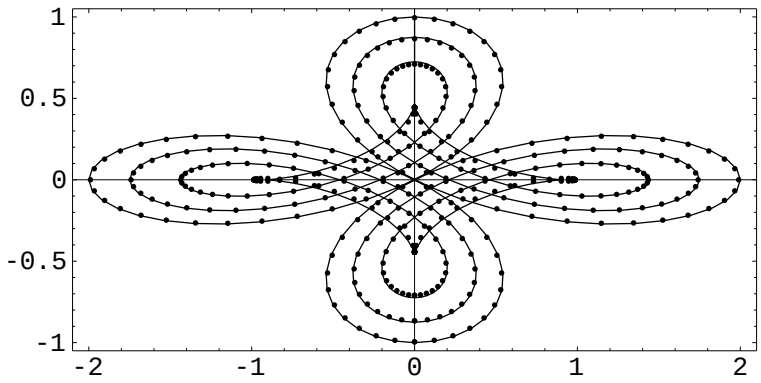

Figure 16: Comparison of two different methods for evolution of selfintersecting quatrefoil curve, $\beta(k) = k^{1/3}$. Tick marks - method (2.17), solid lines - method (2.6)-(2.8). The evolving curve is plotted at the same discrete time moments until the "hair" singularity is formed [48, 10]. The method (2.6)-(2.8) cannot continue beyond singularity.

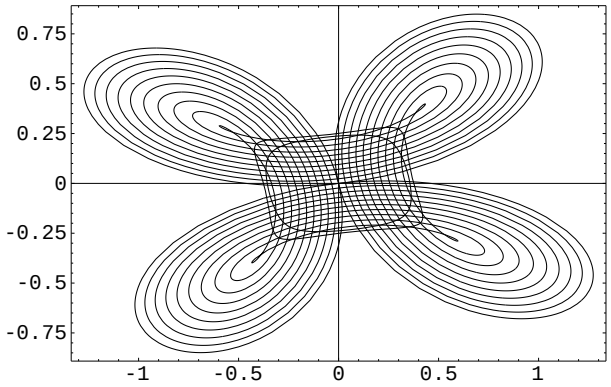

Figure 17: Evolution of the affine transformed quatrefoil through "hair" singularities computed by the method (2.17), $\beta(k) = k^{1/3}$.

given by the power like function, where $m > 0$ and $\gamma(\nu) > 0$ is a given anisotropy function satisfying

$$0 < C_1^{-1} \leq \gamma(\nu) \leq C_1, \quad |\gamma'(\nu)| \leq C_1 \qquad \text{for any } \nu \in \mathbb{R} \tag{2.19}$$

where $C_1 > 0$ is a constant.

The approach from the previous Section where we solve the intrinsic heat equation can be generalized, theoretical results about existence of the solution can be proved and computational algorithm can be significantly improved by tangential stabilizing terms. In [100] Mikula and Ševčovič established the short time existence of a family of regular smooth plane curves satisfying the geometric equation (2.18), suggested the tangential redistribution conserving relative local length and presented numerical experiments showing the important role of tangential redistribution in computational algorithm. In the theory of curve evolution, it extends the result due to Angenent, Sapiro and Tannenbaum obtained for the power $m = 1/3$ to the general fast diffusion powers $0 < m < 1$ as well as for degenerate slow diffusion cases where $1 < m \leq 2$. Some further interesting theoretical results can be found in [6, 24].

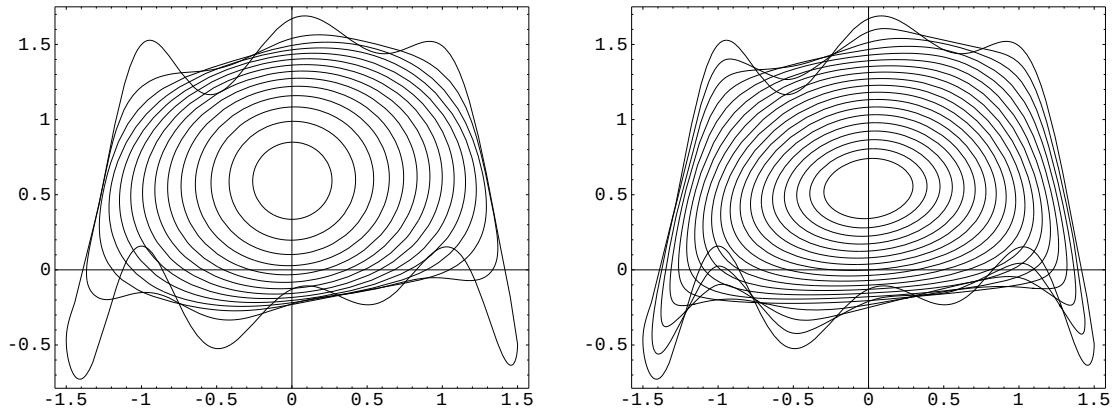

Figure 18: Evolution of initial nonconvex curve computed by the method (2.17), $\beta(k) = k$ (left) and $\beta(k) = k^{1/3}$ (right).

The idea how to describe a family of evolving plane curves is to parameterize Γ_t by a solution $x \in C^2(Q_T, \mathbb{R}^2)$ to a slightly more general intrinsic heat equation as in the previous Section, namely

$$\frac{\partial x}{\partial t} = \frac{1}{\theta_1}\frac{\partial}{\partial s}\left(\frac{1}{\theta_2}\frac{\partial x}{\partial s}\right), \quad x(.,0) = x^0(.) \tag{2.20}$$

where θ_1, θ_2 are geometric quantities for the curve $\Gamma_t = \text{Image}(x(.,t))$, i.e. functions whose definition is independent of particular parametrization of Γ_t and such that

$$\theta_1\theta_2 = \frac{k}{\beta(k,\nu)} \ . \tag{2.21}$$

By using (2.21) and Frenet's formulae, equation (2.20) can be rewritten into the following equivalent form

$$\frac{\partial x}{\partial t} = \beta\vec{N} + \alpha\vec{T}, \quad x(.,0) = x^0(.) \tag{2.22}$$

where $\beta = \beta(k,\nu)$ is the normal velocity of the evolving curve and α is the tangential velocity given by

$$\alpha = \frac{1}{\theta_1}\frac{\partial}{\partial s}\left(\frac{1}{\theta_2}\right) \ . \tag{2.23}$$

The normal component v of the velocity $\partial_t x$ is therefore equal to $\beta(k,\nu)$. By [14, Lemma 4.1] the family $\Gamma_t = \text{Image}(x(.,t))$ parametrized by a solution x of the geometric equation (2.22) can be converted into a solution of $\partial_t x = \beta\vec{N} + \bar{\alpha}\vec{T}$ for any continuous function $\bar{\alpha}$ by changing the space parametrization of the original curve. In particular, it means that one can take $\bar{\alpha} = 0$ without changing the shape of evolving curves. On the other hand, as it can be observed from our numerical simulations, the presence of a suitable tangential velocity term $\alpha\vec{T}$ is necessary for construction of a numerical scheme which is capable of suitable redistribution of numerical grid points along computed curve.

In the previous Section we have studied the intrinsic heat equation (2.20) with particular choice $\theta_1 = \theta_2 = (k/\beta(k))^{1/2}$. In this case equation (2.20) has the form $\partial_t x = \partial^2_{s_*} x$ where $ds_* = \theta_1 ds$. Using such θ_1, θ_2 we were able to simulate the evolution of plane convex and non-convex curves for the case where $v = |k|^{m-1}k$. Satisfactory results were obtained only for $0 < m \leq 1$ whereas various numerical instabilities appeared for the case $m > 1$. The mathematical explanation for such a behavior is simple. If $\theta_1 = \theta_2 = |k|^{\frac{m-1}{2}}$ then, by (2.23), $\alpha = \frac{m-1}{2}|k|^{m-3}k\partial_s k = \frac{1}{2}\partial_s(|k|^{m-1})$. In the case $m > 1$ numerical grid points were driven by the tangential velocity $\alpha\vec{T}$ towards pieces of the curve with the increasing curvature where they fastly accumulate and the Lagrangian algorithm broke down soon due to computer zeroes in denominators of (2.17). The effect of α is just opposite when $0 < m < 1$. This observation leads us to study formulation where tangential velocity is not given a-priori, as in the previous Section, but can be controlled and thus is capable to give an adequate grid points redistribution.

To that goal, first we derive a system of PDEs governing the evolution of the curvature k and some other geometric quantities for $x = x(u,t)$ a solution to the curve evolution equation (2.18). Notice that such an equation for the curvature is well-known for the case when $\alpha = 0$ and it reads as follows: $\partial_t k = \partial_s^2\beta + k^2\beta$ (indeed, in Section 2.1 we have solved this equation written in ν-parametrization, cf. [49, 11]).

Let us denote $\vec{p} = \partial_u x$. Then by using Frenet's formulae one has

$$\begin{aligned}
\partial_t\vec{p} &= |\partial_u x|((\partial_s\beta + \alpha k)\vec{N} + (-\beta k + \partial_s\alpha)\vec{T}) \\
\vec{p}\,.\,\partial_t\vec{p} &= |\partial_u x|\ \vec{T}\,.\,\partial_t\vec{p} = |\partial_u x|^2(-\beta k + \partial_s\alpha) \\
\vec{p}\wedge\partial_t\vec{p} &= |\partial_u x|\ \vec{T}\wedge\partial_t\vec{p} = |\partial_u x|^2\ (\partial_s\beta + \alpha k) \\
\partial_t\vec{p}\wedge\partial_u\vec{p} &= -|\partial_u x|\partial_u|\partial_u x|\ (\partial_s\beta + \alpha k) + |\partial_u x|^3\ (-\beta k + \partial_s\alpha)
\end{aligned} \tag{2.24}$$

because $p_u = \partial_u^2 x = \partial_u(|\partial_u x|\ \vec{T}) = \partial_u|\partial_u x|\ \vec{T} + k|\partial_u x|^2\ \vec{N}$. Since $\partial_u(\vec{p}\wedge\partial_t\vec{p}) = \partial_u\vec{p}\wedge\partial_t\vec{p} + \vec{p}\wedge\partial_u\partial_t\vec{p}$ we have $\vec{p}\wedge\partial_u\partial_t\vec{p} = \partial_u(\vec{p}\wedge\partial_t\vec{p}) + \partial_t\vec{p}\wedge\partial_u\vec{p}$. As $k = (\vec{p}\wedge\partial_u\vec{p})\,|\vec{p}|^{-3}$ (see (2.1)) we obtain

$$\begin{aligned}
\partial_t k &= -3|p|^{-5}(\vec{p}\,.\,\partial_t\vec{p})(\vec{p}\wedge\partial_u\vec{p}) + |\vec{p}|^{-3}\,((\partial_t\vec{p}\wedge\partial_u\vec{p}) + (\vec{p}\wedge\partial_u\partial_t\vec{p})) \\
&= -3k|\vec{p}|^{-2}(\vec{p}\,.\,\partial_t\vec{p}) + 2|\vec{p}|^{-3}(\partial_t\vec{p}\wedge\partial_u\vec{p}) + |\vec{p}|^{-3}\partial_u(\vec{p}\wedge\partial_t\vec{p})
\end{aligned}$$

Finally, by applying identities (2.24) we end up with the second order nonlinear parabolic *equation for the curvature*

$$\partial_t k = \partial_s^2\beta + \alpha\partial_s k + k^2\beta, \quad k(.,0) = k^0(.)\ . \tag{2.25}$$

The identities (2.24) can be used in order to derive an evolutionary equation for the local length $|\partial_u x|$. Indeed, $|\partial_u x|_t = (\partial_u x\,.\,\partial_u\partial_t x)/|\partial_u x| = (\vec{p}\,.\,\partial_t\vec{p})/|\partial_u x|$ and by (2.24) we have the *local length equation*

$$\frac{\partial}{\partial t}|\partial_u x| = -|\partial_u x|\,k\beta\ +\ \frac{\partial\alpha}{\partial u}, \qquad |\partial_u x(.,0)| = |\partial_u x^0(.)|\ . \tag{2.26}$$

where $(u,t) \in Q_T$. By integrating equation (2.26) over the interval $[0,1]$ and taking into account that α satisfies periodic boundary conditions we obtain the *total length equation*

$$\frac{d}{dt}L_t + \int_{\Gamma_t} k\beta(k,\nu)ds = 0 \tag{2.27}$$

where $L_t = L(\Gamma_t)$ is the total length of the curve Γ_t, $L_t = \int_{\Gamma_t} ds = \int_0^1 |\partial_u x(u,t)|\, du$. If $k\beta(k,\nu) \geq 0$ then the evolution of plane curves represents a curve shortening flow, i.e. $L_{t_2} \leq L_{t_1} \leq L_0$ for any $0 \leq t_1 \leq t_2 \leq T$. The condition $k\beta(k,\nu) \geq 0$ is obviously satisfied in the case $\beta(k,\nu) = \gamma(\nu)|k|^{m-1}k$ where $m > 0$ and γ is a nonnegative anisotropy function.

The area enclosed by an embedded nonselfintersecting curve $\Gamma = \text{Image}(x)$ can be computed as $A = \frac{1}{2}\int_0^1 x \wedge \partial_u x\, du$. Applying the identities (2.24) and taking into account that $0 = \int_0^1 \partial_u(x \wedge \partial_t x)\, du = \int_0^1 (\vec{p} \wedge \partial_t x + x \wedge \partial_t \vec{p})\, du$ we obtain the *area equation*

$$\frac{d}{dt}A^t + \int_{\Gamma_t} \beta(k,\nu) ds = 0 \ . \tag{2.28}$$

If $\beta(k,\nu)$ is nonnegative along the evolution then the area is a non-increasing function of the time.

Denote by $[\partial_t, \partial_s]$ the commutator of the differential operators ∂_t and ∂_s, i.e. $[\partial_t, \partial_s] = \partial_t\partial_s - \partial_s\partial_t$. Since $ds = |\partial_u x| du$ it follows from the local length equation (2.26) that

$$[\partial_t, \partial_s] = (\beta k - \partial_s \alpha)\partial_s \ . \tag{2.29}$$

Recall that the tangential vector ν to a curve $\Gamma = \text{Image}(x)$ is given by $\nu = \arg(\vec{T})$, i.e. $(\cos\nu, \sin\nu) = \partial_s x$. From (2.29) we obtain $\partial_t \nu = \partial_s x \wedge \partial_t \partial_s x = \partial_s x \wedge \partial_s \partial_t x + (\beta k - \partial_s \alpha)(\partial_s x \wedge \partial_s x)$. Applying Frenet's formulae and (2.22) we obtain $\partial_t \nu = \partial_s \beta + \alpha k$, and using $\partial_s \beta(k,\nu) = \beta'_k \partial_s k + \beta'_\nu \partial_s \nu = \beta'_k \partial_s^2 \nu + \beta'_\nu k$ we get the second order nonlinear parabolic *equation for the tangential angle*

$$\partial_t \nu = \beta'_k \partial_s^2 \nu + k(\alpha + \beta'_\nu), \quad \nu(.,0) = \nu^0(.) \ . \tag{2.30}$$

Now we are in a position to write a closed system of governing equations for the geometric motion satisfying equation (2.18):

$$\begin{aligned} \frac{\partial k}{\partial t} &= \frac{1}{g}\frac{\partial}{\partial u}\left(\frac{1}{g}\frac{\partial}{\partial u}\beta(k,\nu)\right) + \frac{\alpha}{g}\frac{\partial k}{\partial u} + k^2\beta(k,\nu) \\ \frac{\partial \nu}{\partial t} &= \frac{\beta'_k(k,\nu)}{g}\frac{\partial}{\partial u}\left(\frac{1}{g}\frac{\partial \nu}{\partial u}\right) + k(\alpha + \beta'_\nu(k,\nu)) \\ \frac{\partial g}{\partial t} &= -gk\beta(k,\nu) + \frac{\partial \alpha}{\partial u} \end{aligned} \tag{2.31}$$

$(u,t) \in [0,1] \times (0,T)$. A solution to (2.31) is subject to the initial conditions

$$k(.,0) = k^0, \quad \nu(.,0) = \nu^0, \quad g(.,0) = g^0 \tag{2.32}$$

and periodic boundary conditions except of ν for which we require $\nu(1,t) = \nu(0,t) + 2\pi$. Notice that the initial conditions for k^0, ν^0, g^0 are related through the identity $\partial_u \nu^0 = g^0 k^0$.

In general, the function α is a free parameter in the model. The main idea behind a proper construction of α is to analyze the relative local length function defined as the ratio $\frac{|\partial_u x(u,t)|}{L_t}$ where L_t is the total length of Γ_t and $|\partial_u x(u,t)|$ represents the local length of Γ_t. The idea is to keep this ratio constant with respect to time, i.e.

$$\frac{d}{dt}\left(\frac{|\partial_u x(u,t)|}{L_t}\right) = 0 \tag{2.33}$$

for any $u \in [0,1]$ and $t \in I = (0,T)$. Taking into account (2.26) and (2.27) one sees that (2.33) is fulfilled iff

$$\frac{\partial \alpha}{\partial s} = k\beta(k,\nu) - \frac{1}{L}\int_\Gamma k\beta(k,\nu)\,ds \tag{2.34}$$

where $\Gamma = \Gamma_t$, $L = L(\Gamma)$, k is the curvature of Γ and β is the given normal velocity function. Let ϑ be new variable, such that $\theta_2 = \exp(\vartheta)$. Since $\theta_1 = k/(\beta\theta_2)$ we get

$$\alpha = \frac{1}{\theta_1}\frac{\partial}{\partial s}\left(\frac{1}{\theta_2}\right) = -\frac{\beta}{k}\frac{\partial}{\partial s}\ln\theta_2 = -\frac{\beta}{k}\frac{\partial \vartheta}{\partial s}$$

and, using (2.34), ϑ should be a solution to the *stationary intrinsic heat equation*

$$-\frac{\partial}{\partial s}\left(\frac{\beta}{k}\frac{\partial \vartheta}{\partial s}\right) = k\beta - \frac{1}{L}\int_\Gamma k\beta\,ds\ . \tag{2.35}$$

Due to [100] there exists unique solution of (2.35) as well as solution of the fully nonlinear system (2.31) by which we can construct solution of (2.20) and correspondingly the flow (2.22). So we can state the main theoretical result of [100]:

2.2 Theorem *Suppose that* $\beta(k,\nu) = \gamma(\nu)|k|^{m-1}k$ *where* $0 < m \le 2$ *and* γ *satisfies* (2.19). *Let* $\Gamma^0 = \mathrm{Image}(x^0)$ *be a smooth regular plane curve. Then there exists* $T > 0$ *and a family of regular plane curves* $\Gamma_t = \mathrm{Image}(x(.,t)), t \in [0,T]$ *such that*

1. $x, \partial_u x \in (C(\overline{Q_T}))^2,\ \ \partial_u^2 x,\ \partial_t x,\ \partial_u\partial_t x \in (L_\infty(Q_T))^2$;
2. *the flow* $\Gamma_t = \mathrm{Image}(x(.,t)), t \in [0,T]$ *of regular plane curves satisfies the geometric equation*

$$\partial_t x = \beta\vec{N} + \alpha\vec{T}$$

where $\beta = \beta(k,\nu)$ *and* α *is the tangential velocity preserving the relative local length, i.e.* α *satisfies* (2.34) *and*

$$\frac{|\partial_u x(u,t)|}{L_t} = \frac{|\partial_u x^0(u)|}{L_0}$$

for any $t \in [0,T]$ *and* $u \in [0,1]$.

Now we describe a numerical procedure which can be used for computing the curve evolution satisfying the geometric equation (2.18) accompanied with equation (2.34) for tangential velocity α. To this end, we propose a scheme solving the coupled system of intrinsic heat equations (2.20) for the position vector x and (2.35) for the redistribution parameter ϑ.

Approximation scheme for the curve evolution solving intrinsic heat equation with tangential redistribution [100]:

A smooth solution x is approximated by discrete plane points $x_i^j, i = 1,...,n,\ j = 0,...,m$, where index i represents space discretization and index j a discrete time stepping. The approximation of a curve in time $j\tau$ (with uniform time step $\tau = \frac{T}{m}$) is given by the polygon

with vertices $x_i^j, i = 1, ..., n$. In order to obtain such an approximation of an evolving curve in j-th time step we use the following fully discrete semi-implicit scheme

$$\frac{1}{2}(g_i^{j-1} + g_{i+1}^{j-1})\frac{x_i^j - x_i^{j-1}}{\tau} = \frac{x_{i+1}^j - x_i^j}{h_{i+1}^{j-1}} - \frac{x_i^j - x_{i-1}^j}{h_i^{j-1}}, \tag{2.36}$$

$i = 1, ..., n$, for every $j = 1, ..., m$. The coefficients in (2.36) (for simplicity we omit upper index $j-1$) are given by the following expressions

$$g_i = |r_i|\theta_{1,i}, \quad h_i = |r_i|\theta_{2,i}, \quad r_i = x_i - x_{i-1}, \quad \theta_{1,i} = \frac{k_i}{\beta_i \theta_{2,i}},$$

$$k_i = \frac{1}{2|r_i|}\mathrm{sgn}(r_{i-1} \wedge r_{i+1}) \arccos\left(\frac{r_{i+1}.r_{i-1}}{|r_{i+1}||r_{i-1}|}\right), \tag{2.37}$$

$$\nu_i = \arccos(r_{i_1}/|r_i|) \text{ if } r_{i_2} \geq 0, \quad \nu_i = 2\pi - \arccos(r_{i_1}/|r_i|) \text{ if } r_{i_2} < 0,$$

$$\beta_i = \beta(k_i, \nu_i), \quad \theta_{2,i} = \exp(\vartheta_i),$$

and the system (2.36) is subject to the periodic boundary conditions $x_{i+n}^j = x_i^j$ $(i = 0, 1)$. In order to compute $\vartheta_i, i = 1, ..., n$, governing tangential redistribution of flowing points we solve

$$-\frac{\frac{\beta_i}{k_i} + \frac{\beta_{i+1}}{k_{i+1}}}{|r_i| + |r_{i+1}|}(\vartheta_{i+1} - \vartheta_i) + \frac{\frac{\beta_i}{k_i} + \frac{\beta_{i-1}}{k_{i-1}}}{|r_i| + |r_{i-1}|}(\vartheta_i - \vartheta_{i-1})$$

$$= |r_i|\left(k_i\beta_i - \left(\sum_{l=1}^{n} |r_l|k_l\beta_l\right)\left(\sum_{l=1}^{n} |r_l|\right)^{-1}\right) \tag{2.38}$$

for $i = 1, ..n$, accompanied by the periodic boundary conditions $\vartheta_{i+n} = \vartheta_i$ $(i = 0, 1)$.

The system (2.38) can be represented by a symmetric positive semidefinite tridiagonal matrix with kernel containing n-dimensional vector each component of which is equal 1. Since $\sum_{i=1}^{n} b_i = 0$, where b_i are the components of the right hand side of (2.38), we have assured the existence of a solution which is also unique up to an additive constant. We choose the unique solution by imposing the constraint condition $\vartheta_0 = \vartheta_n = 0$.

Then, the linear systems (2.36) can be represented by two symmetric positive definite tridiagonal matrices for which we have the existence and uniqueness of a solution. In each discrete computational time step $j\tau$ the scheme (2.36)-(2.38) leads to solving of three tridiagonal systems, namely one for the redistribution of points along the curve and two for finding the new curve position.

2.3 Remark The scheme (2.36)-(2.38) can be derived using so-called *flowing finite volume method* (c.f. [100, 101, 102, 103]). Let us consider points $x_i, i = 1, ..., n$, belonging to a smooth curve $\Gamma_t = \mathrm{Image}(x(., t))$ where x is a solution of (2.20) at time t. By $[x_{i-1}, x_i]$ we

denote the arc of the curve between the points x_{i-1} and x_i. Let us consider a dual volume V_i around x_i consisting of part of the arc connecting centers $\tilde{x}_i, \tilde{x}_{i+1}$ of arcs $[x_{i-1}, x_i]$, $[x_i, x_{i+1}]$, respectively. Such a centered control volume is flowing and changing a length during the evolution respecting the new positions of the points x_i along the curve. Let us integrate intrinsic diffusion equation (2.20) along the flowing control volume V_i. We obtain

$$\int\limits_{V_i} \theta_1 \frac{\partial x}{\partial t} ds = \left[\frac{1}{\theta_2} \frac{\partial x}{\partial s} \right]_{\tilde{x}_i}^{\tilde{x}_{i+1}} . \tag{2.39}$$

Let us consider piecewise linear approximation of x, i.e. a polygon connecting points $x_i, i = 1, ..., n$. From (2.37) we can compute constant geometrical quantities k_i, ν_i, β_i for each line segment $[x_{i-1}, x_i]$. The quantity ϑ_i can be computed numerically again by solving flowing finite volume approximation of the intrinsic equation (2.34). Integrating (2.34) along $[x_{i-1}, x_i]$ yields

$$- \left[\frac{\beta}{k} \frac{\partial \vartheta}{\partial s} \right]_{x_{i-1}}^{x_i} = |r_i| \left(k_i \beta_i - \left(\sum_{l=1}^{n} |r_l| k_l \beta_l \right) \left(\sum_{l=1}^{n} |r_l| \right)^{-1} \right) . \tag{2.40}$$

Approximating $\frac{\partial \vartheta}{\partial s}(x_i)$ by $2\frac{\vartheta_{i+1} - \vartheta_i}{(|r_i| + |r_{i+1}|)}$ and $\frac{\beta}{k}(x_i)$ by $\frac{1}{2}(\frac{\beta_i}{k_i} + \frac{\beta_{i+1}}{k_{i+1}})$ we end up with the system (2.38). Now, approximating $\frac{\partial x}{\partial t}$ by $\dot{x}_i$ inside V_i we obtain from (2.39) the system of ordinary differential equations

$$\frac{1}{2}(|r_i|\theta_{1,i} + |r_{i+1}|\theta_{1,i+1})\dot{x}_i = \frac{1}{\theta_{2,i+1}} \frac{x_{i+1} - x_i}{|r_{i+1}|} - \frac{1}{\theta_{2,i}} \frac{x_i - x_{i-1}}{|r_i|} . \tag{2.41}$$

There is a range of possibilities how to solve this system. In order to obtain the scheme (2.36) we approximate time derivative by time difference of the new and previous discrete curve position and all nonlinear terms are taken from the previous time step and linear terms are considered at a new time level. The numerical simulations show that such approximation is sufficient in very general cases regarding accuracy and efficiency of computations.

We test properties of the model and the numerical scheme in evolution of convex as well as nonconvex (and nonrectifiable) initial curves in the presence of nonlinearity and anisotropy in the shape of function β. The effect of redistribution of discrete points representing evolving curve is documented at the same time. We have found several examples where the grid redistribution based on relative local length conservation of flowing curve segments is an important tool in correct handling of the curve evolution without other artificial operations like points removing or artificial cutting of the so-called swallow tails. The redistribution of grid points based on (2.34) preserves the initial discretization of a curve and thus makes its discrete representation smooth enough during evolution. First such examples are given in Fig. 19. In those experiments $\beta(k) = k$, i.e. we have classical curve shortening, and we start with initial curve with large variations in the curvature, namely

$$\begin{aligned} x_1(u) &= \cos(2\pi u), \\ x_2(u) &= \frac{1}{2}\sin(2\pi u) + \sin(x_1(u)) + \sin(2\pi u)(0.2 + \sin(2\pi u)\sin(6\pi u)\sin(6\pi u)) \end{aligned}$$

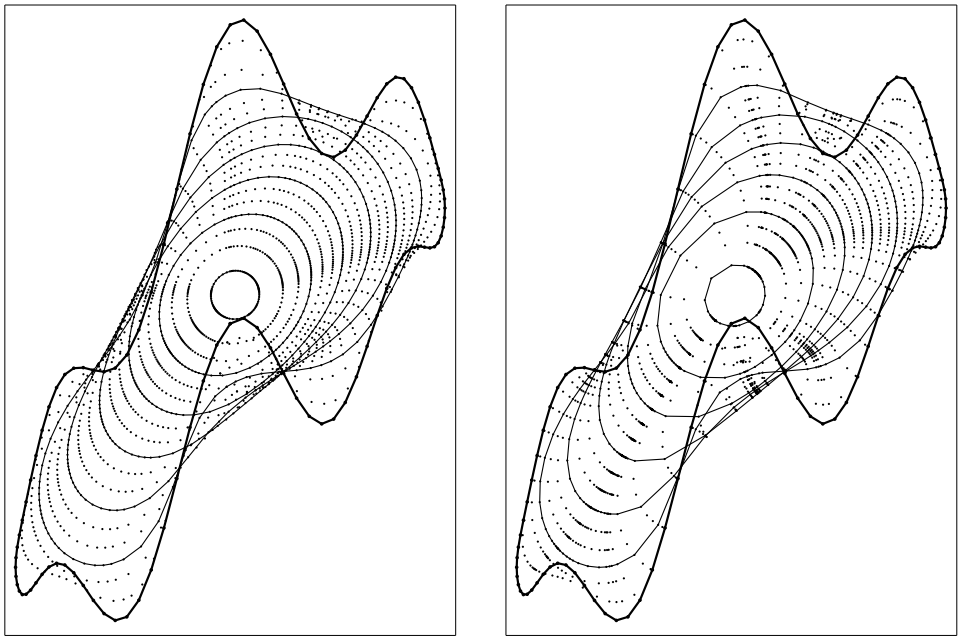

Figure 19: $\beta(k) = k$, discrete evolution using tangential redistribution of points (left) and without redistribution, only normal component of velocity is used (right).

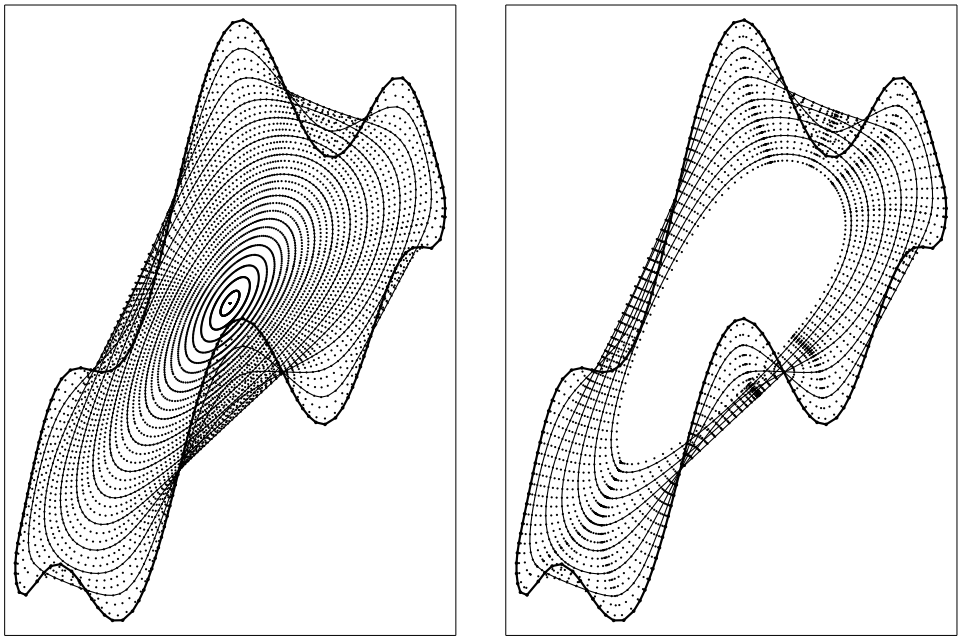

Figure 20: $\beta(k) = k^{1/3}$, discrete evolution using tangential redistribution preserving relative local length (left) and without redistribution, computation collapses due to vanishing of the local length element $|\partial_u x|$ (right).

$u \in [0,1]$, and initial discretization is given by uniform division of the range of parameter u. The curve is represented by 100 discrete points. Addition of a nontrivial tangential velocity obeying (2.34) leads to the evolution plotted in Fig. 19 left. In Fig. 19 right, the points move only in the normal direction and one can see their fast merging in several regions and very poor discrete representation in other pieces of the curve. In all experiments we have used the uniform time step $\tau = 0.001$. The blow up time for the curvature was $T_{max} = 0.363$. Isoperimetric ratio starting with 3.02 tends to 1.0 which is consistent with Grayson's theorem [52]. In both subfigures, we plot each 20-th discrete time step using discrete points representing the evolving curve and in each 60-th time step we plot also piecewise linear curve connecting those points.

In the next Fig. 20 we computed affine evolution of the same initial curve for the affine scale case $\beta(k) = k^{1/3}$. The initial curve has been discretized almost uniformly. In Fig. 20 left we show how this discretization is then preserved in evolution when using the scheme (2.34). The blow up time $T_{max} = 0.694$, a solution converges to an ellipse with the isoperimetric ratio stabilized on 1.33. This is in a good agreement with analytical results of Sapiro and Tannenbaum [121]. On the other hand, without any grid redistribution we can see rapid merging of several points leading to degeneracy in the distance $|r_i|$ corresponding to discretization of the term $|\partial_u x|$ and subsequent collapse of computation. In Fig. 20 right, one can see evolution until $t = 0.38$ just before collapse of the numerical solution.

In the next figures we show evolutions of initial "∞-like" curve. In the left and right parts of Fig. 21 the tangential velocity preserving relative local length has been used whereas in the middle, one can see that computation without tangential redistribution cannot prevent vanishing of the term $|\partial_u x|$. In Fig. 22 evolution of general nonconvex curves are plotted.

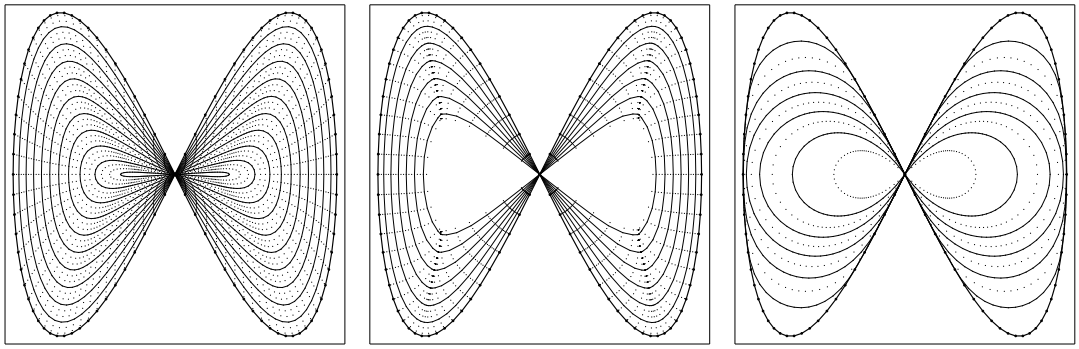

Figure 21: Evolution of "∞-like" curve; $\beta(k) = k^{1/4}$, using redistribution (left); $\beta(k) = k^{1/4}$, without redistribution leading to merging of points (middle); $\beta(k) = k^2$, using redistribution (right).

In Figures 23 - 24 the affine invariant evolution of initial ellipse with half-axes ratio 3:1 is shown. In Fig. 23 the exact blow up time $T_{max} = 1.560$ while the numerically computed one is equal 1.570 using time step $\tau = 0.001$ and 100 grid points for curve representation. The half-axes ratio as well as isoperimetric ratio were perfectly conserved during numerical evolution. Without any tangential velocity (i.e. $\alpha = 0$ and $\theta_2 = 1$), the numerical solution collapses as it should be obvious from Fig. 24.

In Figures 25 - 26 we present various computations including anisotropy in the model. The last numerical experiment represents affine invariant evolution of a spiral. In Fig. 27 we

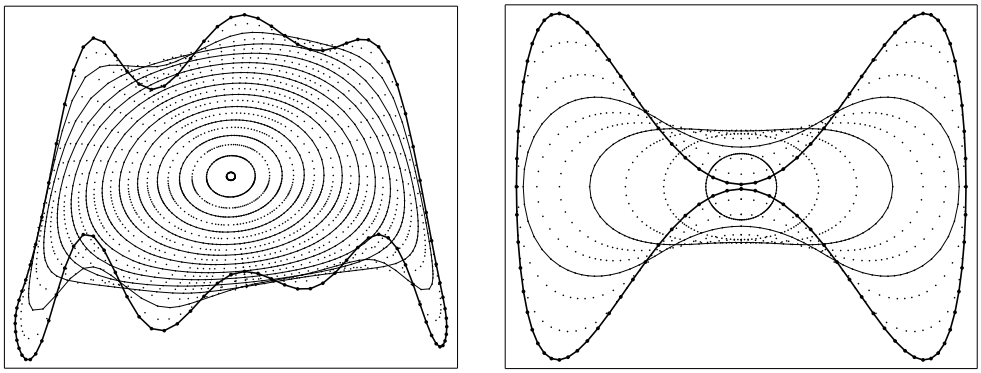

Figure 22: Evolution of general nonconvex curve using tangential redistribution of points, $\beta(k) = k^{1/2}$ (left), $\beta(k) = k^2$ (right).

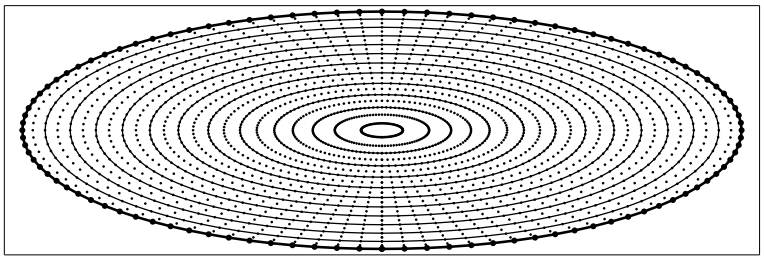

Figure 23: Affine invariant motion of ellipse using tangential redistribution of points.

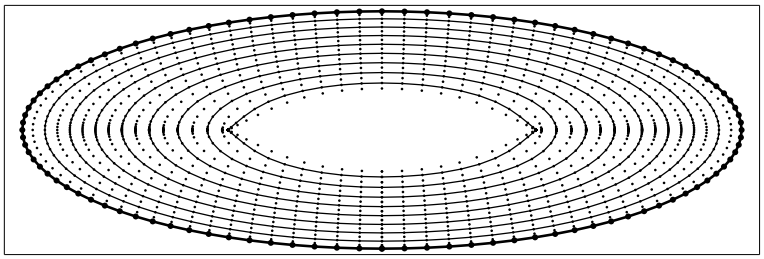

Figure 24: Computation using only normal component of velocity.

present several time moments of the motion until it is shrinking to an ellipse-like point.

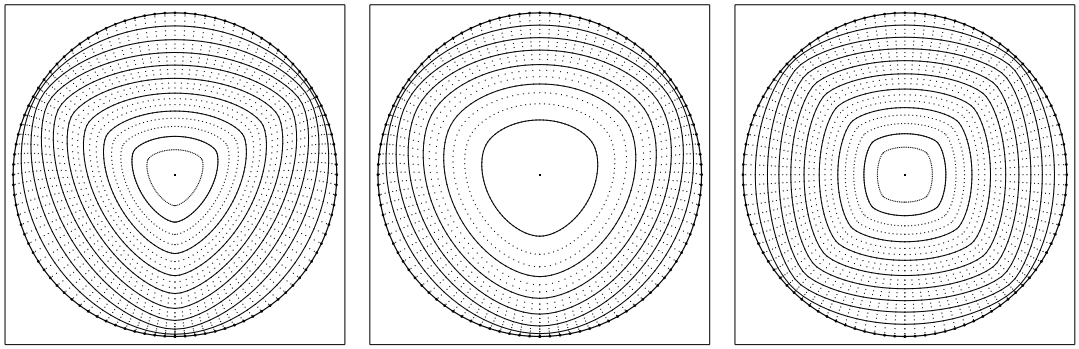

Figure 25: Anisotropic evolution of the unit circle using redistribution, $\beta(k,\nu) = (1 - 7/9\cos(3\nu))k$ (left), $\beta(k,\nu) = (1 - 7/9\cos(3\nu))k^2$ (middle), $\beta = (1 - 0.8\cos(4(\nu - \pi/4)))k$ (right).

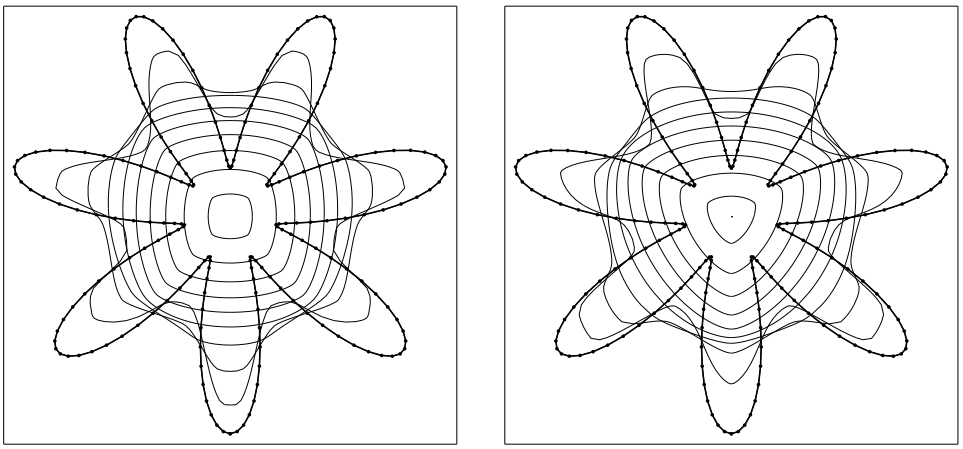

Figure 26: Anisotropic evolution of nonconvex curve using redistribution, $\beta = (1 - 0.8\cos(4(\nu - \pi/4)))k^{3/4}$ (left), $\beta = (1 - 7/9\cos(3\nu))k^{3/4}$ (right).

2.4 Solving the intrinsic system for geometric quantities

In this Section we develop a method where, additionally to previous Sections, normal velocity v may depend also on the curve position vector x. For the sake of simplicity and due to applications in mind, namely motion of interfaces with external forces, geodesic curvature flow and image segmentation (cf. Sections 1.8, 1.9), we will assume a linear dependence on the curvature k, i.e. we consider the normal velocity of the form

$$v = \beta(x,k,\nu) = a(x,\nu)\,k + c(x,\nu) \tag{2.42}$$

where $a > 0$ and c are smooth functions depending on x and ν. One could treat also nonlinear dependence of β on curvature k using ideas of the previous Sections, but we are not going to study such situation here.

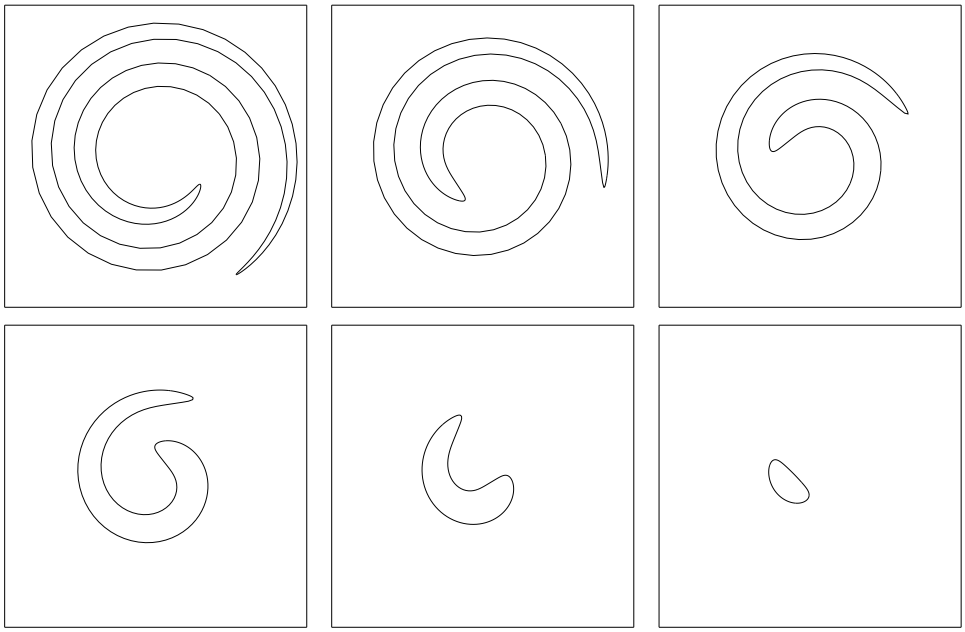

Figure 27: The sequence of evolving spirals for $\beta(k,\nu) = k^{1/3}$ using redistribution. The limiting curve is an ellipse rounded point.

Whereas in the previous Section the nonlinear system of governing equations (2.31) was only a theoretical tool to get analytical results for evolving curves, in [101, 102, 103] Mikula and Ševčovič discretize such a system to compute numerically the curve evolution. Since in (2.42) the flow depends on x itself, we must slightly modify (2.31) and close the system by adding equation for the position vector. Since $\partial_s \nu = k$ and $\partial_s \beta(x,k,\nu) = \beta'_k \partial_s k + \beta'_\nu \partial_s \nu + \nabla_x \beta . \vec{T}$ we end up with the following closed system of parabolic-ordinary differential equations:

$$\partial_t k = \partial_s^2 \beta + \alpha \partial_s k + k^2 \beta \,, \tag{2.43}$$

$$\partial_t \nu = \beta'_k \partial_s^2 \nu + (\alpha + \beta'_\nu) \partial_s \nu + \nabla_x \beta . \vec{T} \,, \tag{2.44}$$

$$\partial_t g = -gk\beta + \partial_u \alpha \,, \tag{2.45}$$

$$\partial_t x = \beta \vec{N} + \alpha \vec{T} \tag{2.46}$$

where $(u,t) \in [0,1] \times (0,T)$, $ds = g\,du$, $\vec{T} = \partial_s x = (\cos\nu, \sin\nu)$, $\vec{N} = \vec{T}^\perp = (-\sin\nu, \cos\nu)$, $\beta = \beta(x,k,\nu)$. A solution (k,ν,g,x) to (2.43)–(2.46) is subject to initial conditions

$$k(.,0) = k_0 \,,\ \nu(.,0) = \nu_0 \,,\ g(.,0) = g_0 \,,\ x(.,0) = x_0(.)$$

and periodic boundary conditions at $u = 0, 1$ except of ν for which we require the boundary condition $\nu(1,t) = \nu(0,t) + 2\pi$. The initial conditions for k_0, ν_0, g_0 and x_0 must satisfy natural compatibility constraints:

$$g_0 = |\partial_u x_0| > 0 \,,\ k_0 = g_0^{-3} \partial_u x_0 \wedge \partial_u^2 x_0 \,,\ \partial_u \nu_0 = g_0 k_0$$

following from (2.43) and Frenet's formulae applied to the initial curve $\Gamma_0 = \mathrm{Image}(x_0)$.

Notice that the functional α is still undetermined and it may depend on variables k, ν, g, x in various ways. One suitable choice of α was given in the previous Section, here we will give

further appropriate tangential velocities and embed the previous approach to a more general framework . As we have already seen, the construction of α is rather simple and consists in the analysis of the relative local length g/L. Let us take quantity θ defined as follows:

$$\theta = \ln(g/L).$$

As in the previous Section, taking into account local and global length equations we have

$$\partial_t \theta + k\beta - \langle k\beta \rangle_\Gamma = \partial_s \alpha \,. \tag{2.47}$$

By a choice of $\partial_s \alpha$ on the right hand side of (2.47) appropriately we can therefore control behavior of θ. Equation (2.47) can be also viewed as a kind of a *constitutive relation* determining redistribution of grid points along a curve.

Non-locally dependent tangential velocity functional:

We first analyze the case when $\partial_s \alpha$ (and so does α) depends on other geometric quantities k, β and g in a non-local way. The simplest possible choice of $\partial_s \alpha$ is:

$$\partial_s \alpha = k\beta - \langle k\beta \rangle_\Gamma \tag{2.48}$$

yielding $\partial_t \theta = 0$ in (2.47). Consequently,

$$\frac{g(u,t)}{L_t} = \frac{g(u,0)}{L_0} \quad \text{for any } u \in S^1,\ t \in [0, T_{max}) \,.$$

Notice that α can be uniquely computed from (2.48) under the additional renormalization constraint $\alpha(0,t) = 0$. Tangential redistribution driven by a solution α to (2.48) is refereed to as *a parametrization preserving relative local length.* It has been first utilized by Hou et al. for linear curve shortening in curvature equation formulation [61] and by Mikula and Ševčovič [100] for intrinsic heat equation formulation given in the previous Section.

A more general choice of α is based on the following setup [101, 102, 103]:

$$\partial_s \alpha = k\beta - \langle k\beta \rangle_\Gamma + \left(e^{-\theta} - 1\right) \omega(t) \tag{2.49}$$

where $\omega \in L_1^{loc}([0, T_{max}))$. If we additionally suppose

$$\int_0^{T_{max}} \omega(\tau)\, d\tau = +\infty \tag{2.50}$$

then, after insertion of (2.49) into (2.47) and solving the ODE $\partial_t \theta = \left(e^{-\theta} - 1\right) \omega(t)$, we obtain $\theta(u,t) \to 0$ as $t \to T_{max}$ and hence

$$\frac{g(u,t)}{L_t} \to 1 \quad \text{as } t \to T_{max} \quad \text{uniformly w.r. to } u \in S^1.$$

In this case redistribution of grid points along a curve becomes uniform as t approaches the maximal time of existence T_{max}. We will refer to the parametrization based on (2.49) to as *an asymptotically uniform parametrization.*

Asymptotically uniform redistribution of grid points is of a particular interest in the case when the family $\{\Gamma_t, t \in [0,T)\}$ shrinks to a point as $t \to T_{max}$, i.e. $\lim_{t \to T_{max}} L_t = 0$.

Then one can choose $\omega(t) = \kappa_2\langle k\beta\rangle_{\Gamma_t}$ where $\kappa_2 > 0$ is a positive constant. By (2.27), $\int_0^t \omega(\tau)\,d\tau = -\kappa_2 \int_0^t \ln L_\tau d\tau = \kappa_2(\ln L_0 - \ln L_t) \to +\infty$ as $t \to T_{max}$. On the other hand, if the length L_t is away from zero and $T_{max} = +\infty$ one can choose $\omega(t) = \kappa_1$, where $\kappa_1 > 0$ is a positive constant in order to meet the assumption (2.50).

Summarizing, in both types of grid points redistributions discussed above, a suitable choice of the tangential velocity functional α is given by a solution to

$$\partial_s\alpha = k\beta - \langle k\beta\rangle_\Gamma + (L/g - 1)\,\omega\,,\ \alpha(0) = 0\,, \tag{2.51}$$

where $\omega = \kappa_1 + \kappa_2\langle k\beta\rangle_\Gamma$ and $\kappa_1, \kappa_2 \geq 0$ are given constants.

If we insert tangential velocity functional α computed from (2.51) into (2.43)–(2.46) and make use of the identity $\alpha\partial_s k = \partial_s(\alpha k) - k\partial_s\alpha$ then the system of governing equations can be rewritten as follows:

$$\partial_t k = \partial_s^2\beta + \partial_s(\alpha k) + k\langle k\beta\rangle_\Gamma + (1 - L/g)\,k\omega\,, \tag{2.52}$$

$$\partial_t\nu = \beta'_k\partial_s^2\nu + (\alpha + \beta'_\nu)\partial_s\nu + \nabla_x\beta.\vec{T}\,, \tag{2.53}$$

$$\partial_t g = -g\langle k\beta\rangle_\Gamma + (L - g)\omega\,, \tag{2.54}$$

$$\partial_t x = \beta\vec{N} + \alpha\vec{T}\,. \tag{2.55}$$

It is worth to note that the strong local length shrinking term $k\beta$ in (2.45) which influences also strong reaction term $k^2\beta$ in (2.43) has been replaced by the averaged term $\langle k\beta\rangle_\Gamma$ in (2.54) and (2.52). The pointwise influence of these terms (e.g. in numerical solution) is replaced by the integral average. This is very important feature and indeed the main point behind the tangential redistribution. It allows us to construct a stable Lagrangian numerical scheme for curve evolution equation (2.42).

Locally dependent tangential velocity functional:

Another possibility for grid points redistribution along evolved curves is based on a tangential velocity functional defined locally. If we take $\alpha = \partial_s\theta$, i.e. $\partial_s\alpha = \partial_s^2\theta$ then the constitutive equation (2.47) reads as follows: $\partial_t\theta + k\beta - \langle k\beta\rangle_\Gamma = \partial_s^2\theta$. Since this equation has a parabolic nature one can expect that θ will be redistributed along the curve Γ due to the diffusion process. The advantage of the particular choice

$$\alpha = \partial_s\theta = \partial_s\ln(g/L) = \partial_s\ln g \tag{2.56}$$

has been already observed by Deckelnick in [35]. He analyzed the mean curvature flow of planar curves (i.e. $v = k$) by means of a solution to the intrinsic heat equation

$$\partial_t x = \frac{\partial_u^2 x}{|\partial_u x|^2}\,, \quad u \in S^1, t \in (0,T),$$

describing evolution of the position vector x of a curve $\Gamma_t = \mathrm{Image}(x(.,t))$. By using Frenet's formulae we obtain $\partial_t x = k\vec{N} + \alpha\vec{T}$ where $\alpha = \partial_s\ln g = \partial_s\ln(g/L) = \partial_s\theta$.

Inserting the tangential velocity functional $\alpha = \partial_s\theta = \partial_s(\ln g)$ into (2.43)–(2.46) we obtain the following system of governing equations:

$$\partial_t k = \partial_s^2 \beta + \alpha \partial_s k + k^2 \beta, \tag{2.57}$$
$$\partial_t \nu = \beta_k' \partial_s^2 \nu + (\alpha + \beta_\nu')\partial_s \nu + \nabla_x \beta . \vec{T}, \tag{2.58}$$
$$\partial_t g = -gk\beta + g\partial_s^2(\ln g), \tag{2.59}$$
$$\partial_t x = \beta \vec{N} + \alpha \vec{T}\,. \tag{2.60}$$

Notice that equation (2.59) is a nonlinear parabolic equation whereas (2.54) is a non-local ODE for the local length g.

2.4.1 Local existence and uniqueness of classical solutions to intrinsic system for geometrical quantities

In [101] has been proven local in time existence and uniqueness of a classical solution of the governing system of equations (2.43)–(2.46) by means of the abstract theory of nonlinear analytic semigroups developed by Angenent in [7]. If we denote $\Phi = (k, \tilde{\nu}, g, x)$ where $\tilde{\nu}(u) = \nu(u) + 2\pi u, u \in S^1$, then the system of governing equations can be rewritten as a fully nonlinear PDE of the form

$$\partial_t \Phi = f(\Phi), \qquad \Phi(0) = \Phi_0\,, \tag{2.61}$$

where $f(\Phi) = F(\Phi, \alpha(\Phi))$ and $F(\Phi, \alpha)$ is the right hand side of (2.52)–(2.55) if α is defined as in (2.51), or (2.57)–(2.60) if α is defined as in (2.56), resp. We had to shift the function ν by $2\pi u$ because of the boundary condition $\nu(1) = \nu(0) + 2\pi$ imposed on the tangential angle ν. Let $0 < \varrho < 1$ be fixed. By E_k^n, E_k^l we denote the following Banach spaces

$$\begin{aligned} E_k^n &= c^{2k+\varrho} \times c^{2k+\varrho} \times c^{1+\varrho} \times (c^{2k+\varrho})^2 \\ E_k^l &= c^{2k+\varrho} \times c^{2k+\varrho} \times c^{2k+\varrho} \times (c^{2k+\varrho})^2 \end{aligned}$$

where $k = 0, 1$, and $c^{2k+\varrho} = c^{2k+\varrho}(S^1)$ is the "little" Hölder space, i.e. the closure of $C^\infty(S^1)$ in the topology of the Hölder space $C^{2k+\varrho}(S^1)$ (see [8, 9, 7]). By the superscript "n" resp. "l" we distinguished the functional space setting for two different choices of the functional α depending on whether α is defined non-locally or locally, i.e,

$$\begin{aligned} E_k &= E_k^n \qquad \text{if } \alpha \text{ is defined as in (2.51)} \\ E_k &= E_k^l \qquad \text{if } \alpha \text{ is defined as in (2.56)} \end{aligned} \tag{2.62}$$

Then we have the following result (for proof we refer to [101]):

2.4 Theorem *Assume $\Phi_0 = (k_0, \tilde{\nu}_0, g_0, x_0) \in E_1$ where k_0 is the curvature, ν_0 is the tangential vector, $g_0 = |\partial_u x_0| > 0$ is the local length element of an initial regular curve $\Gamma_0 = \mathrm{Image}(x_0)$ and the Banach space E_k is defined as in (2.62). Assume $\beta = \beta(x, k, \nu)$ is a C^4 smooth and 2π-periodic function in the ν variable such that $\min_{\Gamma_0} \beta_k'(x_0, k_0, \nu_0) > 0$ and α is defined either as in (2.51) or (2.56). Then there exists a unique solution $\Phi = (k, \tilde{\nu}, g, x) \in C([0,T], E_1) \cap C^1([0,T], E_0)$ of the governing system of equations (2.43)–(2.46) defined on some small time interval $[0,T]$, $T > 0$. Moreover, if Φ is the maximal solution defined on $[0, T_{max})$ then either $T_{max} = +\infty$ or $\liminf_{t \to T_{max}^-} \min_{\Gamma_t} \beta_k'(x, k, \nu) = 0$ or $T_{max} < +\infty$ and $\max_{\Gamma_t} |k| \to \infty$ as $t \to T_{max}$.*

2.4.2 Full space-time discretization scheme

To describe the full space-time discretization scheme, we consider the normal velocity

$$v = \beta(x,k,\nu) = a(x,\nu)k + c(x,\nu)$$

and the tangential velocity functional α given by a linear combination of non-local and local tangential redistributions discussed above. Let us denote $\eta = \ln g$. Then we have $\theta = \ln(g/L) = \eta - \ln L$, and, for the redistribution functional α, we obtain

$$\partial_s\alpha = \varepsilon_1(k\beta - \langle k\beta\rangle_\Gamma) + \omega\,(L/g - 1) + \varepsilon_2\partial_s^2\eta \tag{2.63}$$

where $\varepsilon_1, \omega, \varepsilon_2$ are weights for parametrization preserving relative local length, asymptotically uniform parametrization and locally diffusive parametrization, respectively. Recall that the parameter setting: $\varepsilon_1 = 1, \varepsilon_2 = 0, \omega = \kappa_1 + \kappa_2\langle k\beta\rangle_\Gamma$ with $\kappa_1, \kappa_2 \geq 0$ is associated with the non-locally dependent tangential velocity functional α whereas the choice $\varepsilon_1 = 0, \varepsilon_2 = 1, \omega = 0$ corresponds to the locally defined α. The governing system of equations (2.43)–(2.46) can be rewritten in the form suitable for numerical approximation:

$$\partial_t k = \partial_s^2\beta + \partial_s(\alpha k) + k(k\beta - \partial_s\alpha), \tag{2.64}$$

$$\partial_t\nu = \beta_k'\partial_s^2\nu + (\alpha + \beta_\nu')\partial_s\nu + \nabla_x\beta.\vec{T}, \tag{2.65}$$

$$\partial_t\eta = -k\beta + \partial_s\alpha, \quad g = \exp(\eta), \tag{2.66}$$

$$\partial_t x = a(x,\nu)\partial_s^2 x + \alpha\partial_s x + \vec{c}(x,\nu) \tag{2.67}$$

where $\vec{c}(x,\nu) = c(x,\nu).\vec{N} = c(x,\nu)(-\sin\nu, \cos\nu)$. By using Frenet's formulae one can easily verify that the last equation (2.67) is equivalent to (2.46) in the case of linear dependence β on the curvature k.

In our computational method a numerical solution to the system (2.63)–(2.67) is represented by discrete plane points x_i^j where the index $i = 0, ..., n$, denotes space discretization and the index $j = 0, ..., m$, denotes a discrete time stepping. The approximation of an evolving curve in j-th discrete time step is thus given by a polygon with vertices $x_i^j, i = 0, ..., n$, for which the periodicity condition $x_0^j = x_n^j$ is required. If we take a uniform division of the time interval $[0, T]$ with a time step $\tau = \frac{T}{m}$ and a uniform division of the fixed parametrization interval $[0, 1]$ with a step $h = \frac{1}{n}$, a point x_i^j corresponds to $x(ih, j\tau)$.

To construct the approximation of an evolved curve we will derive systems of difference equations corresponding to (2.63)–(2.67) to be solved at every discrete time step. Difference equations will be given for discrete quantities α_i^j, η_i^j, r_i^j, k_i^j, ν_i^j, x_i^j, $i = 1, ..., n$, $j = 1, ..., m$, representing approximations of the unknowns α, η, gh, k, ν, x. The fully discrete quantities represent time stepping of time dependent functions $\alpha_i(t)$, $\eta_i(t)$, $r_i(t) = |x_i(t) - x_{i-1}(t)|$, $k_i(t)$, $\nu_i(t)$, $x_i(t)$ which will be also used in the sequel. The function $\alpha_i(t)$ represents tangential velocity of a flowing node $x_i(t)$. Functions $\eta_i(t)$, $r_i(t)$, $k_i(t)$, $\nu_i(t)$ represent piecewise constant approximations of the corresponding quantities in a flowing-in-time linear segment, the so-called *flowing finite volume* $[x_{i-1}(t), x_i(t)]$. We will also use the corresponding flowing dual volumes defined as: $[\tilde{x}_{i-1}, \tilde{x}_i]$, where $\tilde{x}_i = \frac{x_{i-1}+x_i}{2}$.

Our algorithm is semi-implicit in time. It means that all non-linear terms in equations are treated from the previous time step whereas linear terms are solved at the current time level. Such a discretization leads to a solution of linear systems of equations at every discrete

time level. At the j-th time step, $j = 1, .., m$, we first find discrete values of the tangential velocity functional α_i^j. Then the values of the redistribution parameter η_i^j are computed and subsequently utilised for updating discrete local lengths r_i^j. Using already computed local lengths, tridiagonal systems with periodic boundary conditions are constructed and solved for discrete curvature k_i^j, tangent angle ν_i^j and position vector x_i^j.

In order to construct a discretization of (2.63)–(2.66) we subsequently integrate equations over flowing finite volume $[x_{i-1}, x_i]$. Then, at any time t, for the tangential velocity functional α we have

$$\int_{x_{i-1}}^{x_i} \partial_s \alpha ds = \int_{x_{i-1}}^{x_i} \varepsilon_1 (k\beta - \langle k\beta \rangle_\Gamma)\, ds + \int_{x_{i-1}}^{x_i} \omega\,(L/g - 1) + \varepsilon_2 \partial_s^2 \eta \; ds$$

and thus

$$\alpha_i - \alpha_{i-1} = \varepsilon_1 (r_i k_i \beta(\tilde{x}_i, k_i, \nu_i) - r_i \langle k\beta \rangle_\Gamma) + \omega\,(L/n - r_i) + \varepsilon_2 \left(\frac{\eta_{i+1} - \eta_i}{q_i} - \frac{\eta_i - \eta_{i-1}}{q_{i-1}} \right).$$

By taking discrete time stepping in the previous relation we obtain the following expression for *discrete values of the tangential velocity functional* α_i^j

$$\begin{aligned} \alpha_i^j = \alpha_{i-1}^j \quad &+ \quad \omega(M^{j-1} - r_i^{j-1}) + \varepsilon_1 \left(r_i^{j-1} k_i^{j-1} \beta(\tilde{x}_i^{j-1}, k_i^{j-1}, \nu_i^{j-1}) - r_i^{j-1} B^{j-1} \right) \\ &+ \quad \varepsilon_2 \left(\frac{\eta_{i+1}^{j-1} - \eta_i^{j-1}}{q_i^{j-1}} - \frac{\eta_i^{j-1} - \eta_{i-1}^{j-1}}{q_{i-1}^{j-1}} \right) \end{aligned}$$

where

$$q_i^j = \frac{r_i^j + r_{i+1}^j}{2}, \quad \tilde{x}_i^{j-1} = \frac{x_{i-1}^{j-1} + x_i^{j-1}}{2}, \; i = 1, ..., n,$$

$\alpha_0^j = 0$, i.e. the point x_0^j is moved in the normal direction, and

$$\begin{aligned} M^{j-1} &= \frac{1}{n} L_{j-1}, \quad L_{j-1} = \sum_{l=1}^{n} r_l^{j-1}, \\ B^{j-1} &= \frac{1}{L_{j-1}} \sum_{l=1}^{n} r_l^{j-1} k_l^{j-1} \beta(\tilde{x}_l^{j-1}, k_l^{j-1}, \nu_l^{j-1}) \end{aligned}$$

and $\omega = \kappa_1 + \kappa_2 B^{j-1}$ with κ_1, κ_2 being redistribution parameters.

Concerning discretization of equation (2.66) we proceed along the following lines:

$$\begin{aligned} \int_{x_{i-1}}^{x_i} \partial_t \eta ds &= \int_{x_{i-1}}^{x_i} -k\beta + \varepsilon_1 (k\beta - \langle k\beta \rangle_\Gamma)\, ds + \int_{x_{i-1}}^{x_i} \omega\,(L/g - 1) + \varepsilon_2 \partial_s^2 \eta \, ds, \\ r_i \frac{d\eta_i}{dt} &= (\varepsilon_1 - 1) r_i k_i \beta(\tilde{x}_i, k_i, \nu_i) - \varepsilon_1 r_i \langle k\beta \rangle_\Gamma + \omega\,(L/n - r_i) + \varepsilon_2 \left[\partial_s \eta \right]_{x_{i-1}}^{x_i}. \end{aligned}$$

Replacing the time derivative by time difference, approximating $\partial_s \eta$ in nodal points, taking all linear terms at the new time level j and all the remaining terms from the previous time

level $j-1$ we obtain

$$r_i^{j-1}\frac{\eta_i^j-\eta_i^{j-1}}{\tau} = (\varepsilon_1-1)r_i^{j-1}k_i^{j-1}\beta(\tilde{x}_i^{j-1},k_i^{j-1},\nu_i^{j-1}) - \varepsilon_1 r_i^{j-1}B^{j-1} + \omega(M^{j-1}-r_i^{j-1}) + \varepsilon_2\left(\frac{\eta_{i+1}^j-\eta_i^j}{q_i^{j-1}} - \frac{\eta_i^j-\eta_{i-1}^j}{q_{i-1}^{j-1}}\right),$$

for $i=1,...,n$, $\eta_0^j=\eta_n^j$, $\eta_{n+1}^j=\eta_1^j$. Note that this is either an updating formula in the case $\varepsilon_2=0$ or a tridiagonal system (if $\varepsilon_2\neq 0$) for *new values of redistribution parameter* η. Next we *update local lengths* by the rule:

$$r_i^j=\exp(\eta_i^j),\quad i=1,...,n,\quad r_0^j=r_n^j,\quad r_{n+1}^j=r_1^j.$$

Subsequently, new local lengths are used for approximation of intrinsic derivatives in (2.64)–(2.67). First, we derive a discrete analogy of the curvature equation (2.64). We have

$$\int_{x_{i-1}}^{x_i}\partial_t k\,ds = \int_{x_{i-1}}^{x_i}\partial_s^2\beta(x,k,\nu)\,ds + \int_{x_{i-1}}^{x_i}\partial_s(\alpha k)ds + \int_{x_{i-1}}^{x_i}k(k\beta-\partial_s\alpha)\,ds\,,$$

$$r_i\frac{dk_i}{dt} = [\partial_s\beta(x,k,\nu)]_{x_{i-1}}^{x_i} + [\alpha k]_{x_{i-1}}^{x_i} + r_i k_i(k_i\beta(\tilde{x}_i,k_i,\nu_i) - (\alpha_i-\alpha_{i-1})).$$

Now, by replacing the time derivative by time difference, approximating k in nodal points by the average value of neighboring segments, taking all linear terms at the new time level j and taking all the remaining terms from the previous time level $j-1$ we obtain a *tridiagonal system* subject to periodic boundary conditions imposed on *new discrete values of curvature*:

$$a_i^j k_{i-1}^j + b_i^j k_i^j + c_i^j k_{i+1}^j = d_i^j,\quad i=1,...,n,\quad k_0^j=k_n^j,\quad k_{n+1}^j=k_1^j,$$

where

$$\begin{aligned}
a_i^j &= \frac{\alpha_{i-1}^j}{2} - \frac{a(\tilde{x}_{i-1}^{j-1},\nu_{i-1}^{j-1})}{q_{i-1}^j},\\
b_i^j &= r_i^j\left(\frac{1}{\tau} - k_i^{j-1}\beta(\tilde{x}_i^{j-1},k_i^{j-1},\nu_i^{j-1}) + \alpha_i^j - \alpha_{i-1}^j\right)\\
&\quad -\frac{\alpha_i^j}{2} + \frac{\alpha_{i-1}^j}{2} + \frac{a(\tilde{x}_i^{j-1},\nu_i^{j-1})}{q_{i-1}^j} + \frac{a(\tilde{x}_i^{j-1},\nu_i^{j-1})}{q_i^j},\\
c_i^j &= -\frac{\alpha_i^j}{2} - \frac{a(\tilde{x}_{i+1}^{j-1},\nu_{i+1}^{j-1})}{q_i^j},\\
d_i^j &= \frac{r_i^j}{\tau}k_i^{j-1} + \frac{c(\tilde{x}_{i+1}^{j-1},\nu_{i+1}^{j-1}) - c(\tilde{x}_i^{j-1},\nu_i^{j-1})}{q_i^j} - \frac{c(\tilde{x}_i^{j-1},\nu_i^{j-1}) - c(\tilde{x}_{i-1}^{j-1},\nu_{i-1}^{j-1})}{q_{i-1}^j}.
\end{aligned}$$

In the next step we solve the tangent angle equation (2.65) using the following approximation:

$$\int_{x_{i-1}}^{x_i}\partial_t\nu ds = \beta_k'(\tilde{x}_i,k_i,\nu_i)\int_{x_{i-1}}^{x_i}\partial_s^2\nu ds + \int_{x_{i-1}}^{x_i}\alpha\partial_s\nu\,ds$$
$$+\beta_\nu'(\tilde{x}_i,k_i,\nu_i)\int_{x_{i-1}}^{x_i}\partial_s\nu\,ds + \int_{x_{i-1}}^{x_i}\nabla_x\beta(\tilde{x}_i,\nu_i,k_i).\vec{T}\,ds,$$

$$r_i \tfrac{d\nu_i}{dt} = a(\tilde{x}_i, \nu_i)\,[\partial_s \nu]_{x_{i-1}}^{x_i} + [\alpha\nu]_{x_{i-1}}^{x_i}$$
$$-\nu_i \int_{x_{i-1}}^{x_i} \partial_s \alpha \, ds + \beta'_\nu(\tilde{x}_i, k_i, \nu_i)\,[\nu]_{x_{i-1}}^{x_i} + r_i \nabla_x \beta(\tilde{x}_i, \nu_i, k_i).(\cos\nu_i, \sin\nu_i)\,.$$

Again, values of ν in nodal points are approximated by the average of neighboring segments values, the time derivative is replaced by the time difference. By applying a semi-implicit approach we obtain

$$r_i^j \tfrac{\nu_i^j - \nu_i^{j-1}}{\tau} = a(\tilde{x}_i^{j-1}, \nu_i^{j-1}) \left(\tfrac{\nu_{i+1}^j - \nu_i^j}{q_i^j} - \tfrac{\nu_i^j - \nu_{i-1}^j}{q_{i-1}^j} \right) + \alpha_i^j \tfrac{\nu_{i+1}^j + \nu_i^j}{2} - \alpha_{i-1}^j \tfrac{\nu_i^j + \nu_{i-1}^j}{2} - \nu_i^j(\alpha_i^j - \alpha_{i-1}^j)$$
$$+\beta'_\nu(\tilde{x}_i^{j-1}, k_i^{j-1}, \nu_i^{j-1}) \left(\tfrac{\nu_{i+1}^j - \nu_{i-1}^j}{2} \right) + r_i^{j-1} \nabla_x \beta(\tilde{x}_i^{j-1}, \nu_i^{j-1}, k_i^j).(\cos\nu_i^{j-1}, \sin\nu_i^{j-1})\,.$$

Collecting the corresponding terms we again end up with a *tridiagonal system* with periodic boundary conditions *for new values of the tangent angle*

$$A_i^j \nu_{i-1}^j + B_i^j \nu_i^j + C_i^j \nu_{i+1}^j = D_i^j, \quad i = 1, ..., n\,, \quad \nu_0^j = \nu_n^j - 2\pi, \quad \nu_{n+1}^j = \nu_1^j + 2\pi,$$

where

$$\begin{aligned}
A_i^j &= \frac{\alpha_{i-1}^j + \beta'_\nu(\tilde{x}_i^{j-1}, k_i^j, \nu_i^{j-1})}{2} - \frac{a(\tilde{x}_i^{j-1}, \nu_i^{j-1})}{q_{i-1}^j}, \\
B_i^j &= \frac{r_i^j}{\tau} - (A_i^j + C_i^j), \\
C_i^j &= -\frac{\alpha_i^j + \beta'_\nu(\tilde{x}_i^{j-1}, k_i^j, \nu_i^{j-1})}{2} - \frac{a(\tilde{x}_i^{j-1}, \nu_i^{j-1})}{q_i^j}, \\
D_i^j &= \frac{r_i^j}{\tau}\nu_i^{j-1} + r_i^{j-1} \nabla_x \beta(\tilde{x}_i^{j-1}, \nu_i^{j-1}, k_i^j).(\cos\nu_i^{j-1}, \sin\nu_i^{j-1})\,.
\end{aligned}$$

In order to construct discretization for (2.67) we integrate it in the dual volume $[\tilde{x}_{i-1}, \tilde{x}_i]$. We obtain

$$\int_{\tilde{x}_i}^{\tilde{x}_{i+1}} \partial_t x \, ds = \int_{\tilde{x}_i}^{\tilde{x}_{i+1}} a(x,\nu) \partial_s^2 x \, ds + \int_{\tilde{x}_i}^{\tilde{x}_{i+1}} \alpha \partial_s x \, ds + \int_{\tilde{x}_i}^{\tilde{x}_{i+1}} \vec{c}(x,\nu) ds,$$
$$q_i \tfrac{dx_i}{dt} = a(x_i, \tfrac{\nu_i + \nu_{i+1}}{2})\,[\partial_s x]_{\tilde{x}_i}^{\tilde{x}_{i+1}} + \alpha_i(\tilde{x}_{i+1} - \tilde{x}_i) + q_i \vec{c}(x_i, \tfrac{\nu_i + \nu_{i+1}}{2}),$$
$$q_i \tfrac{dx_i}{dt} = a(x_i, \tfrac{\nu_i + \nu_{i+1}}{2}) \left(\tfrac{x_{i+1} - x_i}{r_{i+1}} - \tfrac{x_i - x_{i-1}}{r_i} \right) + \alpha_i(\tilde{x}_{i+1} - \tilde{x}_i) + q_i \vec{c}(x_i, \tfrac{1}{2}(\nu_i + \nu_{i+1})).$$

By replacing $\tilde{x}_i$ with the average of grid points, time derivative by time difference and using a semi-implicit approach in nonlinear terms we end up with *two tridiagonal systems for updating the position vector*

$$\mathcal{A}_i^j x_{i-1}^j + \mathcal{B}_i^j x_i^j + \mathcal{C}_i^j x_{i+1}^j = \vec{\mathcal{D}}_i^j\,, \quad i = 1, ..., n\,, \quad x_0^j = x_n^j, \quad x_{n+1}^j = x_1^j,$$

where

$$\begin{aligned}
\mathcal{A}_i^j &= -\frac{a(x_i, \frac{1}{2}(\nu_i + \nu_{i+1})}{r_i^j} + \frac{\alpha_i^j}{2}, \\
\mathcal{B}_i^j &= \frac{q_i^j}{\tau} - (\mathcal{A}_i^j + \mathcal{C}_i^j), \\
\mathcal{C}_i^j &= -\frac{a(x_i, \frac{1}{2}(\nu_i + \nu_{i+1})}{r_{i+1}^j} - \frac{\alpha_i^j}{2}, \\
\vec{\mathcal{D}}_i^j &= \frac{q_i^j}{\tau} x_i^{j-1} + q_i^j \vec{c}(x_i^{j-1}, \frac{1}{2}(\nu_i^j + \nu_{i+1}^j)).
\end{aligned}$$

Given a discretized initial curve x_i^0 further initial quantities for the algorithm are computed as follows:

$$\begin{aligned}
R_i &= (R_{i_1}, R_{i_2}) = x_i^0 - x_{i-1}^0, \quad i = 1, ..., n, \quad R_0 = R_n, \quad R_{n+1} = R_1, \\
r_i^0 &= |R_i|, \quad i = 0, ..., n+1, \quad \eta_i^0 = \exp(r_i^0), \quad i = 0, ..., n+1, \\
k_i &= \frac{1}{2r_i^0} \mathrm{sgn}(R_{i-1} \wedge R_{i+1}) \arccos\left(\frac{R_{i+1}.R_{i-1}}{r_{i+1}^0 r_{i-1}^0}\right), i = 1, ..., n, \quad k_0^0 = k_n^0, \; k_{n+1}^0 = k_1^0, \\
\nu_0^0 &= \arccos(R_{i_1}/r_i^0), \text{ if } R_{i_2} \geq 0, \quad \nu_0^0 = 2\pi - \arccos(R_{i_1}/r_i) \text{ if } R_{i_2} < 0, \\
\nu_i^0 &= \nu_{i-1}^0 + r_i^0 k_i^0, \quad i = 1, ..., n+1.
\end{aligned}$$

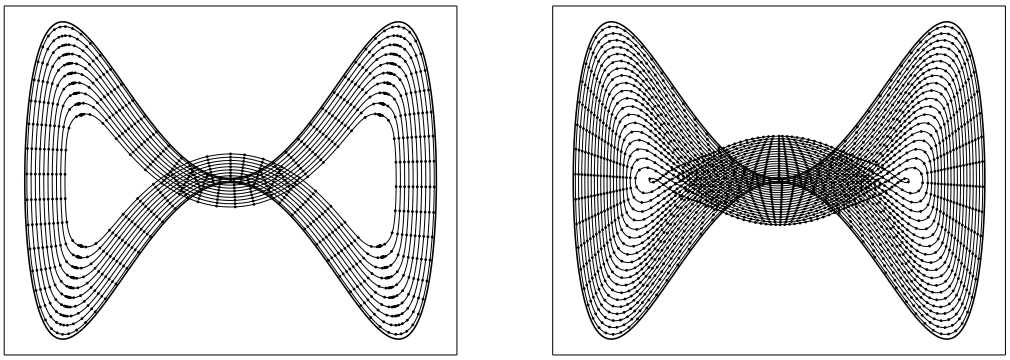

Figure 28: Isotropic curvature driven motion, $\beta(k) = \gamma k + F$, with $\gamma = 1$, $F = 10$, without (left) and with (right) asymptoticaly uniform tangential redistribution of grid points. The merging of the grid points in the left figure is overcome by proper tangential redistribution in the right.

2.4.3 Discussion on numerical experiments

In Figures 28-29 we present numerical solutions computed by the numerical scheme described in the previous Section for the case $v = \beta(k, \nu) \equiv \gamma k + F$. As an initial curve for computation shown in Fig. 28 we chose: $x_1(u) = \cos(2\pi u)$, $x_2(u) = 2\sin(2\pi u) - 1.99\sin^3(2\pi u)$, $u \in [0, 1]$. In Fig. 29 we considered an initial curve $x_1(u) = (1 - C\cos^2(2\pi u))\cos(2\pi u)$, $x_2(u) =$

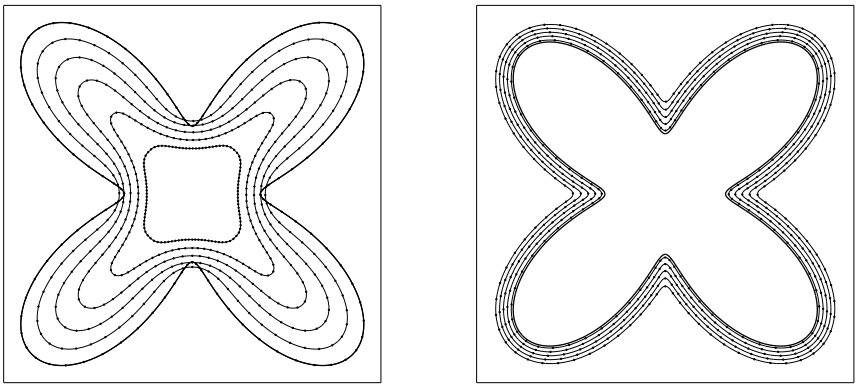

Figure 29: Isotropic curvature driven motion of an initial nonconvex curve including asymptoticaly uniform tangential redistribution of grid points; $\beta(k) = \gamma k + F$, with $\gamma = 1$ and $F = 10$ (left); $\gamma = 0.1$ and $F = -10$ (right). Resolution of sharp corners in the case of a highly dominant forcing term $F = -10$ (right) is possible.

Table 1: The exact T_{max} and numerical T^*_{max} blow-up times for the family of shrinking circles on a surface $\mathcal{M} = Graph(\phi)$.

$\phi(x)$	$\bar{\gamma}$	T_{max}	T^*_{max}
$1 - \|x\|^2$	0	0.187489	0.1876
	1	0.269843	0.2700
$\sqrt{1 - \|x\|^2}$	0	0.143833	0.1440
	1	0.169667	0.1698

$(1 - C\cos^2(2\pi u))\sin(2\pi u)$, $u \in [0,1]$ with $C = 0.7$. In Fig. 28 we chose $\tau = 0.00001$, 400 discrete grid points and we plotted every $150th$ time step. For computations depicted in Fig. 29 we took $\tau = 0.00001$ and 400 (Fig. 29 left) resp. 800 (Fig. 29 right) grid points. In presented experiments we have used the non-local tangential velocity functional α with parameters $\kappa_1 = \kappa_2 = 10$. It is worth to note that the method with tangential redistribution can correctly resolve the sharp corner formation and their further evolution as seen in Fig. 29 right, which is not an easy task at all for any Lagrangian scheme.

Now we consider a flow of curves on a given graph surface driven by the geodesic curvature and external force (1.27). Then the flow of vertically projected planar curves is driven by the geometric equation (1.31) with coefficients $a(x,\nu), b(x,\nu)$ defined as in (1.32).

In the first example we have tested accuracy of the computed numerical blow-up time for the family of shrinking curves with finite extinction time. Comparison of exact and numerical blow-up of a family of shrinking circles on a surface $\mathcal{M} = \{(x,\phi(x)), x \in \Omega \subset \mathbb{R}^2\}$ for various ϕ and $\vec{G} = -(0,0,\bar{\gamma})$ is presented in Table 1. In this example the time step was $\tau = 0.0001$, there were 100 grid points and we chose the circle with radius 0.5 centered at the origin as an initial curve.

In the example shown in Fig. 30 we present inner and outer evolution of circles belonging

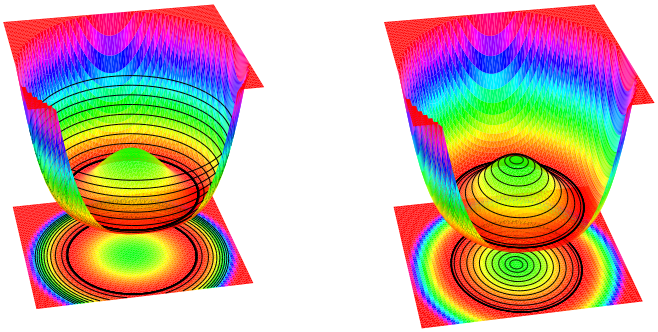

Figure 30: A geodesic flow on the "hat-like" surface and its vertical projection to the plane. Outer and inner evolutions of initial circles Γ_0 with radii $r_0 = 1.5$ (left) and $r_0 = 0.1$ (right).

to a "hat-like" surface and converging towards a circular valley. We chose $\phi(x) = (1 - |x|^2)^2$, $t \in (0, 0.0315)$ and there was a strong external force $\bar{\gamma} = 100$. Profiles of the radius $r = r(t)$ for inner and outer evolution are presented in Fig. 31.

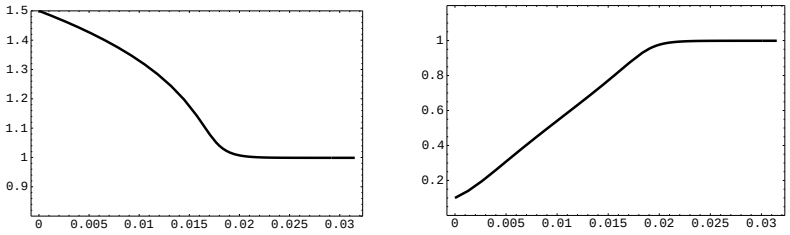

Figure 31: Time evolution of the radius of shrinking circles (left) and expanding circles (right).

The next example having an explicit solution is the family of shrinking circles belonging to a transversal plane. The projection to the base plane is the family of shrinking ellipses. More precisely, we consider a surface $\mathcal{M}$ as a graph of $\phi(x_1, x_2) = kx_1$ where $k \in \mathbb{R}$ is a fixed parameter. Let $r(t), t \geq 0$, be a solution to ODE $\dot{r} = -1/r$, $r(0) = r_0 > 0$. Then $r(t) = \sqrt{2(T-t)}$ where $T = r_0^2/2$ and the normal velocity v of a family of shrinking ellipses $\Gamma_t = \{x(u,t), u \in [0,1]\}$, $x(u,t) = r(t)\left((1+k^2)^{-1/2}\cos(2\pi u), \sin(2\pi u)\right)$ satisfies the geometric equation $v = \beta(x, k, \nu)$ where β is given by (1.31) with zero external force, i.e. $\bar{\gamma} = 0$. Clearly, the family of shrinking circles $\mathcal{G}_t = \{(x, \phi(x)), x \in \Gamma_t\}$ on the surface $\mathcal{M}$ satisfies the geometric equation $\mathcal{V} = \mathcal{K}_g$. In the numerical experiment shown in Fig. 32 we chose $\phi(x_1, x_2) = x_1$, $t \in (0, 0.5)$, $\bar{\gamma} = 0$ and $r_0 = 1$.

An important tool for testing numerical algorithms is the so-called experimental order of convergence (EOC). The idea behind the definition of EOC is rather simple. Suppose that a numerical scheme has an order of convergence α with respect to a spatial discretization parameter h. Here h can be defined as: $h = 1/n$ where n is the number of grid points. It means that the error $err(h)$ (calculated in a certain prescribed norm) of an approximate numerical solution and the true solution satisfies $err(h) \approx h^\alpha$. Now if we halve the discretization step h we can determine the exponent α of EOC as follows:

$$\alpha = \log_2 \left(err(h)/err(h/2) \right) .$$

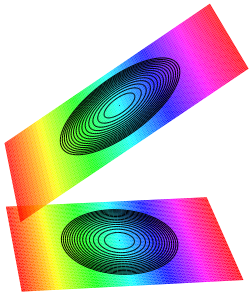

Figure 32: A geodesic flow with no external force ($\bar{\gamma} = 0$) on an affine plane and its vertical projection to the plane. We plot inner evolution of an initial ellipse corresponding to a circle with radius $r_0 = 1$ belonging to transversal plane over the time interval $(0, 0.5)$.

We have tested the experimental order of convergence for the explicit example of shrinking circles on a transversal plane. Since the solved system of governing equations has the parabolic nature we adopted the natural constraint between time stepping and space discretization: $\tau = h^2/2$. In Table 2 we present results obtained by using non-local tangential velocity functional defined as in (2.51) whereas in Table 3 we summarize results obtained by using the locally depending tangential velocity functional defined as in (2.56). Those two methods seem to have the same strength measured in terms of the EOC. Also in case of these highly nonlinear problems the experimental order of convergence in all quantities is at least one, which is usual for the finite volume approximations.

Table 2: Computation using the non-local tangential velocity α defined as in (2.51); $L_p((0,T), L_2(S^1))$ errors and their EOC for x, k, ν and g.

h	p	x	eoc	k	eoc	ν	eoc	g	eoc
0.1	2	0.009398		0.07258		0.1286		0.03289	
	∞	0.01421		0.1162		0.1371		0.05433	
0.05	2	0.004015	1.227	0.03388	1.099	0.06842	0.9109	0.008914	1.884
	∞	0.005955	1.255	0.06471	0.8445	0.07381	0.8939	0.01483	1.873
0.025	2	0.001877	1.097	0.0165	1.038	0.03473	0.978	0.002296	1.957
	∞	0.002761	1.109	0.03347	0.9508	0.03761	0.9727	0.003808	1.961
0.0125	2	0.0009225	1.025	0.00827	0.9961	0.01743	0.9944	0.0005814	1.982
	∞	0.001352	1.031	0.01705	0.9734	0.01889	0.9931	0.0009625	1.984
0.00625	2	0.0004588	1.008	0.004105	1.011	0.008723	0.9991	0.0001454	1.999
	∞	0.0006711	1.01	0.008483	1.007	0.009458	0.9983	0.0002404	2.001

The next example of this Section illustrates a geodesic flow $\mathcal{V} = \mathcal{K}_g$ on a surface with two sufficiently high humps. In Fig. 33 we considered a surface $\mathcal{M}$ defined as a graph of the function $\phi(x) = 6(f(x_1 - 1, x_2) + f(x_1 + 1, x_2))$ where $f(x) = 2^{-1/(1-|x|^2)}$ for $|x| < 1$ and $f(x) = 0$ for $|x| \geq 1$ is a smooth bump function. We took the time step $\tau = 0.0002$. Initial curve was an ellipse centered at the origin with axes 2 and $\sqrt{2}$. The spatial mesh contained

Table 3: Computation using the local tangential velocity α defined as in (2.56); $L_p((0,T),L_2(S^1))$ errors and their EOC for x, k, ν and g.

h	p	x	eoc	k	eoc	ν	eoc	g	eoc
0.1	2	0.009608		0.07163		0.1286		0.03324	
	∞	0.01463		0.1135		0.1371		0.05545	
0.05	2	0.004064	1.241	0.03369	1.088	0.06845	0.9095	0.009231	1.849
	∞	0.006049	1.274	0.06387	0.83	0.07381	0.8939	0.01549	1.84
0.025	2	0.001889	1.106	0.01642	1.037	0.03475	0.9779	0.002389	1.95
	∞	0.00278	1.122	0.03318	0.9447	0.03761	0.9727	0.003985	1.958
0.0125	2	0.0009264	1.028	0.008235	0.9954	0.01744	0.9944	0.0006056	1.98
	∞	0.001356	1.035	0.01692	0.9719	0.01889	0.9931	0.001008	1.984
0.00625	2	0.0004604	1.009	0.004088	1.01	0.008728	0.999	0.0001515	1.999
	∞	0.0006729	1.011	0.00842	1.006	0.009458	0.9983	0.0002517	2.001

400 grid points. The initial curve was evolved until the time $T = 13$. As it can be seen from Fig. 33 the evolving family of surface curves approaches a closed geodesic as $t \to \infty$. The existence of a closed geodesic curve follows from a simple calculation of the lower bound of the length of a curve passing through tops of both humps at the same moment which should be greater than $4\sqrt{3^2+1^2} \approx 12.64$. Since the length of the initial curve is approximately 10.81 and the flow of surface curves is length shortening the family of surface curves converges to a nontrivial closed geodesic with the length strictly less than 10.81.

Finally, we apply our computational method to the image segmentation problem. Let us consider the normal velocity $v = \beta(x,k,\nu)$ where

$$\beta(x,k,\nu) = \phi(x)k - b(\phi(x))\nabla\phi(x).\vec{N}\,,$$

$\phi(x) = 1/(1+|\nabla I(x)|^2)$ and $I(x)$ is a given image intensity function. The numerical experiment is shown in Fig. 34. We look for an edge in a 2D slice of a real 3D echocardiography which was prefiltered by the method of [125]. The testing data set (the image function I) is a courtesy of Prof. Claudio Lamberti, DEIS, University of Bologna. We have inserted an initial ellipse discretized by 400 points into the slice close to an expected edge (Fig. 34 left). Then it was evolved according to the normal velocity described above using the time stepping $\tau = 0.0001$ and non-local redistribution strategy with parameters $\kappa_1 = 20$, $\kappa_2 = 1$ until the limiting curve has been formed (400 time steps). The final curve representing the edge in the slice can be seen in Fig. 34 right.

Next we present results for the image segmentation problem computed by means of a geodesic flow with external force. We consider an artificial image whose intensity function

$$I(x) = \frac{1}{2} + \frac{1}{\pi}\mathrm{arctg}\left(12.5 - 100\left(|x|\frac{2x_1^2+|x|^2}{4x_1^2+|x|^2}\right)^2\right)$$

is depicted in Fig. 14. If we take $\phi(x) = 1/(1+|\nabla I(x)|^2)$ then the surface $\mathcal{M}$ defined as a graph of ϕ has a sharp narrow valley corresponding to points of the image in which the

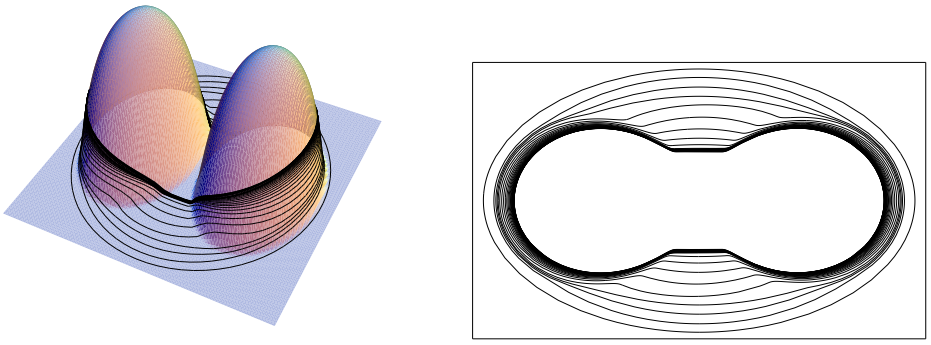

Figure 33: A geodesic flow on a surface with two sufficiently high humps (left) and its vertical projection to the plane (right). The evolving family of surface curves approaches a closed geodesic as $t \to \infty$.

gradient $|\nabla I(x)|$ is very large representing thus an edge in the image. In contrast to the previous example shown in Fig. 34 we will make use of the flow of curves on a surface $\mathcal{M}$ driven by the geodesic curvature and strong "gravitational-like" external force $\mathcal{F}$. According to Section 1.9 such a surface flow can be represented by a family of vertically projected plane curves driven by the normal velocity

$$v = a(x, \nu)k - b(x, \nu)\nabla\phi(x).\vec{N}$$

where coefficients a, b are defined as in (1.32) with strong external force coefficient $\bar{\gamma} = 100$. Results of computation are presented in Fig. 35.

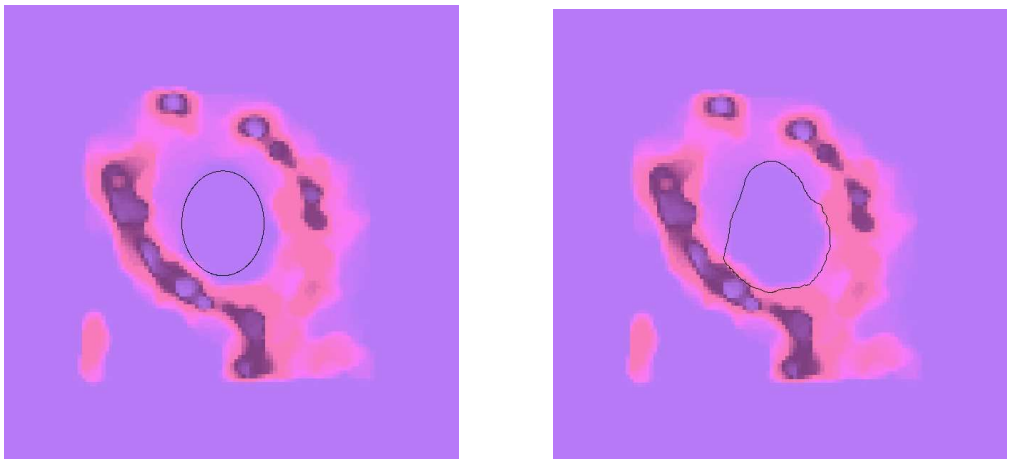

Figure 34: An initial ellipse is inserted into the 2D slice of a prefiltered 3D echocardiography (left), the slice together with the limiting curve representing the edge (right).

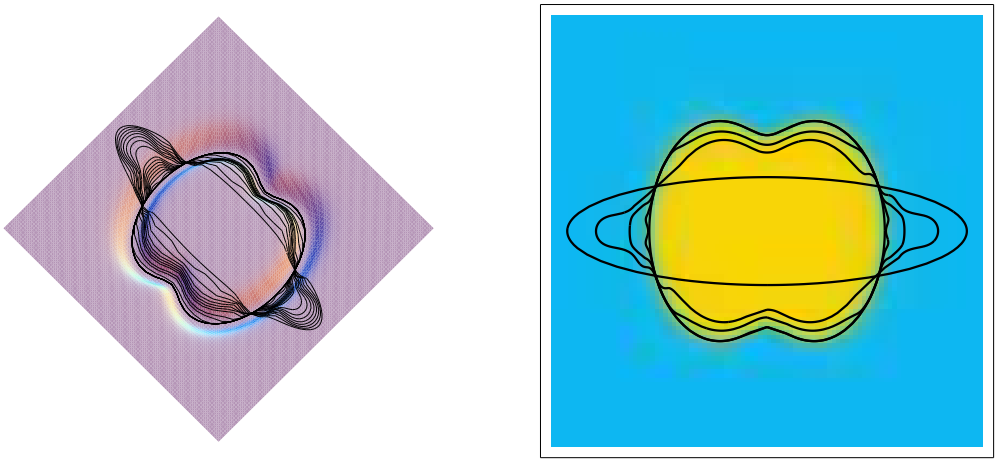

Figure 35: A geodesic flow on a flat surface with a sharp narrow valley (left) and its vertical projection to the plane with density plot of the image intensity function $I(x)$ (right).

3 Computational methods for the regularized Perona-Malik and level-set type equations

The aim of this Chapter is to present numerical schemes for solving some of the nonlinear diffusion equations presented in Chapter 1 and for the level-set formulations of the problems presented in Chapter 2. We will be mainly concentrate on applications to image processing. Since images are given on a discrete grid (pixel/voxel structure), we discretize the PDEs to get a numerical scheme implemented on a computer. One can use a wide range of methods devoted to the numerical solution of nonlinear PDEs. However, semi-implicit schemes [31, 70, 16, 17, 137, 138, 96, 81, 82, 83, 91, 97, 58, 59, 60, 115, 40], where the nonlinear terms of the equation are treated from the previous discrete scale step, and linear terms are considered at the current scale level, have favorable stability and efficiency properties. For space discretization either finite element method [70, 16, 17, 115, 40], finite/complementary volume method [96, 81, 82, 83, 59, 60] or finite difference methods [137, 138] can be used. In this Chapter we discuss discretization in space by variational techniques, i.e., using finite element and finite/complementary volume methods. They are based on integral (weak, variational) formulations of the initial-boundary value problems for PDEs. Variational methods have a strong physical background since they are based on principles like minimization of energy (finite element method) or conservation laws (finite and complemetary volume methods). They allow a clear and physically meaningful derivation of difference equations which are local and easy to implement. Convergence of the schemes to weak solutions of the PDEs can be studied using methods of functional analysis. Such convergence analysis indicates that the discrete model really follows properties of the continuos one when we refine the image resolution. It is an important property, since the continuos PDE is usually designed to respect various differential characteristics of the "continuos image" which is recorded on a photosensitive surface and pixelize.

For our presentation we have chosen two representative geometry-driven diffusion models: the regularized Perona-Malik anisotropic diffusion equation due to Catté, P.L.Lions, Morel and Coll [31]

$$u_t - \nabla.(g(|\nabla G_\sigma * u|)\nabla u) = 0, \tag{3.1}$$

and the nonlinear degenerate diffusion equation of mean curvature flow type due to Alvarez, P.L.Lions and Morel [4]

$$u_t - g(|\nabla G_\sigma * u|)|\nabla u|\nabla.(\frac{\nabla u}{|\nabla u|}) = 0, \tag{3.2}$$

where $u(t,x)$ is an unknown function defined in $Q_T \equiv I \times \Omega$. They are accompanied by the boundary and initial conditions (1.3)–(1.4), and for both equations we assume the hypotheses (1.5)–(1.7). Both models represent a similar view to image selective smoothing, in the sense that edge positions are preserved in the image multiscale analysis, see Chapter 1.

In the first Section of this Chapter we will describe semi-implicit scale discretization of both equations and we establish some of their stability properties. In the next Sections we describe in detail finite element and finite volume spatial discretization of equation (3.1) and complementary volume discretization of equation (3.2).

3.1 Remark In the next paragraphs, we will use the standard notations for the functional spaces $L_p(\Omega)$, $p \geq 1$, and $C^k(\overline{\Omega})$. By V we denote the Sobolev space $W^{1,2}(\Omega)$ of $L_2(\Omega)$-functions with square integrable weak derivates [84]. The absolute value will be denoted by $|\cdot|$ and the norm by $\|\cdot\|$ with a subscript given by the corresponding functional space. By C we denote a general (large) constant.

3.1 Semi-discretizations in scale

We start by the semi-discretizations in scale of the problems given by (3.1) and (3.2), respectively. Choosing $N \in \mathbb{N}$ we obtain the length of the uniform discrete scale step $k = T/N$. We replace the scale derivative in (3.1), (3.2) by backward difference. The nonlinear terms of the equations are treated from the previous scale step while the linear terms are considered at the current scale level – this means semi-implicitness of the method. Let us start with approximation in scale of equation (3.1).

Semi-discrete linear scheme for solving equation (3.1) [70]: *Let $N \in \mathbb{N}$, $k = T/N$ and $\sigma > 0$ be fixed numbers, and let u^0 be given by (1.4). For every $n = 1, \ldots, N$, we look for a function u^n which is a solution of the equation*

$$\frac{u^n - u^{n-1}}{k} - \nabla.(g(|\nabla G_\sigma * u^{n-1}|)\nabla u^n) = 0. \tag{3.3}$$

Due to smoothing properties of convolution,

$$g^{n-1} := g(|\nabla G_\sigma * u^{n-1}|) \geq \nu > 0 \tag{3.4}$$

holds true and then it is not difficult to see that there exist unique variational solution u^n of (3.3) at every discrete scale step for which the stability estimates

$$\|u^n\|_{L_2(\Omega)} \leq \|u^0\|_{L_2(\Omega)}, \qquad \|u^n\|_{L_\infty(\Omega)} \leq \|u^0\|_{L_\infty(\Omega)}, \qquad n = 1, \ldots, N,$$
$$\sum_{n=1}^{N} \|\nabla u^n\|^2_{L_2(\Omega)} k \leq C, \qquad \sum_{n=1}^{N} \|u^n - u^{n-1}\|^2_{L_2(\Omega)} \leq C,$$

hold, too [70, 17]. Moreover, for the so-called Rothe's step function $\bar{u}^{(N)}(t) = u^n$, $(n-1)k < t \leq nk$, Kačur and Mikula [70] proved convergence in $L_2(Q_T)$ to the unique weak solution of (3.1).

In spite of equation (3.1), the equation (3.2) is not in divergence form. For second order partial derivatives, as is usual in variational methods, we would like to use integration by parts or the divergence theorem to get an integral formulation (see the next Sections). Thus, we first move the term in front of the divergence to the time derivative, and then we write semi-implicit discretization of (3.2) in scale

Semi-discrete linear scheme for solving equation (3.2) [59]: *Let $N \in \mathbb{N}$, $k = T/N$ and $\sigma > 0$ be fixed numbers, and let u^0 be given by (1.4). For every $n = 1, \ldots, N$, we look for a function u^n which is a solution of the equation*

$$\frac{1}{g(|\nabla G_\sigma * u^{n-1}|)|\nabla u^{n-1}|}\frac{u^n - u^{n-1}}{k} - \nabla.\left(\frac{\nabla u^n}{|\nabla u^{n-1}|}\right) = 0. \tag{3.5}$$

At this place, let us note another possible approach for the scale discretization of (3.2) based on an interesting approximation of the degenerate diffusion term given in [135]. Following the idea of Walkington one could, instead of (3.5), use the following implicit (nonlinear) semi-discretization

$$\frac{1}{g^{n-1}|\nabla u^{n-1}|}\frac{u^n-u^{n-1}}{\tau}-2\nabla.\left(\frac{\nabla u^n}{|\nabla u^n|+|\nabla u^{n-1}|}\right)=0. \tag{3.6}$$

Walkington considered averaging the gradient terms from the previous and current scale step in the denominator of the divergence term to get an important $W^{1,1}$ estimate, i.e. estimate on the decay of the total variation of discrete solutions. This estimate is a basic property of the flow by mean curvature and of a solution of the level set equation as well [135] and can be interpreted as a curve shortening property which means smoothing of the image level lines (see previous Chapters). Any reasonable numerical approximation should respect this fact. Following [135], one can multiply (3.6) by u^n-u^{n-1} and integrate it over Ω. Then using integration by parts and zero Neumann boundary conditions one gets

$$\int_\Omega \frac{(u^n-u^{n-1})^2}{\tau g^{n-1}|\nabla u^{n-1}|}dx+2\int_\Omega \frac{\nabla u^n.(\nabla u^n-\nabla u^{n-1})}{|\nabla u^{n-1}|+|\nabla u^n|}dx=0 \tag{3.7}$$

where short notation (3.4) has been used. Using the relation

$$2a(a-b)=a^2-b^2+(a-b)^2 \tag{3.8}$$

where a,b are arbitrary real numbers, and by a simple manipulations related to the sum in the denominator we get

$$\begin{aligned}&\int_\Omega \frac{(u^n-u^{n-1})^2}{\tau g^{n-1}|\nabla u^{n-1}|}dx+\int_\Omega \frac{|\nabla u^n|^2-|\nabla u^{n-1}|^2}{|\nabla u^{n-1}|+|\nabla u^n|}dx+\\&+\int_\Omega \frac{|\nabla u^n-\nabla u^{n-1}|^2}{|\nabla u^{n-1}|+|\nabla u^n|}dx=\int_\Omega \frac{(u^n-u^{n-1})^2}{\tau g^{n-1}|\nabla u^{n-1}|}dx+\\&+\int_\Omega \frac{|\nabla u^n-\nabla u^{n-1}|^2}{|\nabla u^{n-1}|+|\nabla u^n|}dx+\left(\int_\Omega |\nabla u^n|dx-\int_\Omega |\nabla u^{n-1}|dx\right)=0\end{aligned} \tag{3.9}$$

which means that

$$\|\nabla u^n\|_{L_1(\Omega)}\le\|\nabla u^{n-1}\|_{L_1(\Omega)} \tag{3.10}$$

and by recursion

$$\|\nabla u^n\|_{L_1(\Omega)}\le\|\nabla u^0\|_{L_1(\Omega)},\quad 1\le n\le N. \tag{3.11}$$

It represents the important stability property of this nonlinear scheme. However, the previous scheme leads in each discrete scale level (after any spatial discretization) to solving of a nonlinear system of equations. This is a rather non-efficient approach. In order to have convergence, which is however very slow, one has to use fixed point-like nonlinear iterations; faster possibilities like Newton's method have no guarantees for convergence [135] and are rather complicated from the implementation point of view.

In [59] Handlovičová, Mikula and Sgallari get the estimate (3.11) also for the scheme (3.5) which is much more simple and efficient. Since it is linear, it allows the use of the fast preconditioned iterative linear solvers at every scale level. Let us multiply (3.5) by $u^n - u^{n-1}$, then integrating it over Ω and using (3.8) we get

$$\int_\Omega \frac{(u^n - u^{n-1})^2}{\tau g^{n-1} |\nabla u^{n-1}|} dx + \frac{1}{2} \int_\Omega \frac{|\nabla u^n|^2 - |\nabla u^{n-1}|^2 + |\nabla u^n - \nabla u^{n-1}|^2}{|\nabla u^{n-1}|} dx = 0.$$

Since

$$|\nabla u^n - \nabla u^{n-1}|^2 = (|\nabla u^n| - |\nabla u^{n-1}|)^2 + \left(\frac{\nabla u^n}{|\nabla u^n|} - \frac{\nabla u^{n-1}}{|\nabla u^{n-1}|} \right)^2 |\nabla u^n| \, |\nabla u^{n-1}|,$$

we get

$$\int_\Omega \frac{(u^n - u^{n-1})^2}{\tau g^{n-1} |\nabla u^{n-1}|} dx + \frac{1}{2} \int_\Omega \frac{|\nabla u^n|^2 - |\nabla u^{n-1}|^2 - (|\nabla u^n| - |\nabla u^{n-1}|)^2}{|\nabla u^{n-1}|} dx$$
$$+ \int_\Omega \frac{(|\nabla u^n| - |\nabla u^{n-1}|)^2}{|\nabla u^{n-1}|} dx + \frac{1}{2} \int_\Omega \left(\frac{\nabla u^n}{|\nabla u^n|} - \frac{\nabla u^{n-1}}{|\nabla u^{n-1}|} \right)^2 |\nabla u^n| dx = 0.$$

Due to positivity of other terms we get for the second term

$$\int_\Omega \frac{|\nabla u^n| \, |\nabla u^{n-1}| - |\nabla u^{n-1}|^2}{|\nabla u^{n-1}|} dx \leq 0$$

which gives

$$\|\nabla u^n\|_{L_1(\Omega)} \leq \|\nabla u^{n-1}\|_{L_1(\Omega)}, \tag{3.12}$$

and thus

$$\|\nabla u^n\|_{L_1(\Omega)} \leq \|\nabla u^0\|_{L_1(\Omega)}, \quad 1 \leq n \leq N \tag{3.13}$$

which is the desired $W^{1,1}$ estimate for the linear semi-implicit scheme (3.5). Since in the general situation there can be zero in denominators of (3.5), the above derivations were formal. However, in the Section devoted to the complementary volume spatial discretization we will regularize the problem, e.g. approximating $|\nabla u^{n-1}| \approx \sqrt{\varepsilon + |\nabla u^{n-1}|^2}$ and show that (3.13) is fulfilled for the regularization parameter ε tending to zero.

3.2 Space discretizations

A discrete image is given on structure of pixels/voxels with rectangular shape in general. Such shape restriction is not necessary for the methods presented bellow, but for simplicity we will use this simple image structure to create a computational grid for the spatial discretization methods.

Concerning the relation of the computational grid to the pixel structure, there will be a difference between the finite element and the complementary volume methods on the one hand, and the finite volume method on the other. The difference is related to the type of approximation of the solution of the partial differential equations assumed in those methods. While in the finite volume method the approximation of the solution is assumed to

be piecewise constant [47], in the complementary volume and finite element methods it is assumed to be continuous and, e.g. piecewise (bi)linear. Thus, in the finite volume method, the computational grid will directly be taken to be the pixel structure of the image and computational domain Ω corresponds to image domain. The initially given and subsequently computed values of discrete intensity are considered as approximations of average of continuous intensity function on pixels. On the other hand, in the finite element and complementary volume methods, the initially given values of discrete intensity, and also the computed values, are considered as approximations of the continuous intensity function in the centers of pixels. The centers of pixels then correspond to the nodes of the finite element or the complementary volume grid (triangulation). We can get such a grid by connecting the centers of pixels by a new rectangular mesh (see Fig. 36). We can take either bilinear approximation of the image on this rectangular grid or further divide every rectangle into two triangles (or six tetrahedra in 3D) and consider linear approximation. By the construction, it also means that in these two methods the computational domain Ω is given as the union of all triangles constructed in this way and Ω thus corresponds to the image domain minus the outer half of every boundary pixel – see Fig. 36. Let us note that the splitting of every pixel into two triangles, as depicted in Fig. 36, is not the only possibility. The orientation of triangles can change locally, e.g. be given by a refinement procedure in a bisection algorithm [15]. Given a triangulation, for the complementary volume method, we will construct a dual mesh. This dual mesh will again, in a sense, copy the pixel structure of the image. Let us note that in the finite element method we will use just the triangulation, in the complementary volume method we use both the triangulation and the dual mesh, and in the finite volume method we use just the pixel structure of the image corresponding to the dual mesh.

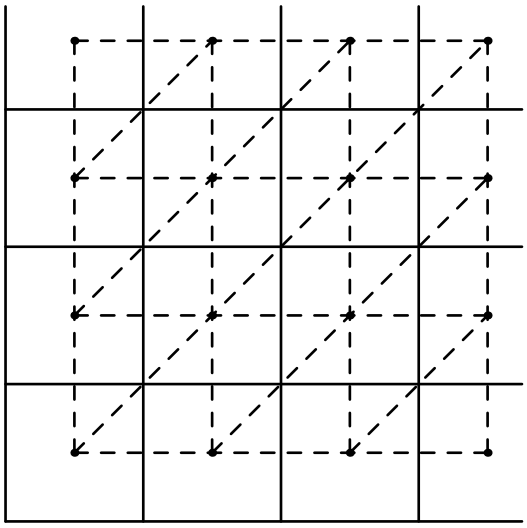

Figure 36: The image pixels (solid lines) corresponding to the finite volume mesh and to the dual mesh for the complementary volume method. Triangulation (dashed lines) for the finite element and complementary volume methods, with nodes (round points) corresponding to the centers of pixels.

We now define quantities which will be used in descriptions of fully discrete schemes (see also [135, 47, 32]). Let us assume that we are given a triangulation $\mathcal{T}$ (e.g. given by a previous

construction). that has no interior angle larger than $\pi/2$. The dual mesh τ will consist of cells p (also called complementary or finite volumes, or co-volumes) associated with the pth node of the triangulation $\mathcal{T}$, $p = 1, \ldots, M$. Since there will be one-to-one correspondence between nodes of triangulation and co-volumes we will use the same notation for them; we also hope that no confusion can appear with τ which denoted time step in Chapter 2 and dual grid here. The co-volume p is bounded by the lines (planes in 3D) that bisect and are perpendicular to the edges emanating from the node. By $m(p)$ we denote measure in $\mathbb{R}^d$ of p. We will denote the edge of $\mathcal{T}$ connecting the pth node to the qth by σ_{pq}, and its length by d_{pq}. We denote by E_{pq} the set of simplices having σ_{pq} as an edge, i.e., $E_{pq} = \{T \in \mathcal{T} | \sigma_{pq} \subset T\}$. Let e_{pq} denote the co-edge (co-plane) that is the perpendicular bisector of σ_{pq}, and let x_{pq} be a point of intersection of e_{pq} and σ_{pq}. By $m(e_{pq})$ we denote the measure of e_{pq} in $\mathbb{R}^{d-1}$. For each $T \in E_{pq}$, let c_{pq}^T be the measure in $\mathbb{R}^{d-1}$ of the portion of e_{pq} that is in T, i.e., $c_{pq}^T = m(e_{pq} \cap T)$. Let $S(p)$ be the set of simplices that have the pth node as a vertex, and for each node of $\mathcal{T}$ let $N(p)$ denote the set of nodes q, $q \neq p$, which are connected to the pth node by an edge and for which $m(e_{pq}) \neq 0$. In the situation depicted in Fig. 36, $N(p)$ consists of four neighbouring nodes q in the direction of the coordinate axes, for every inner node p of the triangulation. We denote by $\mathcal{E}$ the set of pairs of adjacent finite volumes,

$$\mathcal{E} = \{(p, q) \in \tau^2,\ p \neq q,\ m(e_{pq}) \neq 0\}.$$

Given a triangulation $\mathcal{T}$, we define the set $V_h \subset V$ of piecewise linear finite elements, i.e.,

$$V_h = V_h(\mathcal{T}) := \{v \in C^0(\overline{\Omega}) |\ v|_T \in \mathcal{P}_1 \text{ for all } T \in \mathcal{T}\}.$$

For any $v_h \in V_h$ we will use the notation $v_p := v_h(x_p)$, where x_p is the coordinate vector of the pth node of the triangulation. Let $u_h^0 = I_h(u^0) \in V_h(\mathcal{T})$ be the nodal interpolant of u^0. This will be the initial function for the finite element and complementary volume methods. In the finite volume method we denote by $\overline{u}_p$ the representative value for the cell (the bar indicates that we mean the average value in the cell and not a nodal value). The initial condition for the finite volume scheme is then assumed to be

$$\overline{u}_p^0 = \frac{1}{m(p)} \int_p u^0(x)\, dx, \quad p \in \tau. \tag{3.14}$$

Before going to spatial discretizations, let us make the following remark on the realization of the convolution included in the evaluation of the Perona-Malik function g in either (3.3) or (3.5). We use two strategies. The first is the following: Using the Gauss function G_σ as the smoothing kernel, one can replace the term $G_\sigma * u^{n-1}$ by solving the linear heat equation for time σ with the initial condition given by u^{n-1}. This linear equation can be solved numerically at the same grid by just one implicit step with length σ. Thus, as a realization of the convolution, we look for a function u^c which is a solution of the heat equation discretized in time by the backward Euler method with step σ:

$$\frac{u^c - u^{n-1}}{\sigma} = \Delta u^c \tag{3.15}$$

where Δ denotes the Laplace operator. This strategy is very suitable for the finite element and complementary volume methods, since in this case, the numerical solution u^c of (3.15)

is piecewise linear on triangles, its gradients are constant, and thus we can simply evaluate the Perona-Malik function on every triangle.

In the finite volume method we can use another approach. Since we will consider piecewise constant spatial approximations $\overline{u}_p^n$ in every discrete scale step n, we can replace the convolution (integral) by a sum over pixels. For the gradient of the convolution term at any point x we get

$$\nabla G_\sigma * u^{n-1}(x) = \sum_r \overline{u}_r^{n-1} \int_r \nabla G_\sigma(x-s)\,ds, \tag{3.16}$$

where we used the convolution derivative property

$$\frac{\partial}{\partial x_i}(G_\sigma * u^{n-1}(x)) = \frac{\partial G_\sigma}{\partial x_i} * u^{n-1}(x)$$

and

$$\frac{\partial G_\sigma}{\partial x_i} * u^{n-1}(x) = \int_{\mathbb{R}^d} \frac{\partial G_\sigma}{\partial x_i}(x-s)u^{n-1}(s)\,ds = \sum_r \overline{u}_r^{n-1} \int_r \frac{\partial G_\sigma}{\partial z_i}(x-s)\,ds.$$

The sum in (3.16) is evaluated over control volumes r which surround the point x. If we choose a C^∞ compactly supported smoothing kernel with support in a ball $B_{\sigma^*}(0)$ with radius σ^*, e.g. the function

$$G_\sigma(x) = \frac{1}{Z} e^{|x|^2/(|x|^2-\sigma^2)},$$

where $\sigma^* = \sigma$ and the constant Z is chosen so that G_σ has unit mass, then the sum is restricted only to the control volumes contained in $B_{\sigma^*}(x)$, the ball centered at x. If the point x is close to the boundary of the image domain, we use an extension of a discrete solution. The coefficients $\int_r \nabla G_\sigma(x-s)\,ds$ in (3.16) can be computed in advance using a computer algebra system, e.g. Mathematica [141]. The same situation arises when we use the Gauss function and consider as the ball $B_{\sigma^*}(0)$ a "numerical support" of the Gauss function (i.e., we consider a domain in which the values of the Gauss function are above some treshold). Then, again, just a finite sum is evaluated in (3.16).

3.3 Finite element method in image processing

To describe the ideas of finite element space discretization, let us consider the equation (3.1) [70, 16, 17]. Let k, σ be given numbers. Before the discretization we use approach (3.15) for the realization of the convolution, and then we write (3.3) as a couple of integral identities (weak formulations):

$$\int_\Omega u^n v\,dx + k\int_\Omega g(|\nabla u^c|)\nabla u^n \nabla v\,dx = \int_\Omega u^{n-1} v\,dx, \tag{3.17}$$

$$\int_\Omega u^c v\,dx + \sigma\int_\Omega \nabla u^c \nabla v\,dx = \int_\Omega u^{n-1} v\,dx \tag{3.18}$$

that hold for all $v \in V$. Then, at each scale level n, we look for a continuous piecewise linear function $u_h^n \in V_h(\mathcal{T})$ satisfying

$$\int_\Omega u_h^n v_h\,dx + k\int_\Omega g(|\nabla u_h^c|)\nabla u_h^n \nabla v_h\,dx = \int_\Omega u_h^{n-1} v_h\,dx \tag{3.19}$$

for all $v_h \in V_h(\mathcal{T})$, with $u_h^c \in V_h(\mathcal{T})$ being the solution of

$$\int_\Omega u_h^c v_h \, dx + \sigma \int_\Omega \nabla u_h^c \nabla v_h \, dx = \int_\Omega u_h^{n-1} v_h \, dx, \quad \forall v_h \in V_h(\mathcal{T}). \tag{3.20}$$

Considering the standard Lagrangian base functions $\varphi_q \in V_h(\mathcal{T})$, $q = 1, \ldots, M$, given by $\varphi_q(x_p) = \delta_{qp}$ (Kronecker delta) for all nodes of $\mathcal{T}$, the functions u_h^n, u_h^c are given by

$$u_h^n = \sum_{p=1}^{M} u_p^n \varphi_p, \qquad u_h^c = \sum_{p=1}^{M} u_p^c \varphi_p. \tag{3.21}$$

Then using (3.21)) in (3.19)–(3.20) and taking $v_h = \varphi_q$, $q = 1, \ldots, M$, as test functions, we get two Ritz-Galerkin systems of linear equations for the nodal values u_p^n, u_p^c, $p = 1, \ldots, M$, of the piecewise linear functions u_h^n, u_h^c, respectively:

$$\sum_{p=1}^{M} \left(\int_\Omega \varphi_p \varphi_q \, dx + k \int_\Omega g(|\nabla u_h^c|) \nabla \varphi_p \nabla \varphi_q \, dx \right) u_p^n = \int_\Omega u_h^{n-1} \varphi_q \, dx, \quad q = 1, \ldots, M, \tag{3.22}$$

$$\sum_{p=1}^{M} \left(\int_\Omega \varphi_p \varphi_q \, dx + \sigma \int_\Omega \nabla \varphi_p \nabla \varphi_q \, dx \right) u_p^c = \int_\Omega u_h^{n-1} \varphi_q \, dx, \quad q = 1, \ldots, M. \tag{3.23}$$

Thus, in every discrete scale step we need to solve two linear systems with the matrices $\mathbf{M} + k\mathbf{A}(g(|\nabla u_h^c|))$, $\mathbf{M} + \sigma \mathbf{A}(1)$, respectively, where $\mathbf{M}_{q,p} = \int_\Omega \varphi_p \varphi_q \, dx$ is the so-called mass matrix and $\mathbf{A}(w)_{q,p} = \int_\Omega w \nabla \varphi_p \nabla \varphi_q \, dx$ is the stiffness matrix, which are symmetric and positive definite. The discrete solutions can be found efficiently by the preconditioned conjugate gradient method or by Gauss-Seidel (SOR) iterations [119]. It is also customary to use the so-called lumped (diagonalized) mass matrix $\mathbf{M}_{q,p} = \sum_{k=1}^{M} \varphi_p(x_k) \varphi_q(x_k) \int_\Omega \varphi_k \, dx$ in the systems (3.22)–(3.23). In order to improve the efficiency of the finite element method, a choice of different (coarsened) triangulations $\mathcal{T}_n$ in subsequent scale steps $n = 1, \ldots, N$, is possible (see [16, 17, 115] and the next Section).

The analysis of the finite element method for the regularized Perona-Malik equation with a proof of convergence to the weak solution was first given by Kačur and Mikula [70]. Discussion on convergence of the tenzor product finite element methods can be found in [85, 86].

The same ideas as above can be used for the finite element discretization of equation (3.2). The only difference will be in the facts that the mass matrix $\mathbf{M}(w)$ will depend on $w = 1/(g(|\nabla u_h^c|)|\nabla u_h^{n-1}|)$, the stiffness matrix $\mathbf{A}(w)$ will depend on $w = 1/|\nabla u_h^{n-1}|$, and that Evans-Spruck regularization $|\nabla u_h^{n-1}| \approx \sqrt{\varepsilon + |\nabla u_h^{n-1}|^2}$ is used in the denominators. Deep numerical analysis of the finite element schemes for the various level-set type equations can be found in the series of papers by Deckelnick and Dziuk [36, 37, 38, 39].

3.3.1 Adaptivity in the finite element method

Bänsch and Mikula [16] suggested to improve efficiency of the finite element method in image processing by the use of adaptively chosen grids at each scale step. Usually, for time-dependent problems, a modification consisting of refinement and coarsening steps is necessary to adjust the grid at a given time step [15]. However, for the problem (3.1) it

is sufficient to coarsen the initial grid successively. There is no spatial *movement* of edges, hence no refinements of the grids are needed. This access may reduce the computational effort considerably, since with the increasing scale the solution tends to be more flat in large sub-regions of the image. The coarsening of the computational grids rapidly reduces the number of unknowns in the linear systems to be solved at the discrete scale steps of the method.

Concerning the adaptive algorithm, first we generate a triangulation $\mathcal{T}_0$ corresponding to a pixel/voxel structure of the image by (globally) refining a coarse grid $\mathcal{T}^0$, the so-called *macro triangulation*. The refinement procedure generates a sequence $\mathcal{T}^0, \mathcal{T}^1, \mathcal{T}^2, \ldots$ of finer and finer meshes until the desired structure is reached. Then $\mathcal{T}_0 := \mathcal{T}^{k_0}$, where k_0 is the last refinement step. For the refinement we have chosen the so called *bisection method* due to Bänsch, which allows easily for coarsening.

Refinement of the grid by bisection [15]: Before starting the refinement process, one edge of every triangle of the triangulation at kth refinement level is marked (Fig. 37). This edge is called the *refinement edge* (a good choice is the longest one). To divide a single triangle, it is cut through the midpoint of the refinement edge and the vertex opposite to the refinement edge. The new refinement edges are chosen opposite to the new vertex (Fig. 38).

Let us start with $\mathcal{T}^0$. Then for every bisection level k let Σ^+ be the set of those triangles which have to be divided ($\Sigma^+ = \mathcal{T}^k$ in case of uniform refinement). Then *one bisection step* (see also Fig. 39) at level k is given by:

while $\Sigma^+ \neq \emptyset$ **do**

- bisect all $T \in \Sigma^+$ as described above, obtain an intermediate triangulation $\hat{\mathcal{T}}^k$ (possibly non-conforming)
- let now Σ^+ be the set of those tetrahedra with a non-conforming node.

endwhile
$\mathcal{T}^{k+1} := \hat{\mathcal{T}}^k$

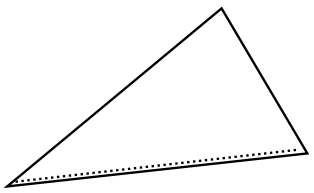

Figure 37: Triangle with refinement edge

To provide a *local coarsening*, we make the following definitions:

1. A simplex $T \in \mathcal{T}$ has level l if T was obtained after l refinement steps.
2. A simplex T is said to have *locally finest level* if the levels of all neighbours are less than or equal to the level of T.

Figure 38: Bisection of a single triangle

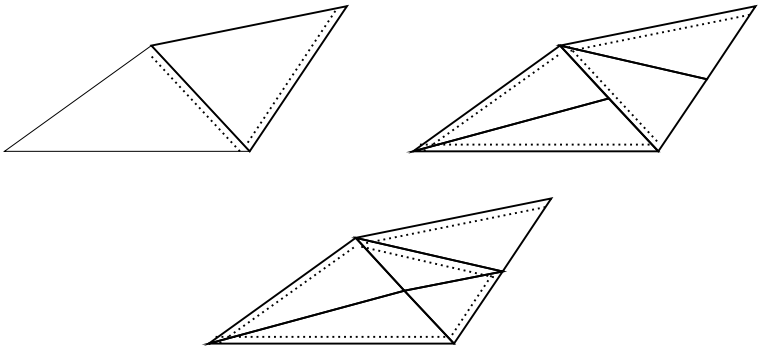

Figure 39: $\mathcal{T}^0$, $\hat{\mathcal{T}}^0$ and $\mathcal{T}^1$

3. Let $T \in \mathcal{T}$, and let T' be the father of T. A vertex P of T which was inserted while bisecting T' is called the *coarsening node* of T.

4. Let K be an edge of the triangulation $\mathcal{T}$ and K' the "father"-edge of K with midpoint Q. Set $M := \{T \in \mathcal{T} | T \cap K' \neq \emptyset\}$. If Q is the coarsening node for all $T \in M$, then M is called a *resolvable patch* (Fig. 40).

If M is a resolvable patch, then all $T \in M$ can be coarsened without interfering with $T' \in \mathcal{T}$ outside M. Therefore resolvable patches are the configurations which we allow to be coarsened. This guarantees that the coarsening process stays local.

Coarsening of the grid [15]: Let $\mathcal{T}_n$ be a triangulation obtained by refinement and coarsening steps. Let $\Sigma^- \subset \mathcal{T}_n$ be the set of triangles to be derefined. Then *one coarsening step* consists of:

```
for each T ∈ Σ⁻ do
    if T belongs to a resolvable patch M then
        if T' ∈ Σ⁻ for all T' ∈ M then
            derefine M
        endif
    endif
enddo
```

Coarsening criterion and our adaptive method [16, 17]: As the local behavior of $\nabla G_\sigma * u$ determines the evolution process and is an indicator for edges, the *coarsening criterion*

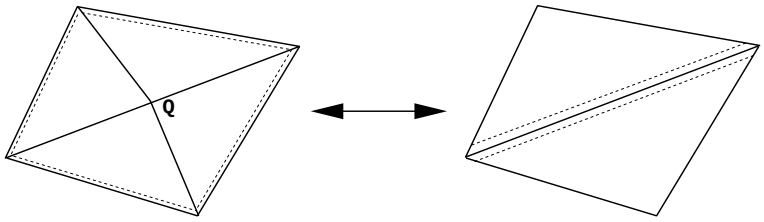

Figure 40: Resolvable patch M with coarsening node Q and coarsened patch

is based on this value. Let $\varepsilon > 0$ be a given tolerance. For the nth scale step and u_h^n, the corresponding numerical solution on the grid $\mathcal{T}_n$, we allow all triangles $T \in \mathcal{T}_n$ to be coarsened, if

$$h_T |\nabla u_h^n| \leq \varepsilon \quad \text{on} \quad T,$$

where h_T is the diameter of triangle T. Thus we have the following *adaptive scheme*:

Let $\mathcal{T}_0, u_h^0$ be given.
for $n = 1, 2, \ldots N$ **do**
  `define` $\Sigma^- := \{T \in \mathcal{T}_{n-1}; h_T |\nabla u_h^{n-1}| \leq \epsilon$ `on` $T\}$
  `derefine` $\mathcal{T}_{n-1}$ `according to` Σ^- `to obtain` $\mathcal{T}_n$
  `set up the matrix` $\mathbf{M} + \sigma \mathbf{A}(1)$
  `compute` $u_h^c \in V_h(\mathcal{T}_n)$
  `set up the matrix` $\mathbf{M} + k\mathbf{A}(g(|\nabla u_h^c|))$
  `compute` $u_h^n \in V_h(\mathcal{T}_n)$
enddo

The same adaptive algorithm can be used in the 3D case, just changing triangles to tetrahedra. For 3D implementation and computational results we refer to [17]. There exist finite element software packages (see e.g. [130]) based on the bisection refinement and coarsening method, thus the adaptivity described above can be implemented also in such an environement.

3.4 Complementary volume spatial discretization

In this Section we will discretize equation (3.2) or, more precisely, the semi-discrete approximation (3.5) by means of the complementary volume method [59]. In order to derive the complementary volume spatial discretization [135], we integrate (3.5) over a co-volume p

$$\int_p \frac{u^n - u^{n-1}}{g^{n-1} |\nabla u^{n-1}| k} \, dx = \int_p \nabla . \left(\frac{\nabla u^n}{|\nabla u^{n-1}|} \right) dx. \tag{3.24}$$

Using the divergence theorem on the right-hand side we get

$$\int_p \nabla \left(\frac{\nabla u^n}{|\nabla u^{n-1}|} \right) dx = \int_{\partial p} \frac{1}{|\nabla u^{n-1}|} \frac{\partial u^n}{\partial \sigma} \, ds = \sum_{q \in N(p)} \int_{e_{pq}} \frac{1}{|\nabla u^{n-1}|} \frac{\partial u^n}{\partial \sigma} \, ds \tag{3.25}$$

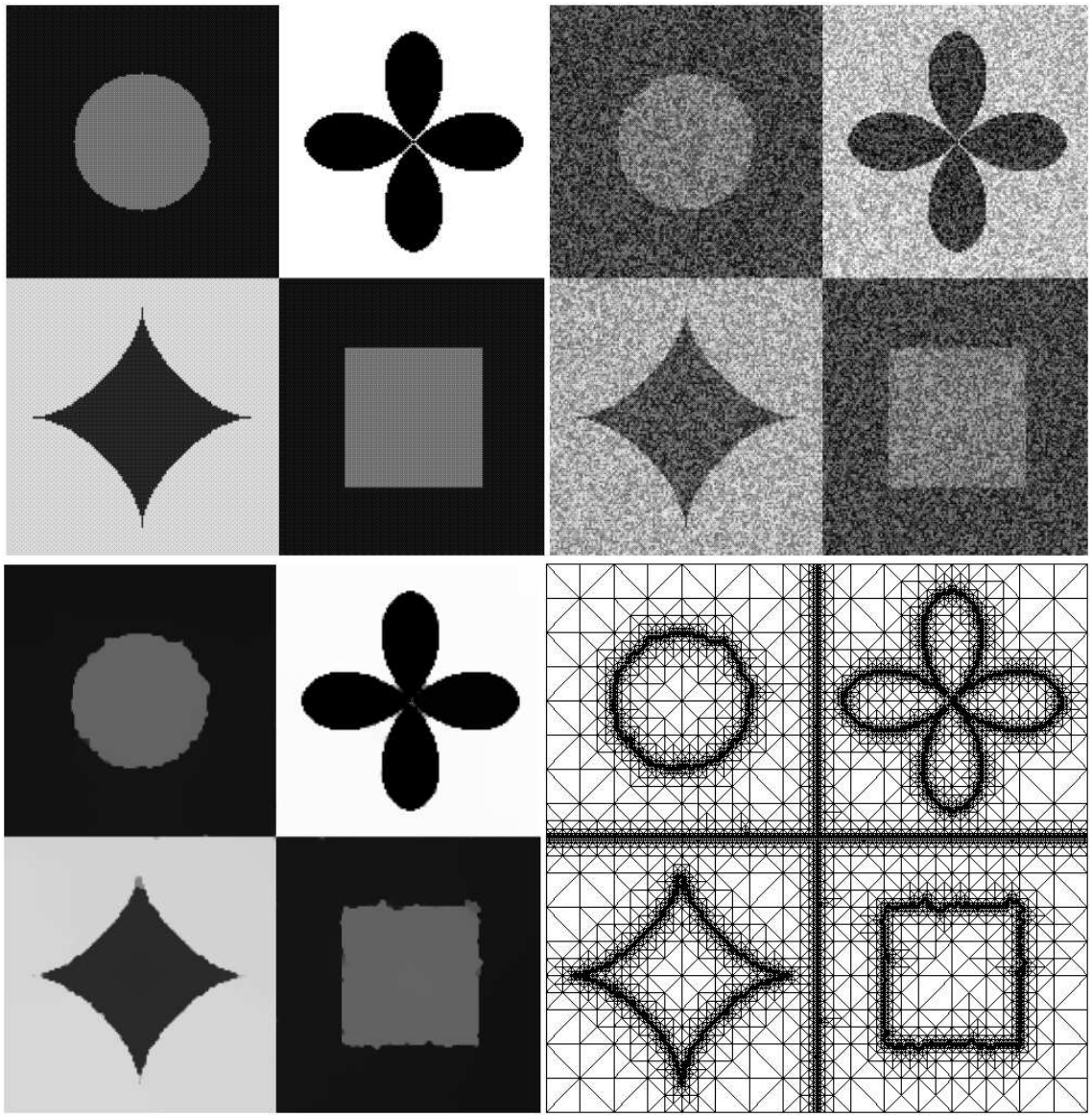

Figure 41: Processing of a noisy image by the adaptive finite element method for the anisotropic diffusion equation (3.1). Upper part: Original image and its noise-corrupted version; lower part: smoothed image after 8 discrete scale steps and corresponding 2D triangulation which is fine only along edges [16].

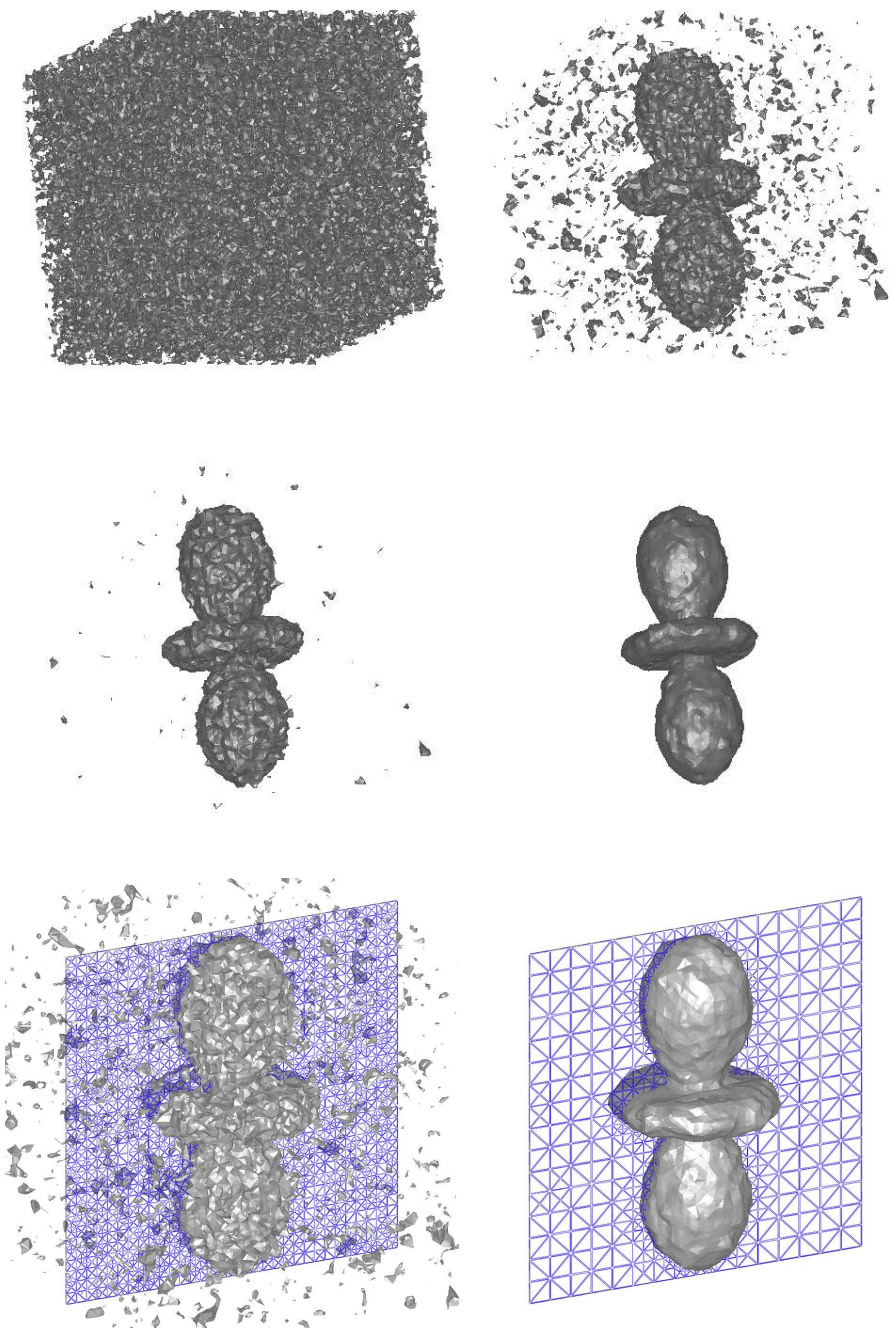

Figure 42: Denoising of an artificial object in a 3D image by the adaptive finite element method for the anisotropic diffusion equation (upper and middle parts) together with cuttings of subsequently coarsened 3D adaptive grids (lower part).

where σ is unit outer normal to co-volume p. If $u_h^n \in V_h(\mathcal{T})$ is a continuous piecewise linear function on a triangulation $\mathcal{T}$ and if its nodal values are denoted by $u_p^n = u_h^n(x_p)$, then

$$\sum_{q\in N(p)} \int_{e_{pq}} \frac{1}{|\nabla u_h^{n-1}|} \frac{\partial u_h^n}{\partial \sigma}\, ds = \sum_{q\in N(p)} \left(\sum_{T\in E_{pq}} \frac{c_{pq}^T}{|\nabla u_T^{n-1}|} \right) \frac{u_q^n - u_p^n}{d_{pq}}, \tag{3.26}$$

where $|\nabla u_T^{n-1}|$ denotes the constant value of the gradient of u_h^{n-1} in the simplex T. The complementary volume method approximates the left-hand side of (3.24) by

$$\frac{m(p)(u_p^n - u_p^{n-1})}{kg(|\nabla u_p^c|)|\nabla u_p^{n-1}|}, \tag{3.27}$$

where $|\nabla u_p^{n-1}|$, $|\nabla u_p^c|$ denote an approximation of the gradient in co-volume p. For that purpose we have chosen the average value of gradients in the co-volume [135]

$$|\nabla u_p| \approx \sum_{T\in S(p)} \frac{m(T\cap p)}{m(p)} |\nabla u_T|. \tag{3.28}$$

Let $\delta > 0$, $\varepsilon > 0$. For any $u_h \in V_h$ and each $T \in \mathcal{T}_h$ we define

$$|\nabla u_T|_\delta = \begin{cases} |\nabla u_T| & \text{if } |\nabla u_T| > \delta \\ \delta & \text{if } |\nabla u_T| \le \delta, \end{cases} \tag{3.29}$$

and for any function $u_h \in V_h$ define

$$|\nabla u_h|_\varepsilon = \sqrt{\varepsilon^2 + |\nabla u_h|^2} \quad \text{so that} \quad |\nabla u_T|_\varepsilon = \sqrt{\varepsilon^2 + |\nabla u_T|^2}, \quad T \in \mathcal{T}_h. \tag{3.30}$$

The difference between regularizations (3.29) and (3.30), respectively, is that in the first case we replace by δ only vanishing or small gradients, while in the second case we add small regularization parameter to gradient everywhere. Let us denote by

$$|\nabla u_p|_\delta = \sum_{T\in S(p)} \frac{|T\cap p|}{|p|} |\nabla u_T|_\delta, \quad |\nabla u_p|_\varepsilon = \sum_{T\in S(p)} \frac{|T\cap p|}{|p|} |\nabla u_T|_\varepsilon,$$

the regularized approximations (3.28) of the gradient in co-volume p. If we denote

$$b_p^{n-1} = \frac{m(p)}{g(|\nabla u_p^c|)|\nabla u_p^{n-1}|_\delta}, \tag{3.31}$$

$$a_{pq}^{n-1} = \frac{1}{d_{pq}} \sum_{T\in E_{pq}} \frac{c_{pq}^T}{|\nabla u_T^{n-1}|_\delta}, \tag{3.32}$$

or

$$b_p^{n-1} = \frac{m(p)}{g(|\nabla u_p^c|)|\nabla u_p^{n-1}|_\varepsilon}, \tag{3.33}$$

$$a_{pq}^{n-1} = \frac{1}{d_{pq}} \sum_{T\in E_{pq}} \frac{c_{pq}^T}{|\nabla u_T^{n-1}|_\varepsilon}, \tag{3.34}$$

we can write the

Linear fully-discrete complementary volume scheme for solving equation (3.2) [59]: *For $n = 1, \dots, N$ we look for u_p^n, $p = 1, \dots, M$, satisfying the equation*

$$b_p^{n-1} u_p^n + k \sum_{q \in N(p)} a_{pq}^{n-1} (u_p^n - u_q^n) = b_p^{n-1} u_p^{n-1}. \tag{3.35}$$

If coefficients of (3.35) are regularized by (3.29), i.e. we use (3.31)-(3.32), the solution $(u_1^n, \dots, u_M^n)$ of this linear system will be denoted by $u_h^{\delta,n}$. If coefficients of (3.35) are regularized by (3.30), i.e. we use (3.33)-(3.34), the solution will be denoted by $u_h^{\varepsilon,n}$. From the construction of the scheme it is clear that the matrix of the system (3.35) is symmetric and diagonally dominant M-matrix, thus it always has unique solution. So we have

3.2 Proposition *Let coefficients of the scheme* (3.35) *be given by* (3.31)-(3.32). *Then there exists unique solution $u_h^{\delta,n} = (u_1^n, \dots, u_M^n)$ of the scheme* (3.35) *for any $\delta > 0$, $n = 1, \dots, N$.*

3.3 Proposition *Let coefficients of the scheme* (3.35) *be given by* (3.33)-(3.34). *Then there exists unique solution $u_h^{\varepsilon,n} = (u_1^n, \dots, u_M^n)$ of the scheme* (3.35) *for any $\varepsilon > 0$, $n = 1, \dots, N$.*

3.4 Remark With ε or δ very small the diagonal dominance of the system (3.35) can be weak, thus one has to be carefull with a choice of proper solver, we refer to [59] for discusson on this linear algebra problem.

Before solving (3.35), we have to put $|\nabla u_p^c|$ into (3.31), (3.33). The function $u_h^c \in V_h(\mathcal{T})$ is found by the same idea as given in (3.24)–(3.27) applied to (3.15); i.e., we solve (3.35) with u_p^n replaced by u_p^c, and with $b_p^{n-1} \equiv b_p = m(p)$, $a_{pq}^{n-1} \equiv a_{pq} = m(e_{pq})/d_{pq}$. Then $|\nabla u_p^c|$ is computed by (3.28) and put into the Perona-Malik function g.

In order to derive an analogue of the estimate (3.11) for our fully discrete scheme we use the following result (see e.g. [135])

3.5 Lemma *Let $\mathcal{T}_h$ be a two-dimensional mesh having simplicies with interior angles not exceeding $\pi/2$ and let $u, v \in V_h$, and w be piecewise constant on $\mathcal{T}_h$. Then*

$$\int_\Omega w \nabla u . \nabla v dx = \sum_{p=1}^{M} \left(\sum_{q \in N(p)} \alpha_{pq}(w)(u_p - u_q) \right) v_p, \tag{3.36}$$

where $\alpha_{pq}(w) = \frac{1}{d_{pq}} \sum_{T \in E_{pq}} w_T c_{pq}^T$ and w_T denotes value of w in $T \in \mathcal{T}_h$.

Then we can prove the following assertions.

3.6 Theorem *There exists limit u_h^n of a subsequence of $u_h^{\delta,n}$ for $\delta \to 0$ where $u_h^{\delta,n}$ is the solution of the scheme* (3.35) *with coefficients given by* (3.31)-(3.32). *Moreover for this generalized solution u_h^n the following estimates hold*

$$\|u_h^n\|_{L_\infty(\Omega)} \le \|u_h^0\|_{L_\infty(\Omega)}, \quad \|\nabla u_h^n\|_{L_1(\Omega)} \le \|\nabla u_h^0\|_{L_1(\Omega)}, \quad 1 \le n \le N. \tag{3.37}$$

Proof Let us rewrite (3.35) in the form

$$u_p^n + \frac{\tau}{b_p^{n-1}} \sum_{q \in N(p)} a_{pq}^{n-1}(u_p^n - u_q^n) = u_p^{n-1} \tag{3.38}$$

and let $\max u_h^{\delta,n} = \max(u_1^n, \ldots, u_M^n)$ be achieved in the pth node. Then the whole second term on the left hand side is nonnegative and thus value $u_p^n \leq u_p^{n-1} \leq \max(u_1^{n-1}, \ldots, u_M^{n-1})$. In the same way we can prove the relations for minima and together we have

$$\min\ u_p^0 \leq \min\ u_p^n \leq \max\ u_p^n \leq \max\ u_p^0, \quad n \leq N \tag{3.39}$$

which imply

$$\|u_h^{\delta,n}\|_{L_\infty(\Omega)} \leq \|u_h^0\|_{L_\infty(\Omega)}, \quad 1 \leq n \leq N. \tag{3.40}$$

Since estimate (3.40) is independent on δ we can choose convergent subsequence of $u_h^{\delta,n}$ as $\delta \to 0$. The limit of this subsequence we denote by $u_h^n \in V_h$ and it is clear that it fulfills the first estimate of the Theorem. To get the second estimate of the Theorem, let us multiply (3.35) by $u_p^n - u_p^{n-1}$ and sum it over all nodes. We get

$$\sum_{p=1}^{M} b_p^{n-1} \frac{(u_p^n - u_p^{n-1})^2}{\tau} + \sum_{p=1}^{M} \sum_{q \in N(p)} a_{pq}^{n-1}(u_p^n - u_q^n)(u_p^n - u_p^{n-1}) = 0 \tag{3.41}$$

using definition of a_{pq}^{n-1} and (3.36) we obtain

$$\sum_{p=1}^{M} b_p^{n-1} \frac{(u_p^n - u_p^{n-1})^2}{\tau} + \int_\Omega \frac{\nabla u_h^{\delta,n}.\nabla(u_h^{\delta,n} - u_h^{n-1})}{|\nabla u_h^{n-1}|_\delta} dx = 0. \tag{3.42}$$

We denote second term of this equation by II and further we denote

$$\Omega_0 = \{T \in \mathcal{T}_h; |\nabla u_T^{n-1}| \leq \delta\}$$

$$\Omega_1 = \{T \in \mathcal{T}_h; |\nabla u_T^{n-1}| > \delta\}.$$

Using the relation (3.8) we can rewrite the second term in the equation (3.42) as follows

$$\begin{aligned} II \quad &= \int_{\Omega_0} \frac{|\nabla u_h^{\delta,n}|^2}{\delta} dx - \int_{\Omega_0} \frac{\nabla u_h^{\delta,n}.\nabla u_h^{n-1}}{\delta} dx \\ &+ \frac{1}{2} \int_{\Omega_1} \frac{|\nabla u_h^{\delta,n}|^2 - |\nabla u_h^{n-1}|^2 + |\nabla u_h^{\delta,n} - \nabla u_h^{n-1}|^2}{|\nabla u_h^{n-1}|} dx. \end{aligned}$$

Since the following identity holds

$$|\nabla u_h^{\delta,n} - \nabla u_h^{n-1}|^2 = (|\nabla u_h^{\delta,n}| - |\nabla u_h^{n-1}|)^2 + \left| \frac{\nabla u_h^{\delta,n}}{|\nabla u_h^{\delta,n}|} - \frac{\nabla u_h^{n-1}}{|\nabla u_h^{n-1}|} \right|^2 |\nabla u_h^{\delta,n}||\nabla u_h^{n-1}|,$$

we get

$$
\begin{aligned}
II \quad &= \int_{\Omega_0} \frac{|\nabla u_h^{\delta,n}|^2}{\delta} dx - \int_{\Omega_0} \frac{\nabla u_h^{\delta,n}.\nabla u_h^{n-1}}{\delta} dx \\
&+ \frac{1}{2} \int_{\Omega_1} \frac{|\nabla u_h^{\delta,n}|^2 - |\nabla u_h^{n-1}|^2 - (|\nabla u_h^{\delta,n}| - |\nabla u_h^{n-1}|)^2}{|\nabla u_h^{n-1}|} dx \\
&+ \int_{\Omega_1} \frac{(|\nabla u_h^{\delta,n}| - |\nabla u_h^{n-1}|)^2}{|\nabla u_h^{n-1}|} dx + \frac{1}{2} \int_{\Omega_1} \left| \frac{\nabla u_h^{\delta,n}}{|\nabla u_h^{\delta,n}|} - \frac{\nabla u_h^{n-1}}{|\nabla u_h^{n-1}|} \right|^2 |\nabla u_h^{\delta,n}| dx.
\end{aligned}
$$

Because the first term of (3.42) and last two terms in the previous expression are nonnegative, using Cauchy-Schwartz and then Young inequality we obtain

$$
\begin{gathered}
\int_{\Omega_1} |\nabla u_h^{\delta,n}| dx + \int_{\Omega_0} \frac{|\nabla u_h^{\delta,n}|^2}{\delta} dx \le \int_{\Omega_1} |\nabla u_h^{n-1}| dx + \int_{\Omega_0} |\nabla u_h^{\delta,n}| dx \le \\
\int_{\Omega_1} |\nabla u_h^{n-1}| dx + \frac{1}{2} \int_{\Omega_0} \frac{|\nabla u_h^{\delta,n}|^2}{\delta} dx + \frac{1}{2} \int_{\Omega_0} \delta dx
\end{gathered}
$$

from where

$$
\frac{1}{2} \int_{\Omega_0} \frac{|\nabla u_h^{\delta,n}|^2}{\delta} dx + \int_{\Omega_1} |\nabla u_h^{\delta,n}| dx \le \int_{\Omega_1} |\nabla u_h^{n-1}| dx + \frac{1}{2} \delta |\Omega_0|. \tag{3.43}
$$

If we use again

$$
\int_{\Omega_0} |\nabla u_h^{\delta,n}| dx \le \frac{1}{2} \int_{\Omega_0} \frac{|\nabla u_h^{\delta,n}|^2}{\delta} dx + \frac{1}{2} \delta |\Omega_0| \tag{3.44}
$$

we obtain

$$
\|\nabla u_h^{\delta,n}\|_{L_1(\Omega)} \le \|\nabla u_h^{n-1}\|_{L_1(\Omega)} + \delta |\Omega_0|. \tag{3.45}
$$

Let $u_h^{\delta,n}$ be subsequence converging to u_h^n corresponding to vector $u_h^n = (u_{h,1}^n, u_{h,2}^n, \ldots, u_{h,M}^n)$. It is clear that there exists subsequence of the previous one for which $|\nabla u_T^{\delta,n}| \to |\nabla u_T^n|$, $\forall T \in \mathcal{T}_h$ as $\delta \to 0$. Thus $\|\nabla u_h^{\delta,n}\|_{L_1(\Omega)} \to \|\nabla u_h^n\|_{L_1(\Omega)}$ for $\delta \to 0$. From the estimate (3.45) then follows that $\|\nabla u_h^n\|_{L_1(\Omega)} \le \|\nabla u_h^{n-1}\|_{L_1(\Omega)}$ which gives the second estimate of the Theorem. □

3.7 Theorem *There exists limit u_h^n of a subsequence of $u_h^{\varepsilon,n}$ for $\varepsilon \to 0$ where $u_h^{\varepsilon,n}$ is the solution of the scheme* (3.35) *with coefficients given by* (3.33)-(3.34). *Moreover for this generalized solution u_h^n the following estimates hold*

$$
\|u_h^n\|_{L_\infty(\Omega)} \le \|u_h^0\|_{L_\infty(\Omega)}, \quad \|\nabla u_h^n\|_{L_1(\Omega)} \le \|\nabla u_h^0\|_{L_1(\Omega)}, \quad 1 \le n \le N. \tag{3.46}
$$

Proof In the same way as in the proof of Theorem 3.6 we get

$$
\|u_h^{\varepsilon,n}\|_{L_\infty(\Omega)} \le \|u_h^0\|_{L_\infty(\Omega)}, \quad 1 \le n \le N \tag{3.47}
$$

and from there the first estimate of this Theorem. Now, we prove the second estimate. Let us again multiply (3.35) by $u_p^n - u_p^{n-1}$ and sum it over all nodes. As in the previous proof we obtain

$$\sum_{p=1}^{M} b_p^{n-1} \frac{(u_p^n - u_p^{n-1})^2}{\tau} + \int_\Omega \frac{\nabla u_h^{\varepsilon,n}.\nabla(u_h^{\varepsilon,n} - u_h^{n-1})}{|\nabla u_h^{n-1}|_\varepsilon} dx = 0. \tag{3.48}$$

Let us use the notation

$$\nabla_\varepsilon v = (v_x, v_y, \varepsilon), \quad \nabla_0 v = (v_x, v_y, 0).$$

where v_x, v_y denote partial derivatives of a function v in 2D case (in 3D analogously). Then

$$|\nabla_\varepsilon u_h^{n-1}| = |\nabla u_h^{n-1}|_\varepsilon, \quad |\nabla_0 u_h^{\varepsilon,n}| = |\nabla u_h^{\varepsilon,n}|, \quad \nabla_\varepsilon u_h^{n-1}.\nabla_0 u_h^{\varepsilon,n} = \nabla u_h^{\varepsilon,n}.\nabla u_h^{n-1}. \tag{3.49}$$

We again denote second term of equation (3.48) by II. Using the relation (3.8) we have

$$II = \frac{1}{2} \int_\Omega \frac{|\nabla u_h^{\varepsilon,n}|^2 - |\nabla u_h^{n-1}|^2 + |\nabla u_h^{\varepsilon,n} - \nabla u_h^{n-1}|^2}{|\nabla u_h^{n-1}|_\varepsilon} dx.$$

We can compute

$$\begin{aligned}
&|\nabla u_h^{\varepsilon,n} - \nabla u_h^{n-1}|^2 = |\nabla u_h^{\varepsilon,n}|^2 - 2|\nabla u_h^{\varepsilon,n}||\nabla u_h^{n-1}|_\varepsilon + \\
&|\nabla u_h^{n-1}|_\varepsilon^2 + 2|\nabla u_h^{\varepsilon,n}||\nabla u_h^{n-1}|_\varepsilon - 2\nabla u_h^{\varepsilon,n} \cdot \nabla u_h^{n-1} - \varepsilon^2 = \\
&(|\nabla u_h^{\varepsilon,n}| - |\nabla u_h^{n-1}|_\varepsilon)^2 + \left(2 - \frac{2\nabla u_h^{\varepsilon,n} \cdot \nabla u_h^{n-1}}{|\nabla u_h^{\varepsilon,n}||\nabla u_h^{n-1}|_\varepsilon}\right) |\nabla u_h^{\varepsilon,n}||\nabla u_h^{n-1}|_\varepsilon - \varepsilon^2.
\end{aligned}$$

and using (3.49) we get

$$2 - \frac{2\nabla u_h^{\varepsilon,n} \cdot \nabla u_h^{n-1}}{|\nabla u_h^{\varepsilon,n}||\nabla u_h^{n-1}|_\varepsilon} = \left| \frac{\nabla_0 u_h^{\varepsilon,n}}{|\nabla_0 u_h^{\varepsilon,n}|} - \frac{\nabla_\varepsilon u_h^{n-1}}{|\nabla_\varepsilon u_h^{n-1}|} \right|^2$$

which together gives us

$$\begin{aligned}
II \quad &= \frac{1}{2} \int_\Omega \frac{|\nabla u_h^{\varepsilon,n}|^2 - |\nabla u_h^{n-1}|_\varepsilon^2}{|\nabla u_h^{n-1}|_\varepsilon} dx + \frac{1}{2} \int_\Omega \frac{(|\nabla u_h^{\varepsilon,n}| - |\nabla u_h^{n-1}|_\varepsilon)^2}{|\nabla u_h^{n-1}|_\varepsilon} dx + \\
&+ \frac{1}{2} \int_\Omega \left| \frac{\nabla_0 u_h^{\varepsilon,n}}{|\nabla_0 u_h^{\varepsilon,n}|} - \frac{\nabla_\varepsilon u_h^{n-1}}{|\nabla_\varepsilon u_h^{n-1}|} \right|^2 |\nabla u_h^{\varepsilon,n}| dx
\end{aligned}$$

and finally

$$\begin{aligned}
&\sum_{p=1}^{M} b_p^{n-1} \frac{(u_p^n - u_p^{n-1})^2}{\tau} + \int_\Omega \frac{(|\nabla u_h^{\varepsilon,n}| - (|\nabla u_h^{n-1}|_\varepsilon)^2}{|\nabla u_h^{n-1}|_\varepsilon} dx + \\
&\frac{1}{2} \int_\Omega \left| \frac{\nabla_0 u_h^{\varepsilon,n}}{|\nabla_0 u_h^{\varepsilon,n}|} - \frac{\nabla_\varepsilon u_h^{n-1}}{|\nabla_\varepsilon u_h^{n-1}|} \right|^2 |\nabla u_h^{\varepsilon,n}| dx + \\
&\frac{1}{2} \int_\Omega \frac{|\nabla u_h^{\varepsilon,n}|^2 - |\nabla u_h^{n-1}|_\varepsilon^2 - (|\nabla u_h^{\varepsilon,n}| - |\nabla u_h^{n-1}|_\varepsilon)^2}{|\nabla u_h^{n-1}|_\varepsilon} dx = 0.
\end{aligned}$$

Since the first three terms are positive we have for the last one

$$\frac{1}{2}\int_\Omega \frac{2|\nabla u_h^{\varepsilon,n}||\nabla u_h^{n-1}|_\varepsilon - 2|\nabla u_h^{n-1}|_\varepsilon^2}{|\nabla u_h^{n-1}|_\varepsilon} dx \le 0$$

from where

$$\int_\Omega |\nabla u_h^{\varepsilon,n}| dx \le \int_\Omega |\nabla u_h^{n-1}|_\varepsilon dx = \int_\Omega \sqrt{|\nabla u_h^{n-1}|^2 + \varepsilon^2} dx \le \int_\Omega |\nabla u_h^{n-1}| dx + \varepsilon|\Omega|,$$

holding for any $\varepsilon > 0$. The rest of the proof uses the same arguments as in the end of the proof of Theorem 3.6. □

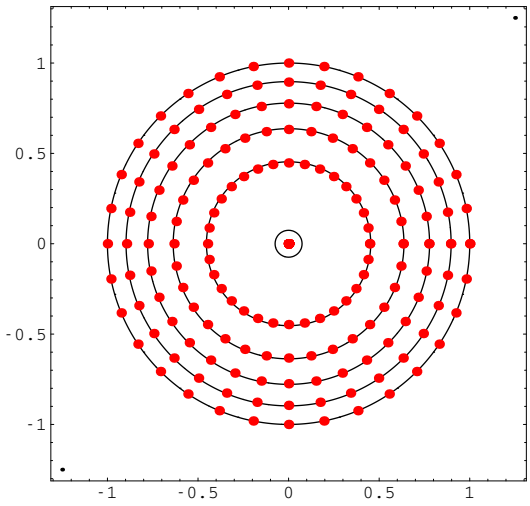

Figure 43: Comparison of the curve evolution given by the scheme (3.35) (solid lines represent zero level set of numerical solution in $t = 0, 1, 2, 3, 4$) and by exact solution given by shrinking unit circle (dots) at the same time moments. (see Example 5)

In Fig. 43 we test our co-volume algorithm (3.35) in simple situation of known exact solution of the level set equation (1.22) given by a shrinking circle into the point. We consider unit circle which extincts at time 0.5. From our comparison one can see precise coincidence of exact and numerical solutions and only very small error in extinction time which is for numerical solution 0.5010. The parameters were $h = 0.01$, time step $\tau = 0.0001$ and $\varepsilon^2 = 10^{-6}$.

In Fig. 44 we test the algorithm (3.35) in the nonconvex curve evolution by mean curvature. We evolve numerically the initial curve given in the top. In all images we plot by solid lines numerical solution by (3.35) and by points numerical solution given by conceptually different method based on discretization of the intrinsic heat equation described in Section 2.3. In case of the scheme (3.35) we use space discretization parameter $h = 0.01$, time step $\tau = 0.001$, $\varepsilon^2 = 10^{-6}$ and both solutions are plotted at the same time moments ($t = 0.05, 0.1, 0.2, 0.3, 0.5, 0.8$) after which the curve shrinks in a circular form into a point. From the comparison one can see a precise coincidence of two methods during evolution. We have also observed very similar behaviour of both studied regularizations.

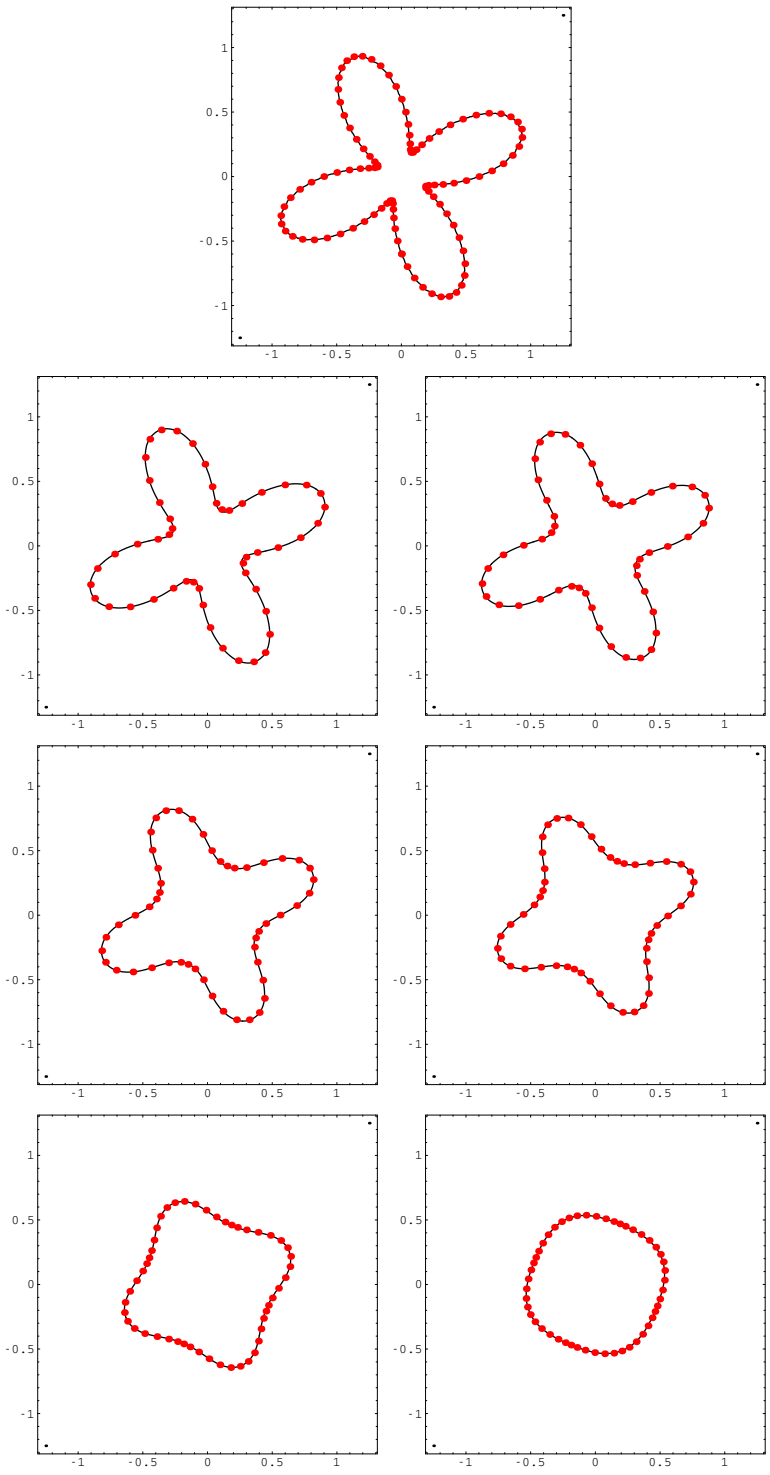

Figure 44: Comparison of numerical solutions using semi-implicit complementary volume scheme for solving level set equation (solid lines) and Lagrangian approach based on solving the intrinsic heat equation (points).

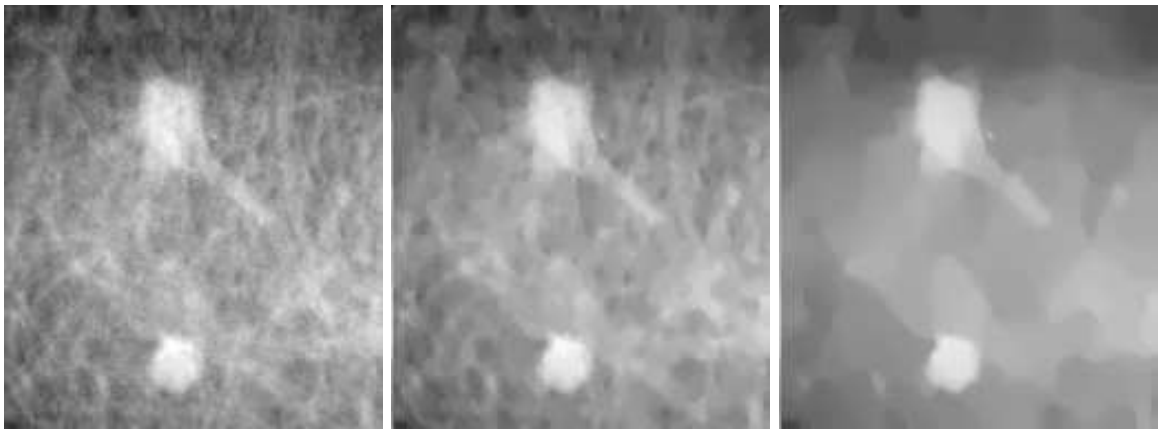

Figure 45: Initial image (left), result of multiscale analysis by equation (3.2) after 30 (middle) and 100 (right) discrete scale steps [59].

Fig. 45 gives an example of an application of the complementary volume scheme to a mammogram image (171×192 pixels).

Using the integration (3.24) and the relation (3.26), one can also derive a complementary volume discretization of equation (3.1) or, more precisely, for the semi-discrete coupling (3.3), (3.15). In such a way, we get the system (3.35) with

$$b_p^{n-1} = m(p), \qquad a_{pq}^{n-1} = \frac{1}{d_{pq}} \sum_{T \in E_{pq}} c_{pq}^T g(|\nabla u_T^c|), \tag{3.50}$$

where u_h^c is computed in the same way as above. Let us note that such a discretization of (3.1) can be considered as a special mass lumping approximation in the finite element method.

3.5 Finite volume discretization

In this Section we will consider the finite volume discretization of equation (3.1). In our approach, the finite volume grid corresponds to the dual mesh τ, and finite volumes correspond to co-volumes as they are identical with the pixel/voxel structure of the image. In general, the finite volume can be either a simplex of the triangulation or a co-volume of the dual mesh [47]; we use the second strategy. The main difference as compared to the finite element and complementary volume techniques, is that in the finite volume method the approximating functions are not in $V_h(\mathcal{T})$, but they are just piecewise constant on finite volumes. Thus, in theoretical analysis of the schemes, we cannot work directly with gradients or normal derivatives since they are either zero (inside finite volumes) or infinite (on their boundaries). However, from conceptual point of view such approach seems to be *the most natural for digital image processing* because pixelwise constant values are given in practice. Using the technique from [47], Mikula and Ramarosy proved convergence of the finite volume scheme [96] to solution of the regularized Perona-Malik equation (3.1). A similar result has been obtained by Mikula and Sgallari [98] also for the 3D problem in cylindrical geometry inspired by a recent fast noninvasive medical acquisition technique. The improvement of

efficiency can be done, similarly as in the finite element method, using adaptively coarsened grids. Such approach based on quad-trees in 2D and oct-trees in 3D has been developed by Krivá and Mikula [81, 82, 83]. In Fig. 46 the result of smoothing and final grid are given after 25 scale steps of the adaptive algorithm applied to a noisy photograph.

The derivation of the finite volume scheme follows the ideas of the previous Section. We integrate the equation (3.1) in every finite volume p. Then, by means of $\overline{u}_p, \overline{u}_q$ representing an approximate values of the solution inside the finite volumes $p, q, p \in \tau, q \in N(p)$, we approximate fluxes through the boundary of p (cf. (3.26)). The value of diffusion coefficient along e_{pq} is approximated by its value at the point x_{pq}. We denote by $T_{pq} = m(e_{pq})/d_{pq}$ the transmissivity coefficient, and get the

Linear fully-discrete finite volume scheme for solving equation (3.1) [96]: *Let $N \in \mathbb{N}$, $k = T/N$ and $\sigma > 0$ be fixed numbers, $t_n = nk$, $n = 0, \ldots, N$. For $n = 1, \ldots, N$ we look for $\overline{u}_p^n, p \in \tau$, satisfying*

$$m(p)\overline{u}_p^n + k \sum_{q \in N(p)} g_{pq}^{\sigma, n-1} T_{pq} \left(\overline{u}_p^n - \overline{u}_q^n\right) = m(p)\overline{u}_p^{n-1}, \tag{3.51}$$

starting with

$$\overline{u}_p^0 = \frac{1}{m(p)} \int_p u^0(x)\, dx, \quad p \in \tau, \tag{3.52}$$

where

$$g_{pq}^{\sigma, n-1} = g(|\nabla G_\sigma * \tilde{u}_{h,k}(x_{pq}, t_{n-1})|) \tag{3.53}$$

and $\tilde{u}_{h,k}$ is an extension of the piecewise constant function $\overline{u}_{h,k}$ ($h = \max_{p \in \tau} \operatorname{diam}(p)$) defined as follows

$$\overline{u}_{h,k}(x,t) = \sum_{n=0}^{N} \sum_{p \in \tau} \overline{u}_p^n \chi_{\{x \in p\}} \chi_{\{t_{n-1} < t \le t_n\}} \tag{3.54}$$

with the boolean function $\chi_{\{A\}} = \begin{cases} 1 & \text{if } A \text{ is true} \\ 0 & \text{elsewhere.} \end{cases}$

The function $\overline{u}_{h,k}$, constructed using discrete values given by the scheme (3.51), is considered as the approximation of the solution and its convergence to a unique weak solution of (3.1) as $h, k \to 0$ has been proved (see [96] for all details and next Section for main ideas). It is clear that (3.51) gives a linear system with a symmetric, strictly diagonally dominant M-matrix, so there exists a unique discrete solution at every discrete scale step. Moreover, using the same trick as in (3.38), we get L_∞-stability of the scheme

$$\min_{p \in \tau} \overline{u}_p^0 \le \min_{p \in \tau} \overline{u}_p^n \le \max_{p \in \tau} \overline{u}_p^n \le \max_{p \in \tau} \overline{u}_p^0, \quad 1 \le n \le N. \tag{3.55}$$

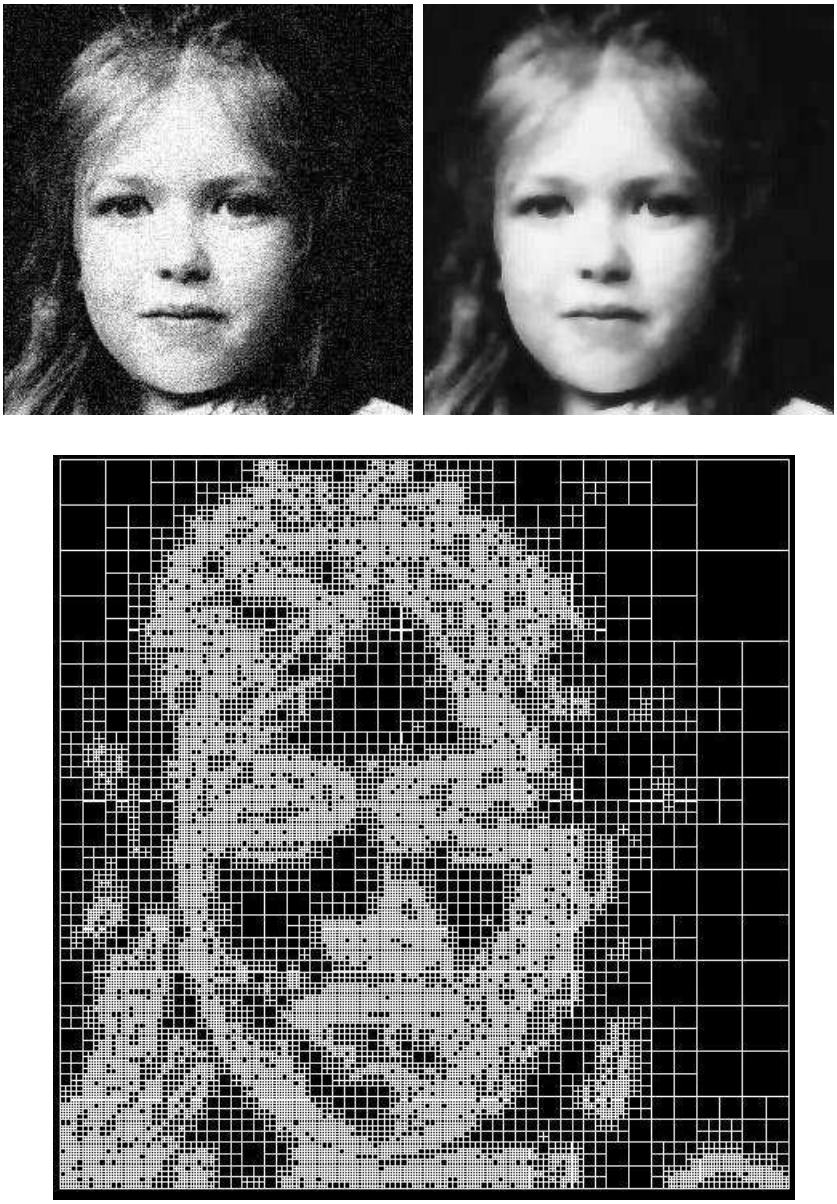

Figure 46: Processing of noisy photograph; noisy original (top left), smoothing after 25 scale steps (top right), final adaptive finite volume grid (down)

3.5.1 Convergence of the finite volume scheme

3.8 Definition A *weak solution* of the regularized Perona-Malik problem (1.2)–(1.4) is a function $u \in L_2(I,V)$ satisfying the identity

$$\int_0^T \int_\Omega u \frac{\partial \varphi}{\partial t}(x,t)\,dx\,dt + \int_\Omega u_0(x)\varphi(x,0)\,dx - \int_0^T \int_\Omega g(|\nabla G_\sigma * u|)\nabla u \nabla \varphi\,dx\,dt = 0 \qquad (3.56)$$

for all $\varphi \in \Psi$, where Ψ is the space of smooth test functions

$$\Psi = \{\varphi \in C^{2,1}(\overline{\Omega} \times [0,T]), \nabla\varphi.\vec{n} = 0 \text{ on } \partial\Omega \times (0,T), \varphi(\cdot,T) = 0\}. \qquad (3.57)$$

In [31] Catté, Lions, Morel and Coll proved that there exists unique weak solution of (1.2)–(1.4) which is also the classical solution of the problem at the same time. To get the existence they used Schauder's fixed point theorem with iterations in entire parabolic equations. In [96] we look for that solution in a computationally natural and efficient way using a semi-implicit finite volume scheme. In this Section we give the main ideas of the proof of the convergence of the finite volume solution to the weak solution of (1.2)–(1.4). Strategy is first to prove some *a priori* estimates of the numerical solution, using the scheme (3.51). These estimates will lead to the so-called *space* and *time translate estimates* for the approximate solution $\overline{u}_{h,k}$. The space and time translate estimates are specific formulations of the equicontinuity in the following well-known criterion (see e.g. [84]):

Kolmogorov's relative compactness criterion in $L_2(Q_T)$ *The set $K \subset L_2(Q_T)$ is relatively compact if and only if*

(i) *K is bounded, i.e., there exists $C > 0$ such that $\|f\| \le C$ for every $f \in K$;*

(ii) *K is mean equicontinous, i.e., for every $\varepsilon > 0$ there exists $\delta > 0$ such that*

$$\int_{Q_T} (f(x+\gamma) - f(x))^2\,dx < \varepsilon^2$$

for each $f \in K$ and γ with $|\gamma| < \delta$.

Proving relative compactness one gets that there exists a limit function $u \in L_2(Q_T)$ of the sequence $\overline{u}_{h,k}$ as $h,k \to 0$. Moreover, the space translates give that this limit is in $L_2(I,V)$, so it is a good candidate for the weak solution. It will be the last step of the convergence proof that u fulfills the weak identity (3.56).

3.9 Lemma (*a priori* estimates) *There exists a positive constant C, independent of h and k, such that*

(i) $\max_{0\le n\le N} \sum_{p\in\tau} (\overline{u}_p^n)^2 m(p) \le C$;

(ii) $\sum_{n=1}^N k \sum_{(p,q)\in\mathcal{E}} T_{pq}(\overline{u}_p^n - \overline{u}_q^n)^2 \le C$;

(iii) $\sum_{n=1}^N \sum_{p\in\tau} (\overline{u}_p^n - \overline{u}_p^{n-1})^2 m(p) \le C$.

Proof Let us multiply the scheme (3.51) by $\overline{u}_p^n$ to obtain

$$(\overline{u}_p^n - \overline{u}_p^{n-1})\overline{u}_p^n m(p) = k \sum_{q \in N(p)} g_{pq}^{\sigma,n-1} T_{pq} (\overline{u}_q^n - \overline{u}_p^n)\overline{u}_p^n. \tag{3.58}$$

Using (3.8) on the left-hand side of (3.58) and summing over $p \in \tau$, we have that

$$\begin{aligned} \frac{1}{2}\sum_{p\in\tau}(\overline{u}_p^n)^2 m(p) - \frac{1}{2}\sum_{p\in\tau}(\overline{u}_p^{n-1})^2 m(p) + \frac{1}{2}\sum_{p\in\tau}(\overline{u}_p^n - \overline{u}_p^{n-1})^2 m(p) \\ = k \sum_{p\in\tau}\sum_{q\in N(p)} g_{pq}^{\sigma,n-1} T_{pq}(\overline{u}_q^n - \overline{u}_p^n)\overline{u}_p^n. \end{aligned} \tag{3.59}$$

The following trick is often used in the finite volume technique for anti-symmetric $a_{pq} = -a_{qp}$:

$$\sum_{p\in\tau}\sum_{q\in N(p)} a_{pq} b_p = \sum_{(p,q)\in\mathcal{E}} a_{pq} b_p = \sum_{(q,p)\in\mathcal{E}} a_{qp} b_q = -\sum_{(p,q)\in\mathcal{E}} a_{pq} b_q,$$

hence

$$2\sum_{p\in\tau}\sum_{q\in N(p)} a_{pq} b_p = -\sum_{(p,q)\in\mathcal{E}} a_{pq}(b_q - b_p) \tag{3.60}$$

whence

$$\sum_{p\in\tau}\sum_{q\in N(p)} g_{pq}^{\sigma,n-1} T_{pq}(\overline{u}_q^n - \overline{u}_p^n)\overline{u}_p^n = -\frac{1}{2}\sum_{(p,q)\in\mathcal{E}} g_{pq}^{\sigma,n-1} T_{pq}(\overline{u}_p^n - \overline{u}_q^n)^2. \tag{3.61}$$

Applying (3.61) in (3.59) and summing over $n = 1, \ldots, m \le N$, we have

$$\begin{aligned} \frac{1}{2}\sum_{p\in\tau}(\overline{u}_p^m)^2 m(p) + \frac{1}{2}\sum_{n=1}^{m}\sum_{p\in\tau}(\overline{u}_p^n - \overline{u}_p^{n-1})^2 m(p) + \frac{1}{2}\sum_{n=1}^{m} k \sum_{(p,q)\in\mathcal{E}} g_{pq}^{\sigma,n-1} T_{pq}(\overline{u}_p^n - \overline{u}_q^n)^2 \\ = \frac{1}{2}\sum_{p\in\tau}(\overline{u}_p^0)^2 m(p). \end{aligned}$$

Since $u^0 \in L_\infty(\Omega)$ we get the results (i) and (iii). We also have

$$\left|\frac{\partial}{\partial x_i} G_\sigma * \tilde{u}_{h,k}(x_{pq}, t_{n-1})\right| \le \int_{\mathbb{R}^d} \left|\frac{\partial}{\partial x_i} G_\sigma(x_{pq} - \xi)\tilde{u}(\xi, t_{n-1})\right| d\xi \le C_\sigma \|\tilde{u}(., t_{n-1})\|_{L_\infty(\Omega)}.$$

Because of (3.55) we have that $|\nabla G_\sigma * \tilde{u}_{h,k}(x_{pq}, t_{n-1})| < \infty$, which in turn implies that there exists a positive constant α such that $g_{pq}^{\sigma,n-1} \ge \alpha > 0$, from which one can deduce the assertion (ii) of the lemma. □

In order to apply Kolmogorov's compactness criterion we have to estimate the integral

$$\begin{aligned} &\int_{Q_T} (\overline{u}_{h,k}(x+\xi, t+s) - \overline{u}_{h,k}(x,t))^2 \, dx\, dt \\ &\le 2\int_{Q_T} (\overline{u}_{h,k}(x+\xi, t+s) - \overline{u}_{h,k}(x, t+s))^2 \, dx\, dt + 2\int_{Q_T} (\overline{u}_{h,k}(x, t+s) - \overline{u}_{h,k}(x,t))^2 \, dx\, dt. \end{aligned}$$

Using an extension of the solution (e.g. by 0 outside of Ω) the main point is to estimate two integrals on the right-hand side restricted to domains $\Omega_\xi \times (0,T)$ with $\Omega_\xi = \{x \in \Omega, [x, x+\xi] \in \Omega\}$ and $\Omega \times (0, T-s)$ with $s \in (0,T)$, respectively [47, 96].

3.10 Lemma (Space translate estimates) *For any vector $\xi \in \mathbb{R}^d$ there exists a positive constant C such that*

$$\int_{\Omega_\xi \times (0,T)} (\overline{u}_{h,k}(x+\xi,t) - \overline{u}_{h,k}(x,t))^2 \, dx \, dt \le C|\xi|(|\xi| + 2h), \tag{3.62}$$

where $\Omega_\xi = \{x \in \Omega, [x, x+\xi] \in \Omega\}$.

Proof Let $\xi \in \mathbb{R}^d$ be a given vector. For all $(p,q) \in \mathcal{E}$, let us denote $\xi_{pq} = \xi/|\xi|.n_{pq}$. For all $x \in \Omega_\xi$, we denote by $E(x,p,q)$ the function defined as follows:

$$E(x,p,q) = \begin{cases} 1 & \text{if the segment } [x, x+\xi] \text{ intersects } e_{pq},\ p \text{ and } q, \text{ and } \xi_{pq} > 0 \\ 0 & \text{otherwise.} \end{cases}$$

For any $t \in (0,T)$ there exists $n \in \mathbb{N}$ such that $(n-1)k < t \le nk$. Then for almost all $x \in \Omega_\xi$ we can see that

$$\overline{u}_{h,k}(x+\xi,t) - \overline{u}_{h,k}(x,t) = \overline{u}^n_{p(x+\xi)} - \overline{u}^n_{p(x)} = \sum_{(p,q)\in\mathcal{E}} E(x,p,q)(\overline{u}^n_q - \overline{u}^n_p),$$

where $p(x)$ is the finite volume $p \in \tau$ such that $x \in p$. By the Cauchy-Schwarz inequality we obtain

$$\begin{aligned} &(\overline{u}_{h,k}(x+\xi,t) - \overline{u}_{h,k}(x,t))^2 \\ &\qquad \le \left(\sum_{(p,q)\in\mathcal{E}} E(x,p,q)\xi_{pq} d_{pq} \right) \left(\sum_{(p,q)\in\mathcal{E}} E(x,p,q) \frac{(\overline{u}^n_q - \overline{u}^n_p)^2}{\xi_{pq} d_{pq}} \right) \end{aligned} \tag{3.63}$$

and using the fact that $\xi_{pq} d_{pq} = \xi/|\xi|.n_{pq} d_{pq} = \xi/|\xi|.(x_q - x_p)$ we have

$$\sum_{(p,q)\in\mathcal{E}} E(x,p,q)\xi_{pq} d_{pq} = \frac{\xi}{|\xi|}.(x_{p(x+\xi)} - x_{p(x)}) \le |x_{p(x+\xi)} - x_{p(x)}| \le 2h + |\xi|.$$

Now, we integrate the relation (3.63) on $\Omega_\xi \times (0,T)$:

$$\begin{aligned} &\int_{\Omega_\xi \times (0,T)} (\overline{u}_{h,k}(x+\xi,t) - \overline{u}_{h,k}(x,t))^2 \, dx \, dt \\ &\qquad \le (2h + |\xi|) \sum_{n=1}^{N} k \sum_{(p,q)\in\mathcal{E}} \frac{(\overline{u}^n_q - \overline{u}^n_p)^2}{\xi_{pq} d_{pq}} \int_{\Omega_\xi} E(x,p,q) \, dx. \end{aligned} \tag{3.64}$$

Taking into account the area of a parallelogram we have

$$\int_{\Omega_\xi} E(x,p,q) \, dx \le m(e_{pq}) \xi.n_{pq} = m(e_{pq}) \frac{\xi}{|\xi|}.n_{pq}|\xi| = m(e_{pq})|\xi|\xi_{pq},$$

and applying this result in (3.64) we obtain

$$\int_{\Omega_\xi\times(0,T)} (\overline{u}_{h,k}(x+\xi,t)-\overline{u}_{h,k}(x,t))^2\,dx\,dt \le (2h+|\xi|)|\xi| \sum_{n=1}^{N} k \sum_{(p,q)\in\mathcal{E}} T_{pq}(\overline{u}_q^n-\overline{u}_p^n)^2. \quad (3.65)$$

Finally, using *a priori* estimate (ii) of Lemma 3.9 we complete the proof. □

In a more technical way, but basically using again the *a priori* estimate (ii) of Lemma 3.9 we get:

3.11 Lemma (Time translate estimate) *There exists a positive constant C such that*

$$\int_{\Omega\times(0,T-s)} (\overline{u}_{h,k}(x,t+s)-\overline{u}_{h,k}(x,t))^2\,dx\,dt \le Cs$$

for all $s\in(0,T)$.

3.12 Lemma (Convergence of $\overline{u}_{h,k}$) *There exists $u\in L_2(Q_T)$ such that for some subsequence of $\overline{u}_{h,k}$*

$$\overline{u}_{h,k}\to u \quad in \quad L_2(Q_T)$$

as $h,k\to 0$. Moreover, this limit function is in $L_2(I,V)$.

Proof From the estimate (i) of Lemma 3.9 we have that $\|\overline{u}_{h,k}\|_{L_2(Q_T)}\le C$, so the space and time translate estimates allow us to use Kolmogorov's relative compactness criterion in $L_2(Q_T)$ and we have the first assertion of the lemma.

Let $\varphi\in C_0^\infty(Q_T)$, $\varepsilon>0$ and $\varphi(x,t)=0$ if $|x-\partial\Omega|<\varepsilon$. Let $0<|\xi|<\varepsilon$. Then by the Cauchy-Schwarz inequality

$$\int_{\Omega\times(0,T)} \frac{\overline{u}_{h,k}(x+\xi,t)-\overline{u}_{h,k}(x,t)}{|\xi|}\varphi(x,t)\,dx\,dt \le \frac{\sqrt{C|\xi|(|\xi|+h)}}{|\xi|}\|\varphi\|_{L_2(Q_T)}.$$

For the limit function u we have

$$\int_{\Omega\times(0,T)} \frac{u(x+\xi,t)-u(x,t)}{|\xi|}\varphi(x,t)\,dx\,dt \le \sqrt{C}\|\varphi\|_{L_2(Q_T)}.$$

On the other hand, by a changing of the variables $y=x+\xi$ we get

$$\begin{aligned}
&\int_{\Omega\times(0,T)} \frac{u(x+\xi,t)-u(x,t)}{|\xi|}\varphi(x,t)\,dx\,dt \\
&\quad= \int_{\Omega\times(0,T)} \frac{u(y,t)}{|\xi|}\varphi(y-\xi,t)\,dy\,dt - \int_{\Omega\times(0,T)} \frac{u(y,t)}{|\xi|}\varphi(y,t)\,dy\,dt \\
&\quad= -\int_{\Omega\times(0,T)} \frac{\varphi(y,t)-\varphi(y-\xi,t)}{|\xi|}u(y,t)\,dy\,dt \\
&\quad\le C\|\varphi\|_{L_2(Q_T)}.
\end{aligned}$$

Let $\xi=\omega e_i$, where e_i is i-th coordinate vector, and let $\omega\to 0$. Then

$$-\int_{\Omega\times(0,T)} \frac{\partial\varphi(x,t)}{\partial x_i}u(x,t)\,dx\,dt \le C\|\varphi\|_{L_2(Q_T)}, \quad \forall\varphi\in C_0^\infty(Q_T).$$

Thus u has generalized spatial derivatives in $L_2(Q_T)$, so it is in $L_2(I,V)$. □

The last step is to prove that u given in Lemma 3.12 fulfills the weak identity (3.56) from Definition 3.8, and thus is a weak solution of the regularized Perona-Malik problem. Since such a solution is unique [31], not only a subsequence of $\overline{u}_{h,k}$ but the whole sequence will converge to u. Let $\varphi \in \Psi$ be given. We obtain a discrete analogy of the weak solution identity multiplying the finite volume scheme

$$(\overline{u}_p^n - \overline{u}_p^{n-1})m(p) = k \sum_{q\in N(p)} g_{pq}^{\sigma,n-1} T_{pq}(\overline{u}_q^n - \overline{u}_p^n)$$

by $\varphi(x_p, t_{n-1})$ and summing the resulting identity over all $p \in \tau$ and $n = 1, \ldots, N$:

$$\sum_{n=1}^{N} k \sum_{p\in\tau} \frac{(\overline{u}_p^n - \overline{u}_p^{n-1})}{k} \varphi(x_p, t_{n-1}) m(p) = \sum_{n=1}^{N} k \sum_{p\in\tau} \sum_{q\in N(p)} g_{pq}^{\sigma,n-1} T_{pq}(\overline{u}_q^n - \overline{u}_p^n)\varphi(x_p, t_{n-1}).$$

Next we perform a discrete integration by parts

$$\sum_{n=1}^{N} (a^n - a^{n-1})b^{n-1} = a^N b^N - a^0 b^0 - \sum_{n=1}^{N} a^n (b^n - b^{n-1})$$

on the left-hand side, and a rearrangement of the sum

$$\sum_{p\in\tau} \sum_{q\in N(p)} a_{pq} b_p = -\frac{1}{2} \sum_{(p,q)\in\mathcal{E}} a_{pq}(b_q - b_p)$$

on the right-hand side, which together with $\varphi(x_p, t_N) = 0$ gives

$$\sum_{n=1}^{N} k \sum_{p\in\tau_h} \overline{u}_p^n \frac{\varphi(x_p, t_n) - \varphi(x_p, t_{n-1})}{k} m(p) + \sum_{p\in\tau_h} \overline{u}_p^0 \varphi(x_p, 0) m(p)$$
$$- \frac{1}{2} \sum_{n=1}^{N} k \sum_{(p,q)\in\mathcal{E}} g_{pq}^{\sigma,n-1} T_{pq}(\overline{u}_q^n - \overline{u}_p^n)(\varphi(x_q, t_{n-1}) - \varphi(x_p, t_{n-1})) = 0.$$

The correspondence of the discrete terms of the previous equation and the continuous integral terms of the weak identity (3.56) can be clearly seen, and the convergence as $h, k \to 0$ can be proved (see [96] for details). Thus we get:

3.13 Theorem *The sequence $\overline{u}_{h,k}$ converges strongly in $L_2(Q_T)$ to the unique weak solution u of (3.1)–(1.4) as $h, k \to 0$.*

References

[1] U. Abresch, J. Langer, *The normalized curve shortening flow and homothetic solutions,* J. Diff. Geom., 23 (1986) pp. 175–196.

[2] H.W. Alt, S. Luckhaus, *Quasilinear elliptic-parabolic differential equations,* Math. Zeitschrift, 183 (1983) pp. 311–341.

[3] L. Alvarez, F. Guichard, P. L. Lions, J. M. Morel, *Axioms and Fundamental Equations of Image Processing,* Archive for Rat. Mech. Anal., 123 (1993) pp. 200–257.

[4] L. Alvarez, P. L. Lions, J.-M. Morel, *Image selective smoothing and edge detection by nonlinear diffusion II,* SIAM J. Numer. Anal., 29 (1992) pp. 845–866.

[5] L. Alvarez, J. M. Morel, *Formalization and computational aspects of image analysis,* Acta Numerica, (1994) pp. 1–59.

[6] B. Andrews, *Evolving convex curves,* Calc. Var. Partial Differ. Equ. 7, (1998) pp. 315–371.

[7] S. B. Angenent, *Nonlinear analytic semiflows,* Proc. R. Soc. Edinb. , Sect. A, 115 (1990) pp. 91–107,

[8] S. B. Angenent, *Parabolic equations for curves on surfaces I: Curves with p-integrable curvature,* Annals of Mathematics, 132 (1990) pp. 451–483.

[9] S. B. Angenent, *Parabolic equations for curves on surfaces II: Intersections, blow-up and generalized solutions,* Annals of Mathematics, 133 (1991) pp. 171–215.

[10] S. B. Angenent, *On the formation of singularities in the curve shortening flow,* J. Diff. Geom., 33 (1991) pp. 601–633.

[11] S. B. Angenent, M. E. Gurtin, *Multiphase thermomechanics with an interfacial structure 2. Evolution of an isothermal interface,* Arch. Rat. Mech. Anal., 108 (1989) pp. 323–391.

[12] S. B. Angenent, M. E. Gurtin,*Anisotropic motion of a phase interface. Well-posedness of the initial value problem and qualitative properties of the interface,* J. Reine Angew. Math., 446 (1994) pp. 1–47.

[13] S. B. Angenent, M. E. Gurtin, *General contact angle conditions with and without kinetics,* Quarterly of Appl. Math., 54, 3 (1996) pp. 557–569.

[14] S. B. Angenent, G. Sapiro, A. Tannenbaum, *On affine heat equation for non-convex curves,* Journal of the Amer. Math. Soc., 11 (1998) pp. 601–634.

[15] E. Bänsch, *Local mesh refinement in 2 and 3 dimensions,* IMPACT of Computing in Science and Engineering, 3 (1991) pp. 181–191.

[16] E. Bänsch, K. Mikula, *A coarsening finite element strategy in image selective smoothing,* Computing and Visualization in Science, Vol.1, No.1 (1997) pp. 53–61.

[17] E. Bänsch, K. Mikula, *Adaptivity in 3D image processing,* Computing and Visualization in Science, Vol.4, No.1 (2001) pp. 21–30.

[18] E. Bänsch, A. Schmidt, *Simulation of dendritic crystal growth with thermal convection,* Interfaces and Free Boundaries, 2 (1) (2000) pp. 95–115.

[19] M. Beneš, K. Mikula, *Simulations of anisotropic motion by mean curvature – comparison of phase field and sharp interface approaches,* Acta Math. Univ. Comenian., 67 (1998) pp. 17–42.

[20] M. Beneš, *Mathematical analysis of phase-field equations with numerically efficient coupling terms,* Interfaces and Free Boundaries, 3 (2) (2001) pp. 201–221.

[21] M. Beneš, *Mathematical and computational aspects of solidification of pure crystallic materials,* Acta Math. Univ. Comenian., 70 (2001) pp. 123–151.

[22] G. Caginalp, *The dynamics of a conserved phase field system: Stefan-like, Hele-Shaw, and Cahn-Hilliard models as asymptotic limits,* IMA J. Appl. Math., 44 (1990) pp. 77–94.

[23] F. Cao, *Application of the Gestalt principles to detection of good continuations and corners in image level lines,* to appear in Computing and Visualization in Science

[24] F. Cao, L. Moisan, *Geometric computation of curvature driven plane curve evolutions,* SIAM J. Numer. Anal., 39 (2001) pp. 624–646

[25] V. Caselles, F. Catté, T. Coll, F. Dibos, *A geometric model for active contours in image processing,* Numerische Matematik, 66 (1993) pp. 1–31.

[26] V. Caselles, R. Kimmel, G. Sapiro, *Geodesic active contours,* in: Proceedings International Conference on Computer Vision'95, Boston 1995, pp. 694–699.

[27] V. Caselles, R. Kimmel, G. Sapiro, *Geodesic active contours,* International Journal of Computer Vision, 22 (1997) pp. 61–79.

[28] V. Caselles, R. Kimmel, G. Sapiro, C. Sbert, *Minimal surfaces: a geometric three dimensional segmentation approach,* Numer. Math., 77 (1997) pp. 423–451.

[29] V. Caselles, R. Kimmel, G. Sapiro, C. Sbert, *Minimal surfaces based object segmentation,* IEEE Trans. Pattern Analysis and Machine Intelligence, 19 (1997) pp. 394–398.

[30] V. Caselles, J.-M. Morel, G. Sapiro (eds.), IEEE Trans. Image Processing, Vol.7 (1998).

[31] V. Catté, P.L. Lions, J.M.. Morel, T. Coll, *Image selective smoothing and edge detection by nonlinear diffusion,* SIAM J. Numer. Anal., 29 (1992) pp. 182–193.

[32] P. F. Ciarlet, *The Finite Element Method For Elliptic Problems,* North-Holland, Amsterdam, 1978.

[33] Y.-G. Chen, Y. Giga, S. Goto, *Uniqueness and existence of viscosity solutions of generalized mean curvature flow equation,* J. Differential Geometry, 33 (1991) pp. 749–786.

[34] M. G. Crandall, H. Ishii, P. L. Lions, *User's guide to viscosity solutions of second order partial differential equations,* Bull. Amer. Math. Soc. (NS), 27 (1992) pp. 1–67.

[35] K. Deckelnick, *Weak solutions of the curve shortening flow,* Calc. Var. Partial Differ. Equ., 5 (1997) pp. 489–510.

[36] K. Deckelnick, G. Dziuk, *Convergence of a finite element method for non-parametric mean curvature flow,* Numer. Math., 72 (1995) pp. 197–222.

[37] K. Deckelnick, G. Dziuk, *Discrete anisotropic curvature flow of graphs,* Math. Model. Numer. Anal., 33 (1999) pp. 1203–1222.

[38] K. Deckelnick, G. Dziuk, *Error estimates for a semi-implicit fully discrete finite element scheme for the mean curvature flow of graphs,* Interfaces and Free Boundaries, 2 (2000) pp. 341–359.

[39] K. Deckelnick, G. Dziuk, *A fully discrete numerical scheme for weighted mean curvature flow,* Numer. Math., 91 (2002) pp. 423–452.

[40] U. Diewald, T. Preusser, M. Rumpf, R. Strzodka, *Diffusion models and their accelerated solution in image and surface processing,* Acta Math. Univ. Comenian., Vol.70, No.1 (2001) pp. 15–34.

[41] G. Dziuk, *Algorithm for evolutionary surfaces,* Numer. Math., 58 (1991) pp. 603–611.

[42] G. Dziuk, *Convergence of a semi discrete scheme for the curve shortening flow,* Mathematical Models and Methods in Applied Sciences, 4 (1994) pp. 589–606.

[43] G. Dziuk, *Discrete anisotropic curve shortening flow,* SIAM J. Numer. Anal., 36 (1999) pp. 1808–1830.

[44] C. M. Elliott, M. Paolini, R. Schätzle, *Interface estimates for the fully anisotropic Allen-Cahn equation and anisotropic mean curvature flow,* Mathematicals Models and Methods in Applied Sciences, 6 (1996) pp. 1103–1118.

[45] C. Epstein, M. Weinstein, *A stable manifold theorem for the curve shortening equation,* Communications on Pure and Applied Mathematics, 40 (1987) pp. 119–139.

[46] L. C. Evans, J. Spruck, *Motion of level sets by mean curvature I,* J. Differential Geometry, 33 (1991) pp. 635–681.

[47] R. Eymard, T. Gallouet, R. Herbin, *The finite volume method,* in: Handbook for Numerical Analysis, Vol.7 (Ph. Ciarlet, J. L. Lions, eds.), Elsevier, 2000.

[48] A. Friedman, B. McLeod, *Blow-up of solutions of nonlinear degenerate parabolic equations,* Arch. Rat. Mech. Anal., 96 (1986) pp. 55–80.

[49] M. Gage, R. S. Hamilton, *The heat equation shrinking convex plane curves,* J. Diff. Geom., 23 (1986) pp. 69–96.

[50] P. M. Girao, *Convergence of a crystalline algorithm for the motion of a simple closed convex curve by weighted curvature,* SIAM J. Numer. Anal., 32 (1995) pp. 886-899.

[51] P. M. Girao, R. V. Kohn, *Convergence of a crystalline algorithm for the heat equation in one dimension and for the motion of a graph by weighted curvature,* Numer. Math., 67 (1994) pp. 41–70.

[52] M. Grayson, *The heat equation shrinks embedded plane curves to round points,* J. Diff. Geom., 26 (1987) pp. 285–314.

[53] F. Guichard, *Axiomatisation des analyses multi-échelles d'images et de films,* Ph.D. Thesis, Université Paris IX Dauphine (1994).

[54] M. Gurtin, *Thermomechanics of Evolving Phase Boundaries in the Plane,* Clarendon Press, Oxford, 1993.

[55] A. Handlovičová, *Error estimates of a linear approximation scheme for nonlinear diffusion problems* Acta Math. Univ. Comenian., 61 (1992) pp. 27–39.

[56] A. Handlovičová, *Error estimates of a fully discrete linear approximation scheme for Stefan problem,* Acta Math. Univ. Comenian., 65 (1996) pp. 65–85.

[57] A. Handlovičová, *Solution of Stefan problems by fully discrete linear schemes,* Acta Math. Univ. Comenian., 67 (1998) pp. 351–372.

[58] A. Handlovičová, K. Mikula, A. Sarti, *Numerical solution of parabolic equations related to level set formulation of mean curvature flow,* Computing and Visualization in Science, 1 (1998) pp. 179–182.

[59] A. Handlovičová, K. Mikula, F. Sgallari, *Semi-implicit complementary volume scheme for solving level set like equations in image processing and curve evolution,* Numer. Math., 93 (2003) pp. 675–695.

[60] A. Handlovičová, K. Mikula, F. Sgallari, *Variational numerical methods for solving nonlinear diffusion equations arising in image processing,* J. Visual Communication and Image Representation, 13 (2002) pp. 217–237.

[61] T.Y. Hou, J. Lowengrub, M. Shelley, *Removing the stiffness from interfacial flows and surface tension,* J. Comput. Phys., 114 (1994) pp. 312–338.

[62] T.Y. Hou, I. Klapper, H. Si, *Removing the stiffness of curvature in computing 3-d filaments,* J. Comput. Phys., 143 (1998) pp. 628–664.

[63] W. Jäger, J. Kačur, *Solution of porous medium type systems by linear approximation schemes,* Numer. Math., 60 (1991) pp. 407–427.

[64] W. Jäger, J. Kačur, *Solution of doubly nonlinear and degenerate parabolic problems by relaxation schemes,* Mathematical Modelling and Numerical Analysis, 29 (1995) pp. 605–627.

[65] P.L. Lions, *Axiomatic derivation of image processing models,* Mathematical Models and Methods in Applied Sciences, 4 (1994) pp. 467–475.

[66] J. Kačur, *Method of Rothe in Evolution Equations,* Teubner-Texte Math. 80, Leipzig, 1985.

[67] J. KAČUR, *Solution of some free boundary problems by relaxation schemes,* SIAM J. Numer. Anal., 36 (1999) pp. 290–316.

[68] J. KAČUR, A. HANDLOVIČOVÁ, M. KAČUROVÁ, *Solution of nonlinear diffusion problems by linear approximation schemes,* SIAM J. Numer. Anal., 30 (1993) pp. 1703–1722.

[69] J. KAČUR, K. MIKULA, *Numerical solution of the anisotropic curve shortening flow,* Proc. of Int. Symp. Numer. Anal. ISNA'92, Praha (1992) pp. 108–121.

[70] J. KAČUR, K. MIKULA, *Solution of nonlinear diffusion appearing in image smoothing and edge detection,* Applied Numerical Mathematics, 17 (1995) pp. 47–59.

[71] J. KAČUR, K. MIKULA, *Slowed anisotropic diffusion,* in: Lecture Notes in Computer Science, 1252, Springer, Berlin (1997) pp. 357–360.

[72] J. KAČUR, K. MIKULA, *Slow and fast diffusion effects in image processing,* Computing and Visualization in Science, 3 (4) (2001) pp. 185–195.

[73] M. KASS, A. WITKIN, D. TERZOPULOS, *Snakes: active contour models,* International Journal of Computer Vision, 1 (1987) pp. 321–331.

[74] S. KICHENASSAMY, *The Perona-Malik paradox,* SIAM J. Appl. Math., Vol.57, No.5 (1997) pp. 1328–1342.

[75] S. KICHENASSAMY, A. KUMAR, P. OLVER, A. TANNENBAUM, A. YEZZI, *Gradient flows and geometric active contours models,* in Proceedings International Conference on Computer Vision'95, Boston (1995)

[76] S. KICHENASSAMY, A. KUMAR, P. OLVER, A. TANNENBAUM, A. YEZZI, *Conformal curvature flows: from phase transitions to active vision* Arch. Rational Mech. Anal., 134 (1996) pp. 275–301.

[77] R. KIMMEL, R. MALLADI, N. SOCHEN, *Images as embedded maps and minimal surfaces: movies, color, texture, and volumetric medical images,* Int. J. Computer Vision, 39 (2) (2000) pp. 111–129.

[78] M.KIMURA, *Accurate numerical scheme for the flow by curvature,* Appl. Math. Letters, 7 (1994) pp. 69–73.

[79] M. KIMURA, *Numerical analysis for moving boundary problems using the boundary tracking method,* Japan J. Indust. Appl. Math., 14 (1997) pp. 373–398.

[80] J. J. KOENDERINK, *The structure of images,* Biol. Cybern., 50 (1984) pp. 363–370.

[81] Z. KRIVÁ, K. MIKULA, *An adaptive finite volume scheme in processing of color images,* in: Proc. ALGORITMY 2000, Conf. on Scientific Computing, Podbanské, Slovakia (2000) pp. 174–188.

[82] Z. KRIVÁ, K. MIKULA, *An adaptive finite volume scheme for solving nonlinear diffusion equations in image processing,* J. Visual Communication and Image Representation, 13 (2002) pp. 22–35.

[83] Z. Krivá, K. Mikula, *Adaptive finite volume schemes in processing of 3D data sets,* J. Electrical Engineering 12/S, 52 (2001) pp. 53-58.

[84] A. Kufner, O. John, S. Fučik, *Function Spaces,* Academia, Prague, 1977.

[85] J.C. Li, *Finite element analysis for a nonlinear diffusion model in image processing,* Applied Mathematics Letters, 15 (2) (2002) pp. 197–202.

[86] J.C. Li, *Finite element analysis and application for a nonlinear diffusion model in image denoising,* Numer. Methods Partial Differ. Equations 18 (5) (2002) pp. 649–662.

[87] E. Magenes,R.H. Nochetto,C. Verdi, *Energy error estimates for a linear scheme to approximate nonlinear parabolic problems,* Math. Mod. Num. Anal., 21 (1987) pp. 655–678.

[88] R. Malladi, J. Sethian, B. Vemuri, *Shape modeling with front propagation: a level set approach,* IEEE Trans. Pattern Analysis and Machine Intelligence, 17 (1995) pp. 158–174.

[89] K. Mikula, *Numerical solution of nonlinear diffusion with finite extinction phenomenon,* Acta Math. Univ. Comenian., 64 (1995) pp. 173–184.

[90] K. Mikula, *Solution of nonlinear curvature driven evolution of plane convex curves,* Applied Numerical Mathematics, 23 (1997) pp. 347–360.

[91] K. Mikula, *Numerical experiments on geometry driven diffusion with application to image processing,* in: Science and Supercomputing at CINECA, Report 1997 (Ed. M.Voli, CINECA Supercomputing Group) (1998) pp. 689–692.

[92] K. Mikula, *Parallel filtering of three dimensional image sequences,* in: Science and Supercomputing at CINECA, Report 2000 (Eds. F.Garofalo, M.Moretti, M.Voli) (2001) pp. 674–677.

[93] K. Mikula, J. Kačur, *Evolution of convex plane curves describing anisotropic motions of phase interfaces,* SIAM J. Sci. Comput., 17 (1996) pp. 1302–1327.

[94] K. Mikula, T. Preusser, M. Rumpf, *Morphological image sequence processing,* to appear in Computing and Visualization in Science (2003)

[95] K. Mikula, T. Preusser, M. Rumpf, F. Sgallari, *On anisotropic geometric diffusion in 3D image processing and image sequence analysis,* in: Trends in Nonlinear Analysis, Springer (2002) pp. 305–319.

[96] K. Mikula, N. Ramarosy, *Semi-implicit finite volume scheme for solving nonlinear diffusion equations in image processing,* Numer. Math., Vol.89, No.3 (2001) pp. 561–590.

[97] K. Mikula, A. Sarti, C. Lamberti, *Geometrical diffusion in 3D-echocardiography,* in: Proc. ALGORITMY'97 – Conf. on Scientific Computing, Zuberec, Slovakia (1997) pp. 167–181.

[98] M K. MIKULA, F. SGALLARI, *Semi-implicit finite volume scheme for image processing in 3D cylindrical geometry,* to appear in Journal of Computational and Applied Mathematics

[99] K. MIKULA, D. ŠEVČOVIČ, *Solution of nonlinearly curvature driven evolution of plane curves,* Applied Numerical Mathematics, 31 (1999) pp. 191–207.

[100] K. MIKULA, D. ŠEVČOVIČ, *Evolution of plane curves driven by a nonlinear function of curvature and anisotropy,* SIAM J. Appl. Math., 61 (2001) pp. 1473–1501.

[101] K. MIKULA, D. ŠEVČOVIČ, *Computational and qualitative aspects of evolution of curves driven by curvature and external force,* to appear in Computing and Visualization in Science (2003)

[102] K. MIKULA, D. ŠEVČOVIČ, *A direct method for solving an anisotropic mean curvature flow of plane curves with an external force,* submitted

[103] K. MIKULA, D. ŠEVČOVIČ, *Evolution of curves on a surface driven by the geodesic curvature and external force,* submitted

[104] L. MOISSAN, *Affine plane curve evolution: A fully consistent scheme,* IEEE Transactions on Image Processing, 7 (1998) pp. 411–420.

[105] M. NIELSEN, P. JOHANSEN, O. F. OLSEN, J. WEICKERT (EDS.), *Scale-Space Theories in Computer Vision,* Lecture Notes in Computer Science, 1682, Springer, Berlin, 1999.

[106] M. NITZBERG, T. SHIOTA, *Nonlinear image filtering with edge and corner enhancement,* IEEE Trans. Pattern Analysis and Machine Intelligence, 14 (8) (1992) pp. 826–833.

[107] R. NOCHETTO, M. PAOLINI, C. VERDI, *Sharp error analysis for curvature dependent evolving fronts,* Mathematical Models and Methods in Applied Sciences, 3 (1993) pp. 711–723.

[108] K. N. NORDSTRÖM, *Biased anisotropic diffusion – A unified approach to edge detection,* Department of Electrical Engineering and Computer Sciences, University of California, Berkeley, 1989.

[109] S.OSHER, R.FEDKIW, *Level set methods and dynamic implicit surfaces* Springer-Verlag, 2003.

[110] S. OSHER, J. SETHIAN, *Fronts propagating with curvature dependent speed: algorithm based on Hamilton-Jacobi formulation,* J. Comput. Phys., 79 (1988) pp. 12–49.

[111] S. OSHER, L. RUDIN, *Feature oriented image enhancement using shock filters,* SIAM J. Numer. Anal., 27 (1990) pp. 919–940.

[112] M. PAOLINI, *Fattening in two dimensions obtained with a nonsymetric anisotropy: Numerical simulations,* Acta Math. Univ. Comenian., Vol.67, No.1 (1998) pp. 43–56.

[113] S. PATANKAR, *Numerical heat transfer and fluid flow,* Hemisphere Publ. Corp., New York, 1980.

[114] P. Perona, J. Malik, *Scale space and edge detection using anisotropic diffusion,* Proc. IEEE Computer Society Workshop on Computer Vision (1987)

[115] T. Preusser, M. Rumpf, *An adaptive finite element method for large scale image processing,* J. Visual Communication Image Representation, 11 (2) (2000) pp. 183–195.

[116] T. Preusser, M. Rumpf, *A level set method for anisotropic geometric diffusion in 3D image processing,* SIAM J. Appl. Math., 62 (2002) pp. 1773–1792.

[117] B.M.t. H. Romeny (Ed.), *Geometry driven diffusion in computer vision,* Kluwer, Dodrecht, 1994.

[118] L. I. Rudin, S. Osher, E. Fatemi, *Nonlinear total variation based noise removal algorithms,* Physica D, 60 (1992) pp. 259–268.

[119] Y. Saad, *Iterative Methods For Sparse Linear Systems,* PWS Publ. Comp., 1996.

[120] G. Sapiro, *Geometric Partial Differential Equations and Image Analysis,* Cambridge University Press, 2001

[121] G. Sapiro, A. Tannenbaum, *On affine plane curve evolution,* J. Funct. Anal., 119 (1994) pp. 79–120.

[122] G. Sapiro, A. Tannenbaum, *Affine invariant scale space,* Int. J. Computer Vision, 11 (1993) pp. 25–44.

[123] G. Sapiro, A. Tannenbaum, *Invariant curve evolution and image processing,* Indiana Univ. Journal of Math., 42 (1993) pp. 985–1009.

[124] G. Sapiro, A. Tannenbaum, *Area and length preserving geometric invariant scale-spaces,* IEEE Trans. Pattern Analysis and Machine Intelligence, 17 (1995) pp. 1066–1070.

[125] A. Sarti, K. Mikula, F. Sgallari, *Nonlinear multiscale analysis of three-dimensional echocardiographic sequences,* IEEE Trans. on Medical Imaging, 18 (1999) pp. 453–466.

[126] A. Sarti, K. Mikula, F. Sgallari, C. Lamberti, *Nonlinear multiscale analysis models for filtering of 3D + time biomedical images,* in: Geometric methods in biomedical image processing (Ed. R.Malladi), Springer (2002) pp. 107–128.

[127] A. Sarti, K. Mikula, F. Sgallari, C. Lamberti, *Evolutionary partial differential equations for biomedical image processing,* Journal of Biomedical Informatics, 35 (2002) pp. 77–91.

[128] A. Schmidt, *Computation of three dimensional dendrites with finite elements,* J. Comput. Phys., 125 (1996) pp. 293–312.

[129] A. Schmidt, *Approximation of crystalline dendrite growth in two space dimensions,* Acta Math. Univ. Comenian., Vol.67, No.1 (1998) pp. 57–68.

[130] A. Schmidt, K. G. Siebert, *ALBERT – Software for scientific computations and applications,* Acta Math. Univ. Comenian., 70 (1) (2001) pp. 105–122.

[131] J. SETHIAN, *Numerical algorithm for propagating interfaces: Hamilton-Jacobi equations and conservation laws,* J. Differential. Geom., 31 (1990) pp. 131–161.

[132] J.A.SETHIAN, *Adaptive fast marching and level set methods for propagating interfaces,* Acta Math. Univ. Comenian., Vol.67, No.1 (1998) pp. 3–16.

[133] J.A. SETHIAN, *Level Set Methods and Fast Marching Methods: Evolving Interfaces in Computational Geometry, Fluid Mechanics, Computer Vision, and Material Science,* Cambridge University Press, New York, 1999.

[134] T.USHIJIMA, S.YAZAKI, *Convergence of a crystalline algorithm for the motion of a closed convex curve by a power of curvature $V = K^{\alpha}$,* SIAM J. Numer. Anal., 37 (2000) pp. 500–522.

[135] N. J. WALKINGTON, *Algorithms for computing motion by mean curvature,* SIAM J. Numer. Anal., 33 (6) (1996) pp. 2215–2238.

[136] J. WEICKERT, *Anisotropic Diffusion in Computer Vision,* Teubner-Stuttgart, 1998.

[137] J. WEICKERT, B. M. T. H. ROMENY, M. A. VIERGEVER, *Efficient and reliable schemes for nonlinear diffusion filtering,* IEEE Trans. Image Processing, 7 (1998) pp. 398–410.

[138] J. WEICKERT, *Coherence-enhancing diffusion of colour images,* Image and Vision Computing, 17 (1999) pp. 201–212.

[139] R WHITACKER, G. GERIG, *Vector-valued diffusion,* in: Geometry Driven Diffusion in Computer Vision (B. M. t. H. Romemy, ed.), Kluwer, Dodrecht, 1994.

[140] A. P. WITKIN, *Scale-space filtering,* in: Proc. Eight Internat. Conf. on Artificial Intelligence, Vol. 2 (1983) pp. 1019–1022.

[141] S. WOLFRAM, *The Mathematica Book, 3rd ed.,* Cambridge Univ. Press, 1996.